DNA 5601F

AD A104689

LABORATORY STUDIES OF CONTAINMENT IN UNDERGROUND NUCLEAR TESTS

J. C. Cizek
A. L. Florence

SRI International
333 Ravenswood Avenue
Menlo Park, California 94025

31 January 1980

Final Report for Period 15 December 1978—31 January 1980

CONTRACT No. DNA 001-79-C-0094

APPROVED FOR PUBLIC RELEASE;
DISTRIBUTION UNLIMITED.

DTIC FILE COPY

Prepared for

Director

DEFENSE NUCLEAR AGENCY

Washington, D. C. 20305

REPORT DOCUMENTATION PAGE	READ INSTRUCTIONS BEFORE COMPLETING FORM

1. REPORT NUMBER DNA 5601F	2. GOVT ACCESSION NO. AD-A104 689	3. RECIPIENT'S CATALOG NUMBER

4. TITLE (and Subtitle) LABORATORY STUDIES OF CONTAINMENT IN UNDERGROUND NUCLEAR TESTS	5. TYPE OF REPORT & PERIOD COVERED Final Report, for Period. 15 Dec 78 — 31 Jan 80
	6. PERFORMING ORG. REPORT NUMBER SRI PYU-8113

7. AUTHOR(s) J. C. Cizek and A. L. Florence	8. CONTRACT OR GRANT NUMBER(s) DNA 001-79-C-0094

9. PERFORMING ORGANIZATION NAME AND ADDRESS SRI International 333 Ravenswood Avenue Menlo Park, CA 94025	10. PROGRAM ELEMENT, PROJECT, TASK AREA & WORK UNIT NUMBERS Subtask J24AAXYX983-64

11. CONTROLLING OFFICE NAME AND ADDRESS Director Defense Nuclear Agency Washington, D.C. 20305	12. REPORT DATE 31 Jan 1980
	13. NUMBER OF PAGES 142

14. MONITORING AGENCY NAME & ADDRESS(if different from Controlling Office)	15. SECURITY CLASS (of this report) UNCLASSIFIED
	15a. DECLASSIFICATION DOWNGRADING SCHEDULE N/A

16. DISTRIBUTION STATEMENT (of this Report)

Approved for public release; distribution unlimited.

17. DISTRIBUTION STATEMENT (of the abstract entered in Block 20, if different from Report)

19. KEY WORDS (Continue on reverse side if necessary and identify by block number)

nuclear	hydrofracture	fault
underground	fracture initiation	interface
explosion	surface fracture	porous flow
containment	overburden	
cavity	tunnel	

20. ABSTRACT (Continue on reverse side if necessary and identify by block number)

As part of the DNA containment program for underground nuclear testing,
laboratory experiments were performed with small explosive charges cast in
compressed grout spheres to assess the effects on containment of the residual

DD FORM 1473 EDITION OF 1 NOV 65 IS OBSOLETE
1 JAN 73

stress field surrounding an exploded cavity. A comparison of constant flow-rate hydrofracture pressures in unvented exploded and unexploded cavities revealed the existence of a residual stress field that was beneficial to containment. Parameters were varied to provide an understanding of mechanisms controlling containment. The effects on containment of geological and test site features were examined.

The data provide results suitable for development of containment theories and for correlation with predictions of existing computer codes.

Unexploded cavity hydrofracture records were interpreted in terms of classical fracture mechanics theory. A simple analysis was applied to examine post test pore water migration and consequent stress relaxation.

PREFACE

RELEVANT CONVERSION FACTORS

To Convert From	To	Multiply By
atmosphere (normal)	kilo pascal (kPa)	1.013 25 X E +2
bar	kilo pascal (kPa)	1.000 000 X E +2
foot	meter (m)	3.048 000 X E -1
inch	meter (m)	2.540 000 X E -2
mil	meter (m)	2.540 000 X E -5
ounce	kilogram (kg)	2.834 952 X E -2
poise	kilogram/meter-second (kg/m·sec)	1.000 000 X E -1
pound-force (1bf avoirdupois)	newton (N)	4.448 222
pound-force/inch² (psi)	kilo pascal (kPa)	6.894 757
pound-mass (1bm avoirdupois)	kilogram (kg)	4.535 924 X E -1

TABLE OF CONTENTS

LIST OF ILLUSTRATIONS

5

LIST OF TABLES

SECTION 1

INTRODUCTION AND SUMMARY

1.1 INTRODUCTION

A requirement of underground nuclear testing is that radioactive
gases be prevented from entering the atmosphere. In general, this
requirement will be met if experimental tunnels leading from the nuclear
device cavity are stemmed successfully and if the cavity gases are
contained by the adjacent surrounding medium. The residual stress field
generated in this surrounding medium by the explosion probably aids
containment. Although containment has been achieved for many years and
stemming has generally been successful in recent nuclear tests, reliability
is uncertain and planned tests still require extensive containment evaluation.

Over the years, the DNA stemming and containment (SAC) program has
consisted of five main parts: code development for ground motion, tunnel
closure, and grout flow calculations; material properties determination;
laboratory investigations; scaled high explosive tests; and field diagnostics.
Over the past several years SRI has been conducting the laboratory
investigations.[1-6]

Laboratory investigations during the last year have focused mainly
on containment. One purpose of the experimental program has been to
compare the containment capability of cavities generated under a variety
of conditions. Another purpose is to validate calculations[7-9] of the
residual stress field as a major containment feature of underground nuclear
tests. The data generated in the laboratory are suitable for correlation
with the predictions of existing codes. The experimental technique has
also been used to determine the influence of major geological and test
site features. Although our basic containment experiment may not be
regarded as a small-scale version of an explosively simulated underground
nuclear test, simulation is close enough to provide the correct important
mechanisms required in a study of containment.

9

In our basic containment experiment, a small spherical charge is cast at the center of a sphere of rock-matching grout (RMG) with properties similar to those of Nevada Test Site tuff. The RMG sphere is hydraulically pressurized to represent overburden. The explosive is detonated, and dyed fluid is immediately pumped into the cavity at a constant flow rate until fracture occurs and a steady radial pressure gradient is established. (In an alternative version of this test, residual cavity gases are vented before the start of hydrofracture.) The internal pressure is removed, and then the external pressure is removed. The cracked sphere is drained and tapped into two parts with a chisel, and the exposed fracture surfaces are photographed. The effect of the explosively generated residual stress field on containment is assessed by conducting a separate hydrofracture test on a sphere with an unexploded cavity equal in size to the exploded cavity.

Exploded and unexploded cavity hydrofracture tests were performed on RMG spheres of 12-inch (30.48-cm) diameter to establish reproducibility of the basic experimental technique. In exploded cavity tests, a 3/8-gram charge of PETN* generated a 3/4-inch (1.90-cm) diameter cavity, which was unvented. In unexploded cavity tests, a smooth and unlined cavity having the same diameter as the explosively formed cavity was cast. The fixed parameters were overburden pressure [1000 psi (6.895 MPa)], rate of fluid flow into the cavity (4.26 cm^3/min), and viscosity of the hydrofracture fluid (1 centipoise). Surface gages monitored fracture and fluid arrival. Embedded gages monitored fluid arrival. Results of the reproducibility tests provide comparison data for assessing the effects on containment of the following features:

- Overburden. External pressures of 0, 1000, and 2000 psi (0, 6.895, and 13.79 MPa) were applied to unexploded cavity spheres.

- Viscosity. Unexploded and exploded cavity spheres were hydrofractured with water (1 centipoise viscosity) and glycerol (660 centipoise viscosity).

---

*Pentaerythritol tetranitrate $(C_5H_8O_{12}N_4)$.

- Material property. Rock-matching grout (RMG 2C4),
  low density rock-matching grout (LD 2C4), and
  granite simulant (GS3) spheres were hydrofractured.

- Cavity lining. Hydrofracture tests were performed on
  unexploded cavities lined with an impermeable membrane.

- Charge holder thickness. Lucite charge holders with
  16-mil (0.406-mm) and 26-mil (0.660-mm) wall thicknesses
  were cast in exploded cavity spheres.

- Uncoupled charge. A 3/16-inch (0.476-cm) air gap
  between charge and surrounding grout was provided
  in exploded cavity tests.

- Geometry. Exploded cavity cylinders 12 inches (30.48 cm)
  in diameter and 12 inches (30.48 cm) long were
  hydrofractured.

- Material interface. Planes of discontinuity in material
  properties were formed in exploded cavity spheres by
  bonding rock-matching grout (RMG 2C4) to low density
  rock-matching grout (LD 2C4) and by bonding RMG 2C4
  to granite simulant (GS3).

- Geological and test site features. Radial tunnels,
  nearby tunnels, and fault planes were cast in exploded
  cavity spheres.

- Stress relaxation. Variations were permitted in the
  decay of residual cavity gas pressure in unvented
  exploded cavities.

In addition, the reproducibility of the 3/8-gram explosive source
was assessed by monitoring the pressure pulse generated in the overburden
fluid during exploded cavity tests. A fracture mechanics analysis was
applied to unexploded cavity tests to explain the dependence of fracture
initiation pressure on hydrofracture fluid viscosity and overburden. A
porous flow analysis was applied to exploded cavity tests to assess the
rate of decay of the explosively generated residual stress field. Particle
velocity measurements obtained in an independent laboratory program[10]
provided additional data for verifying the calculations.

The tests performed during the current phase of the laboratory program
are tabulated according to category in Section 3.1. In general, a minimum
of three tests in each category is desirable to demonstrate reproducibility
or to show a trend developing. However, the extensive variety of experi-
mental configurations limited the number of tests in a few categories to

one or two. Section 2 describes the most recent experimental developments, and Section 3 presents and discusses the hydrofracture results. Appendix A describes the application of a fracture mechanics analysis to hydrofracture. Appendix B examines relaxation of a residual stress field in terms of porous flow theory. Appendix C describes material properties for rock-matching grout RMG 2C4, low density rock-matching grout LD 2C4, and granite simulant GS3. Appendix D describes the sequence of events in unvented exploded cavity tests.

1.2 SUMMARY

The principal findings of the above investigations were as follows:

- Reproducibility of the unexploded cavity hydrofracture records is very good (Figure 3.1).

- Reproducibility of the explosive source is good for both charge holder wall thicknesses tested. The wall thickness variation has negligible effect on hydrofracture.

- Reproducibility of unvented exploded cavities, measured in terms of fracture initiation pressures, is good for water and glycerol hydrofractures. The pressure records depend on the residual cavity gas pressure at the start of hydrofracture.

- Fracture initiation pressures for water hydrofracture of unvented exploded cavities are nearly twice the corresponding values found in unexploded cavity tests.

- Hydrofracture pressures for vented exploded cavity spheres span the range between those for unexploded cavity tests and unvented exploded cavity tests.

- The slope of the fracture initiation pressure versus overburden curve is unity for water and glycerol hydrofractures of unexploded cavity rock-matching grout (RMG 2C4) spheres.

- Increased hydrofracture fluid viscosity results in higher fracture pressures for unexploded cavity rock-matching grout (RMG 2C4) and granite simulant (GS3) spheres.

- Lining an unexploded cavity with an impermeable membrane results in a higher fracture initiation pressure and initially stable crack growth.

- Higher fracture initiation pressures are developed in unexploded cavities surrounded by stronger materials such as GS3.

12

- Air voids in low density grout produce larger exploded cavities, less residual stress, and lower hydrofracture pressures.

- Uncoupling the explosive source from the surrounding medium has negligible effect on hydrofracture pressures.

- Cylindrical exploded cavity specimens yield pressure records comparable to those obtained with spheres.

- A plane interface connecting RMG 2C4 and LD 2C4 has negligible effect on hydrofracture. The effect of a plane interface connecting RMG 2C4 and GS3 is determined by the strength of the bond between the materials.

- Hollow radial tunnels reduce hydrofracture pressure because cavity gases vent to the tunnel which provides an axis for a fracture to initiate.

- Explosive products have been contained in tests with a tunnel passing within one cavity radius of an exploded cavity.

- Containment has been achieved in tests with a fault plane passing within three cavity radii of an exploded cavity.

In summary, an explosively formed residual stress field enhances the containment capability of a cavity by increasing hydrofracture pressures in unvented tests and by stabilizing initial crack growth.

Investigations during the next phase of the containment program will concentrate on the influence of pore water migration and creep on the residual stress field. The program will include:

- Characterizing the residual stress field surrounding an exploded cavity by means of stress, strain, and particle velocity measurements.

- Decreasing the time from charge detonation to fracture initiation in unvented exploded cavity tests.

- Determining the effects on containment of such test site features as nearby chimneys and asymmetric overburden loads.

13

SECTION 2

EXPERIMENTAL DEVELOPMENT

2.1 CONCEPT

The experiment shown schematically in Figure 2.1 was devised[4] to simulate in the laboratory the conditions in an underground nuclear test. A small spherical explosive charge representing the device is sealed in a thin Lucite container and cast in a much larger sphere of rock-matching group (RMG) with properties similar to those of Nevada Test Site tuff [Figure 2.1(a)]. The grout sphere is cured and then hydraulically pressurized to represent overburden [Figure 2.1(b)]. The explosive is detonated and the residual gas pressure is measured [Figure 2.1(c)]. Fluid is immediately pumped into the cavity at a constant flow rate until fracture occurs and a steady flow develops along the fracture surface [Figure 2.1 (d)]. An alternative version of this experiment was developed to allow hydrofracture following the venting of cavity gases.

The hydrofracture portion of the experiment is included to determine the effect of the residual stress field by comparing the cavity pressures required to crack the RMG sphere with and without residual stresses. In the experiments without a residual stress field, spherical cavities are cast in the grout sphere; these unexploded cavities are the same size as the exploded cavities.

2.2 EXPERIMENTAL TECHNIQUES

Figure 2.2 shows the experimental apparatus. A 12-inch-diameter RMG sphere is shown inside a steel vessel containing water that can be pressurized to the desired overburden. The sphere is suspended from the lid by a steel tube cast in the grout. In a vented exploded cavity test, this tube provides a means for positioning the charge, potting in the detonator cables, and drilling into the cavity after detonation. The water in the vessel is maintained at a constant pressure throughout

14
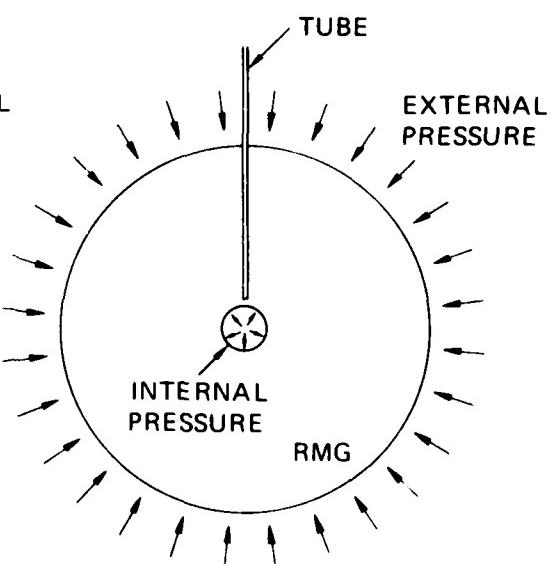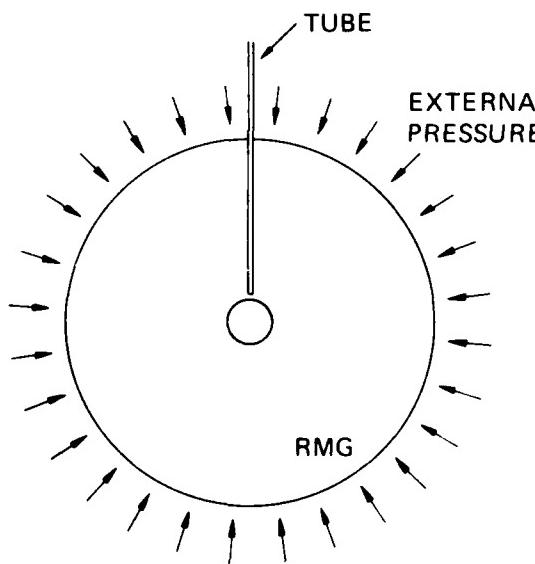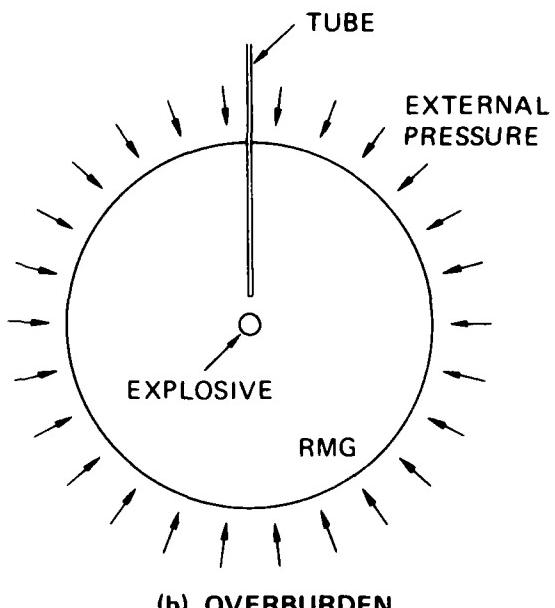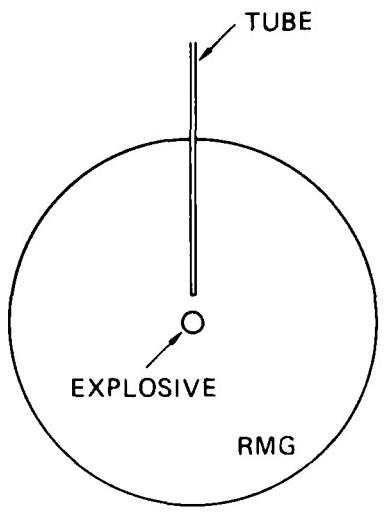
FIGURE 2.1 SEQUENCE OF OPERATIONS IN CONTAINMENT EXPERIMENTS
(Unvented Exploded Cavity)

15
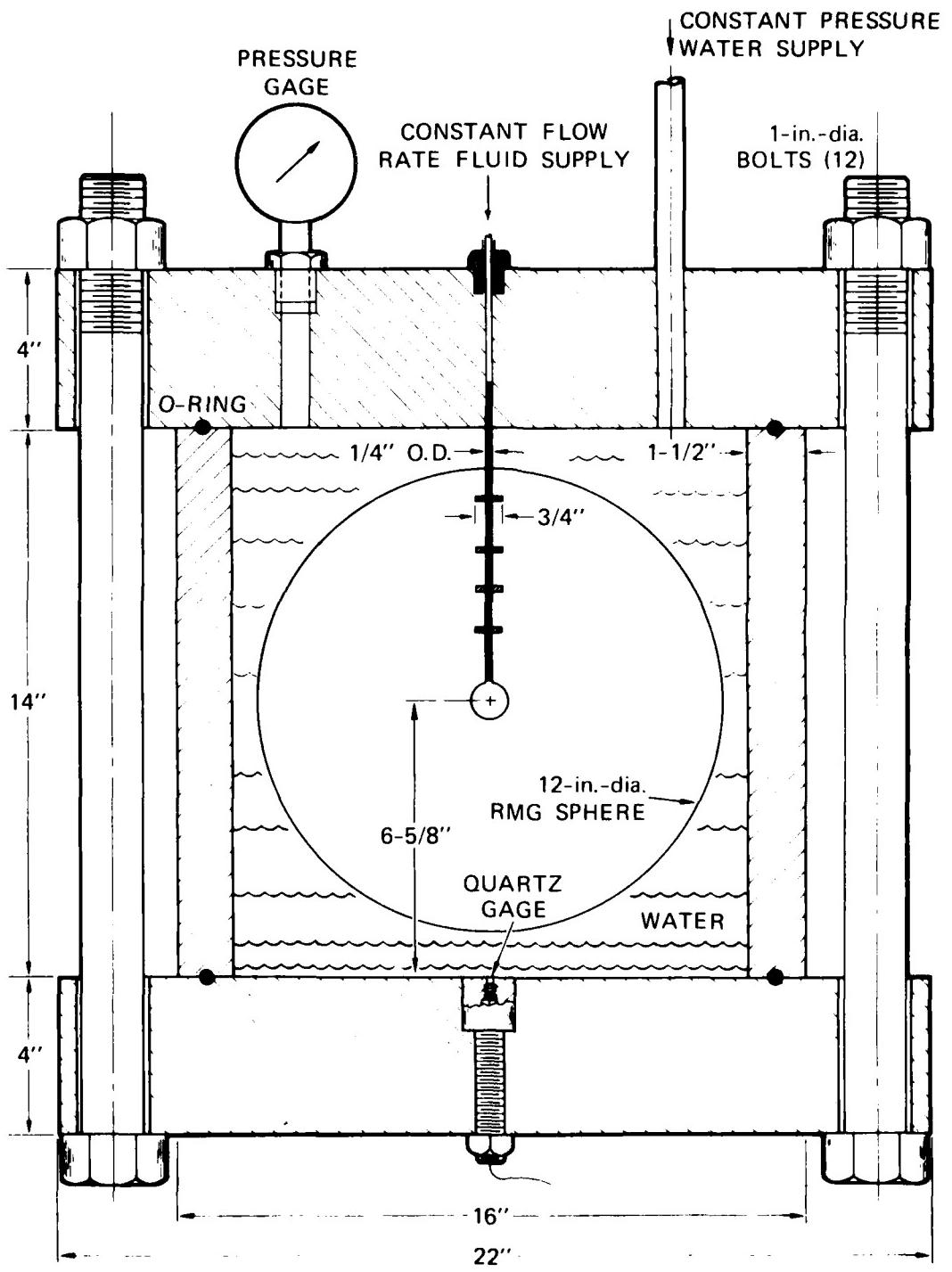
FIGURE 2.2 CONTAINMENT EXPERIMENT APPARATUS

16

the test by incorporating a high-pressure gas reservoir and valve in
the water supply line.

The constant flow rate system shown schematically in Figure 2.3
conforms with standard hydrofracture practice. The specifications of
this system are as follows:

Motor: Dayton Gear motor Model 5K933,
1/4 hp, 6 rpm, 600 in-lb torque

Pump: High Pressure Equipment Co. Model 87-6-5
60-cm^3 capacity, 5000-psi maximum pressure
4.26-cm^3/min flow rate (0.71-cm^3/revolution)

System: Fluid: dyed conductive water or dyed glycerin
Volume (excluding pump): 31.33 cm^3

The motor shaft rotates at a constant angular velocity of 6 rpm. A
slotted tubular coupling allows an extension of the shaft to translate
as well as rotate. The shaft extension is threaded and rotates in a
fixed threaded bearing, resulting in a constant velocity translation
of the pump piston. Hence, fluid is driven at a constant rate of 4.26
cm^3/min into the cavity supply line (Figure 2.2). Fluid flow is recorded
automatically with pen and chart by measuring the voltage change across
an angular potentiometer geared to the rotating shaft; a constant chart
speed introduces time, and calibration test results relate flow to
voltage change. Similarly, pressure is recorded by measuring the voltage
change across a calibrated resistance pressure transducer. Faster or
slower flow rates are possible through a modification of the gear system.

Compliance of the hydrofracture system is measured by performing
a pressure test in which the cavity is replaced by a rigid vessel of
equivalent volume. The pressure-volume curve for this test is then
used to compensate for the effects of system compliance on the hydro-
fracture records.

Details of the experimental techniques for unvented, vented, and
unexploded cavity tests are given below.
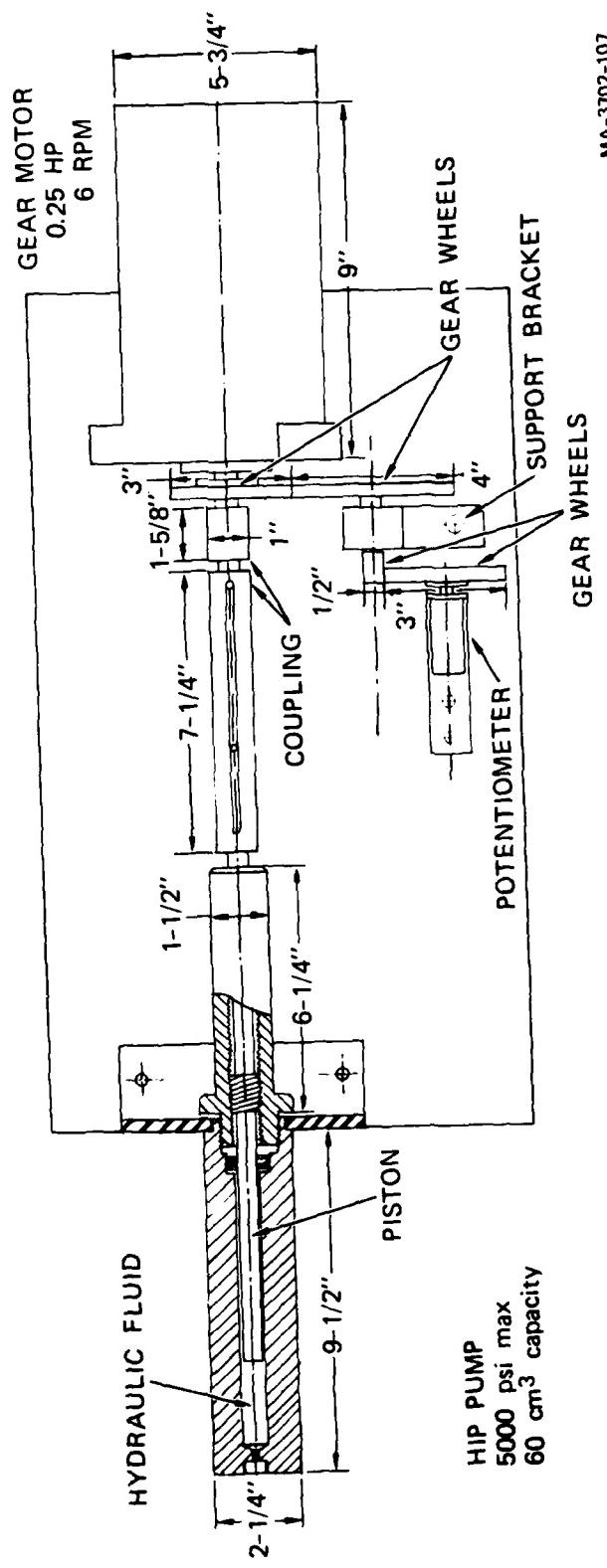
FIGURE 2.3   CONSTANT FLOW-RATE HYDROFRACTURE SYSTEM

MA-3702-107

18

Unvented Cavity Tests

The basic configuration for unvented exploded cavity hydrofracture tests is shown in Figure 2.4. Figure 2.5 shows the initial charge design, which consists of 3/8-gram of PETN in a 3/8-inch-OD (9.52-mm) Lucite case with a wall thickness of 16 mils (0.406 mm). A constant explosive density of 1 g/cm^3 is desired for reproducibility; achievable machining accuracy results in slight variation of PETN weight from charge to charge. Hence 3/8 gram is the nominal weight of the explosive. The charges are assembled by pressing PETN to a density of 1 g/cm^3 into a pair of mating Lucite hemispheres. The bridgewire assembly is then positioned as shown in Figure 2.5, using a notch in one of the hemispheres as a guide, and the hemispheres are snapped together and sealed with Homalite.* Figure 2.6 shows an improved charge design in which the wall thickness of the Lucite charge holder was increased to 26 mils (0.660 mm) to ensure stability under anticipated external loading. A wide-angle ferrule is attached near the end of the access tube to compress the grout around the tube as the cavity expands and prevent a leak path to the overburden from developing. The charge is positioned by gluing the charge holder to the steel ball that serves as a valve during the test; the lead wires are brought out of the sphere along the plane of the equator.

Cavity gas pressure is measured and hydrofracture performed by following the sequence of steps shown in Figure 2.7. Before charge detonation, the entire system is filled with hydrofracture fluid. The steel ball attached to a valve stem seals the end of the access tube [Figure 2.7(a)]. Charge detonation expands the cavity past the end of the tube [Figure 2.7(b)], and when the ball valve is lowered [Figure 2.7(c)], cavity gases pressurize the hydrofracture fluid. Pumping may begin immediately. Cavity gas and hydrofracture pressures are measured by a pressure transducer located in the fluid supply line. Ideally, charge detonation, the start of pumping, and opening of the access tube occur simultaneously. In practice, however, initially high cavity gas pressure delays opening of the access tube for approximately 4 seconds, and cavity pressures are not measured during this time. The process is described schematically in Appendix D.

---

*Homalite Corporation, Wilmington, Delaware.
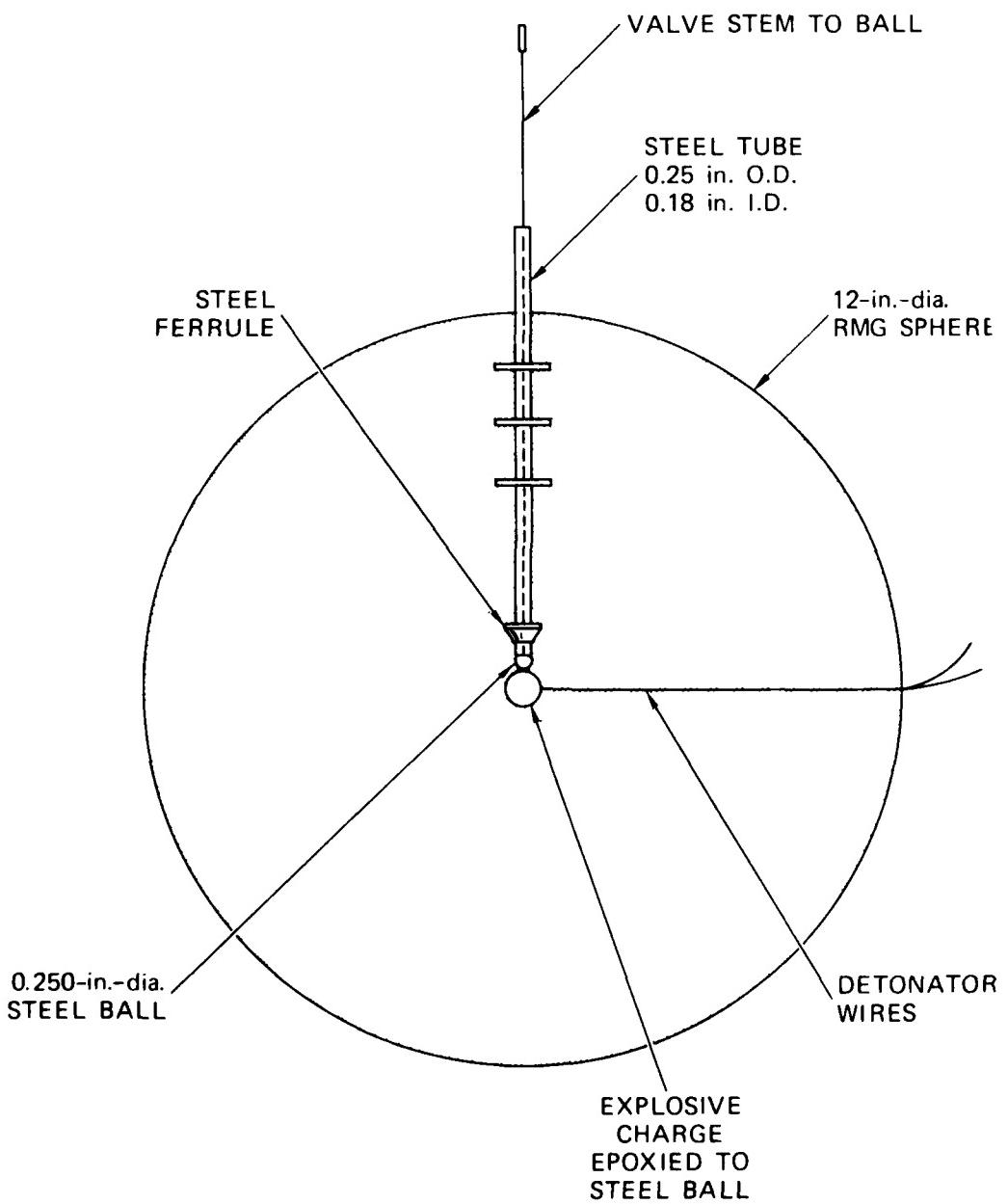
FIGURE 2.4 OVERALL CONFIGURATION FOR UNVENTED EXPLODED CAVITY TESTS

MA-5958-92

SOLID LEAD WIRE
(0.010 in. DIA.)
WITH INSULATION
(0.020 in. DIA.)

HEAT SHRINK
TUBING

EPOXY SEAL

0.343 I.D.

0.375 O.D.

LUCITE CASE

0.003 in. MANGANIN
BRIDGE WIRE
0.050 in. LONG

0.367 g PETN
(1 g/cm^3)
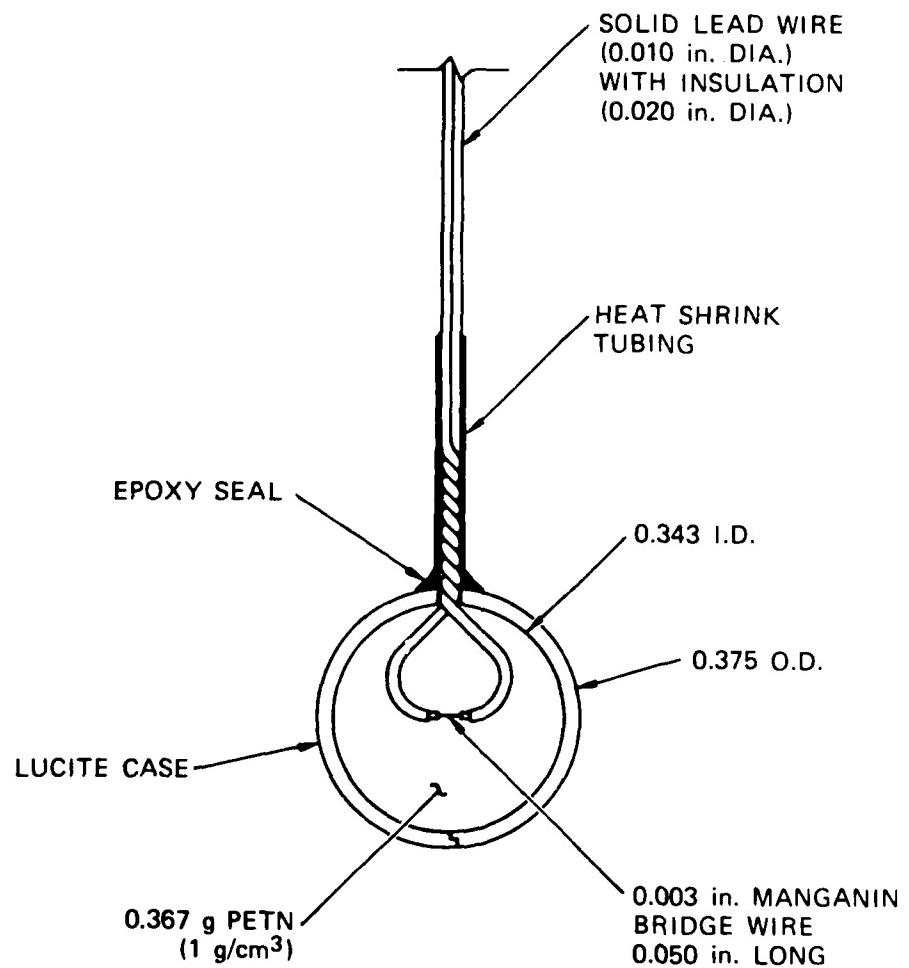
MA-5958-93

FIGURE 2.5   EXPLOSIVE CHARGE

21

SOLID LEAD WIRE
(0.010 in. DIA.)
WITH INSULATION
(0.020 in. DIA.)

EPOXY SEAL

3/8 g PETN
(1 g/cm^3)

0.003 in. MANGANIN
BRIDGE WIRE
0.050 in. LONG

LUCITE CASE
0.343 I.D.
0.394 O.D.
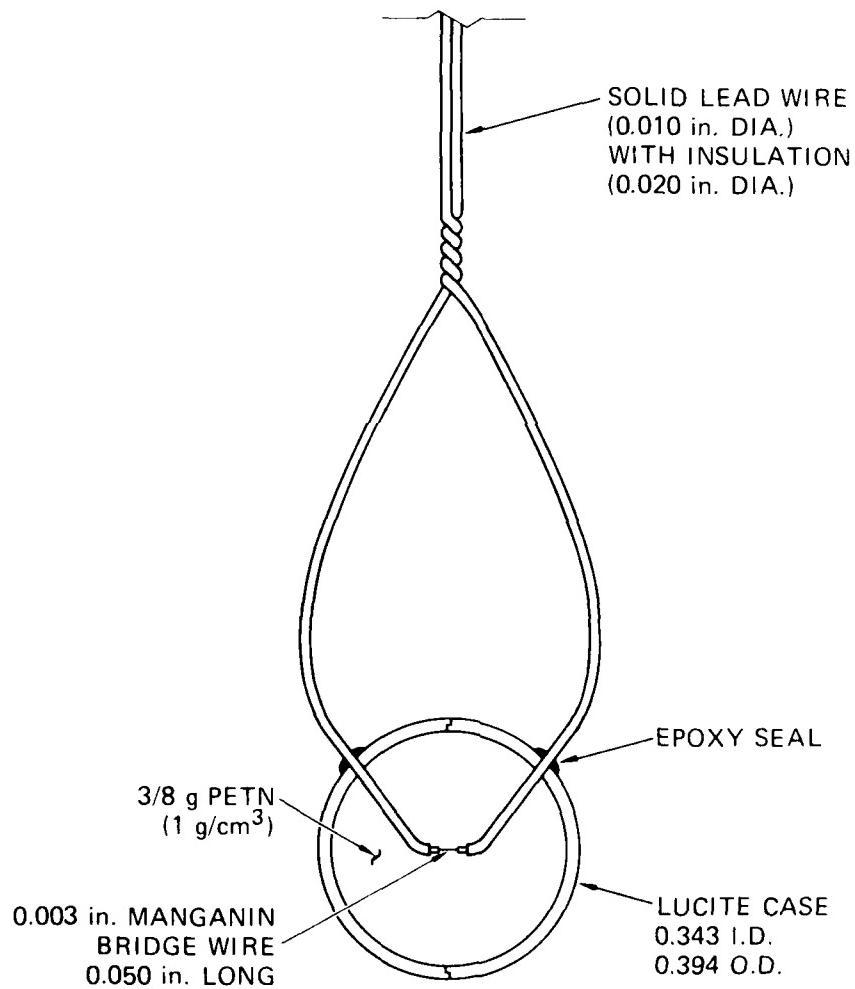
MA-8113-49

FIGURE 2.6   IMPROVED EXPLOSIVE CHARGE
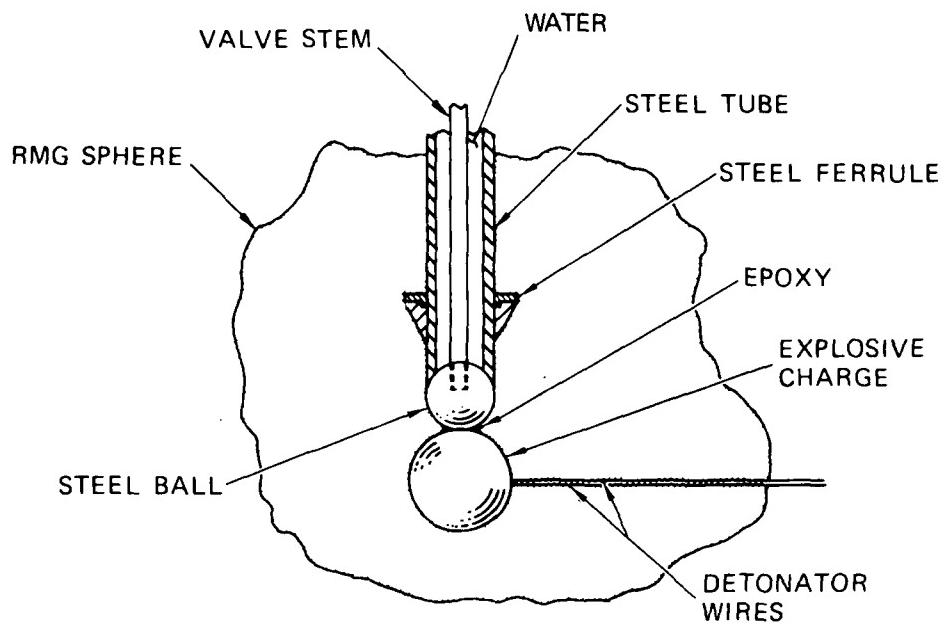
(a) INITIAL CONFIGURATION
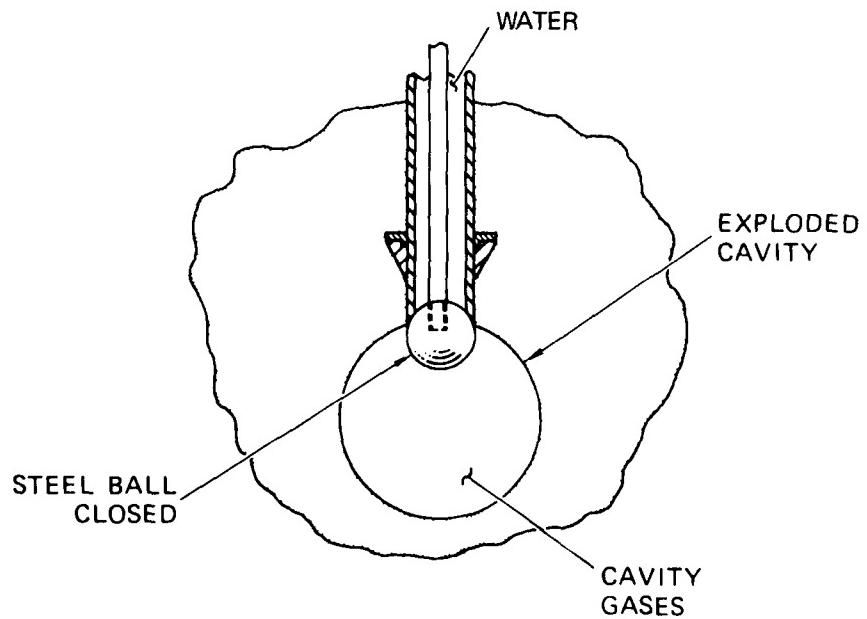
(b) CHARGE EXPLODED

MA-5958-96

FIGURE 2.7   SEQUENCE OF OPERATIONS FOR UNVENTED EXPLODED CAVITY TESTS

23
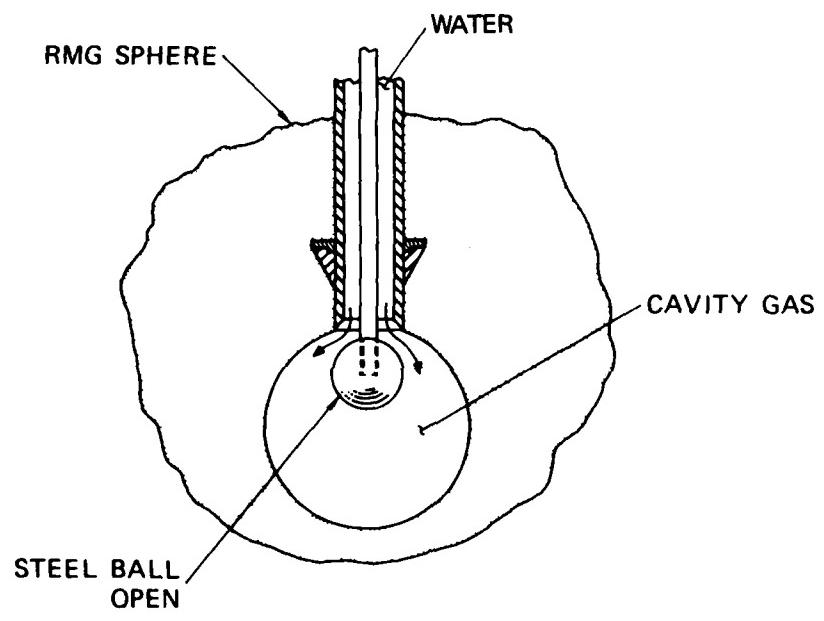
(c) START OF HYDROFRACTURE PROCESS

MA-5958-97

FIGURE 2.7 SEQUENCE OF OPERATIONS FOR UNVENTED EXPLODED CAVITY
TESTS (Concluded)

Accuracy of the cavity gas pressure measurement was assessed by performing a calibration test. In this test the exploded cavity and gases are replaced by a rigid vessel containing an equivalent volume of nitrogen at a known pressure. When the ball valve is lowered, the compliance of the hydrofracture system allows the nitrogen to expand and drop in pressure. To eliminate the pressure drop due to compliance, the hydrofracture system is pressurized to a nominal level of 300 psi (2.068 MPa). This prepressurizing technique was incorporated into the unvented exploded cavity tests.

Vented Cavity Tests

The basic configuration for vented exploded cavity hydrofracture tests is shown in Figure 2.8. The charge is positioned by drawing the lead wires through the access tube and filling the space between charge holder and tube with epoxy. The access tube is filled with epoxy. Venting occurs when the tube is drilled out following charge detonation. The drilling operation results in a 20-minute delay between charge detonation and hydrofracture. The hydrofracture pressures are measured by a pressure transducer located in the fluid supply line.

Unexploded Cavity Tests

The basic configuration for unexploded cavity hydrofracture tests is shown in Figure 2.9. The method of forming the central cavity is determined by the choice of a lined or unlined cavity.

A lined cavity is formed by first casting a balloon-shaped rubber membrane with an outside diameter equal to the desired cavity diameter. The neck of the membrane is then stretched over the end of the access tube and held in place by means of a Teflon ferrule and epoxy seal. The membrane is filled with water to preserve its spherical shape while the grout is poured and cured. After the grout is cured and water removed from the cavity, the membrane remains in place to act as a cavity lining during hydrofracture.

CONSTANT FLUID
FLOW RATE

STEEL TUBE (0.25 in. O.D.)
(0.18 in. I.D.)

12 in. dia
RMG SPHERE

STEEL FERRULE

EXPLODED SPHERICAL
CAVITY

ORIGINAL SPHERICAL
CAVITY

WATER
1000 psi

MA-3702-122A
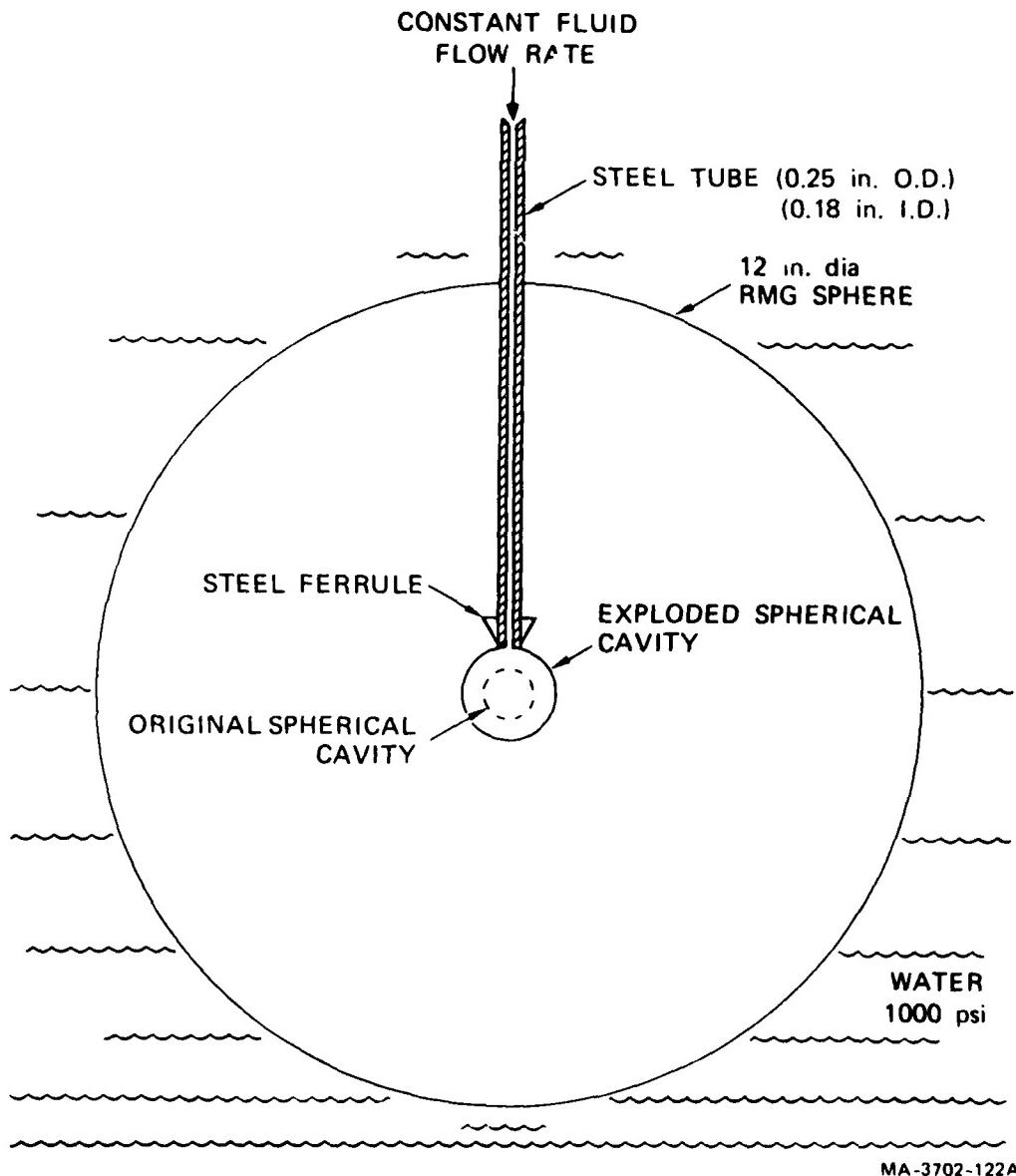
FIGURE 2.8 BASIC CONFIGURATION FOR VENTED EXPLODED CAVITY TESTS

26
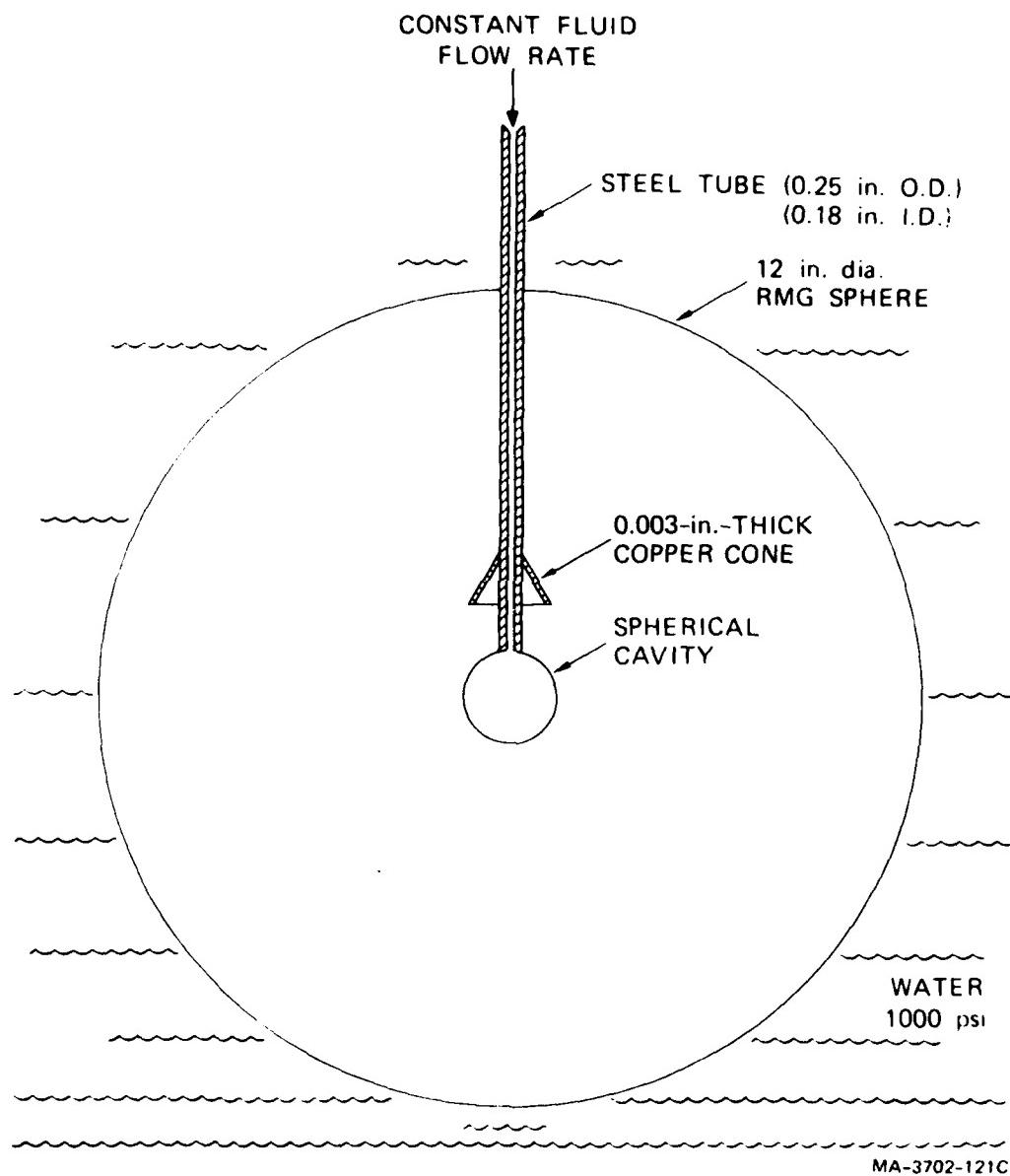
FIGURE 2.9 BASIC CONFIGURATION FOR UNEXPLODED CAVITY TESTS

An unlined cavity is formed by first inserting a rubber membrane (balloon) through the access tube and expanding the tip with water to the desired diameter. A spherical shape is maintained by means of a wire cage, which is temporarily fastened to the end of the tube. After 48 hours, the membrane has assumed a permanent shape and the cage is removed. The membrane and tube are then positioned in a Lucite mold and the grout is cast around them. After the grout has cured, the membrane is removed, leaving a smooth unlined cavity.

2.3 INSTRUMENTATION

The crack growth and fluid motion associated with hydrofracture and the particle velocity associated with charge detonation were monitored by the following sensors:

- Surface fracture gage   (Figure 2.10)
- Surface fluid arrival gage   (Figure 2.10)
- Embedded fluid arrival gage.

In addition, visual observations of surface cracking and fluid arrival were made for unexploded cavity tests conducted without overburden. Finally, relevant particle velocity records, which were generated during an independent laboratory study,[10] were incorporated into these results.

Surface Fracture Gage

Surface fracture of a grout sphere is detected by means of a 1/16-inch-wide (1.59-mm) stripe of electrically conductive silver-based paint. Two copper tabs are first embedded in the surface of the sphere during casting. After the grout is cured, the paint stripe connects the tabs to cover a desired region. During hydrofracture the resistance from tab to tab is monitored. Visual inspection of the surface of the sphere during hydrofracture has shown that a hairline crack in the grout is sufficient to break the paint and produce a noticeable resistance change in the gage. Typical regions of surface covered by the gage are shown in Figure 2.10. Initial gage resistance, which is a function of length, is 100 to 200 ohms for the gage shown. Final resistance, which is a measure of electrical conductivity through the grout, is 40,000 ohms.

0.020 in. DIA.
COPPER WIRE
IN CONTACT WITH
GROUT

TAPE OVER
CONDUCTIVE
WIRE

ELECTRICAL
WIRES

CONDUCTIVE
SILVER PAINT STRIPE

STEEL TUBE

1/8 x 1/4 x 3/16
in. COPPER TABS
IMBEDDED IN
GROUT

RMG SPHERE
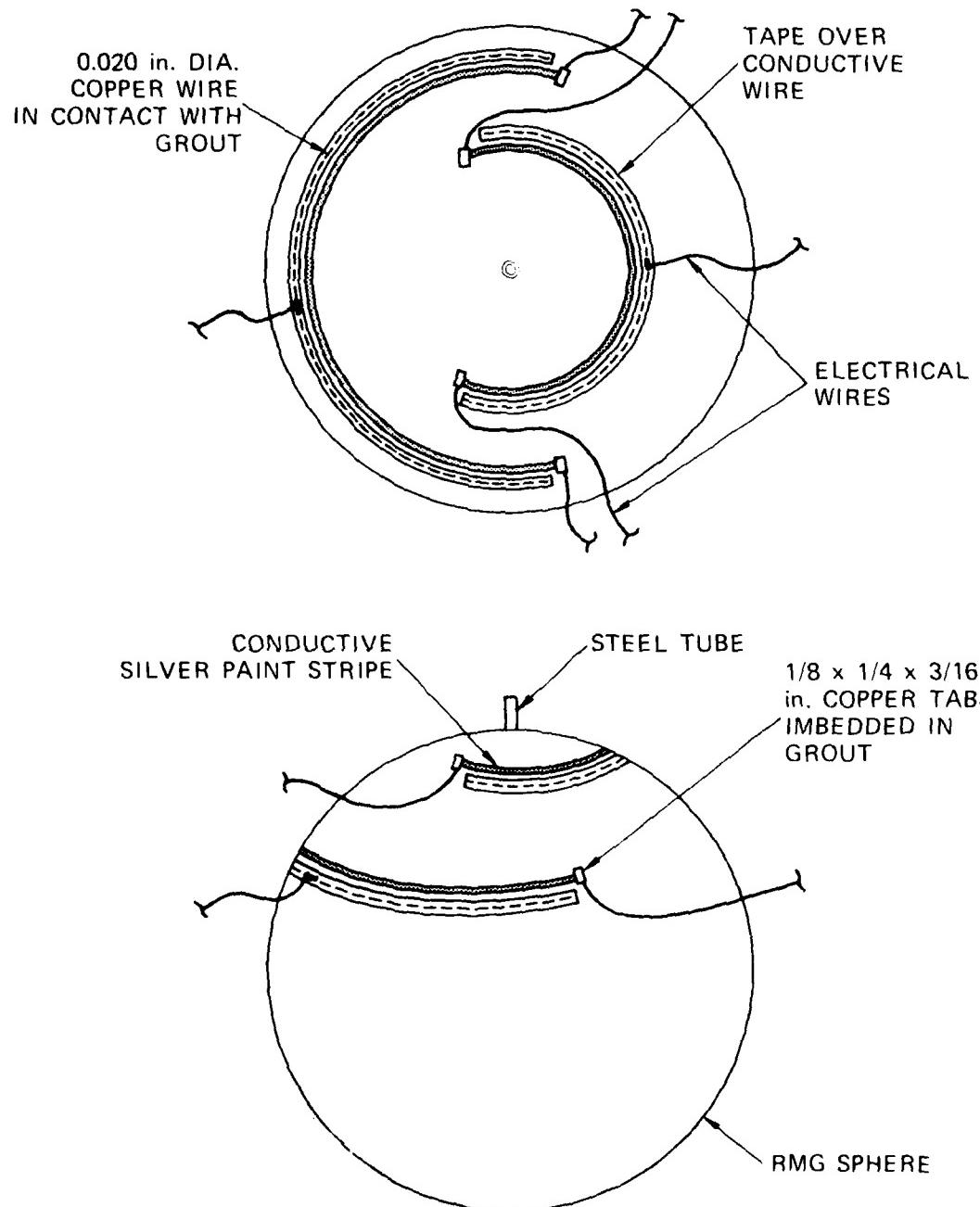
MA-5958-94

FIGURE 2.10   SURFACE CRACK AND FLUID ARRIVAL GAGES

Surface Fluid Arrival Gage

Arrival of hydrofracture fluid at the surface of a sphere is detected by means of a 20-mil (0.51-mm) copper wire taped to the grout. The resistance between access tube and gage is monitored during a test. Conductive hydrofracture fluid flows from the cavity, along a crack, and to the gage, resulting in a decrease in the measured resistance. The portion of the sphere in contact with the gage is coated with a brittle, electrically insulating material to provide a high initial resistance from access tube to copper wire. With this technique, the resistance decreases from 1500 to 700 ohms as fluid reaches the surface. Each copper wire may be positioned adjacent to a surface paint stripe, as shown in Figure 2.10, to allow for a correlation of surface fracture and fluid arrival. The conductive hydrofracture fluid is a mixture of dyed water and copper sulfate.

Embedded Fluid Arrival Gage

Arrival of hydrofracture fluid at some interior point of a grout sphere is detected by means of embedded 2-mil (0.051-mm) copper wire. The technique is similar to that of the surface fluid arrival gage described above. Conductive hydrofracture fluid flows along a crack and changes the resistance between the access tube and the wire. By adjusting the configuration and orientation of the wire, we can detect fluid arrival at any point in the sphere.

Embedded Particle Velocity Gage

Particle velocity records associated with charge detonation in rock-matching grout are shown in Figure 2.11. The results, which were taken from a recent laboratory study of stress waves crossing fault planes,[10] provide additional data for verifying the calculations. Radial velocity 4 cm from the center of the charge was measured. An average profile based on the six records in Figure 2.11 yields a time of arrival of 15 μsec, a peak particle velocity of 11.0 m/sec, and a reversal of motion at 41 μsec.
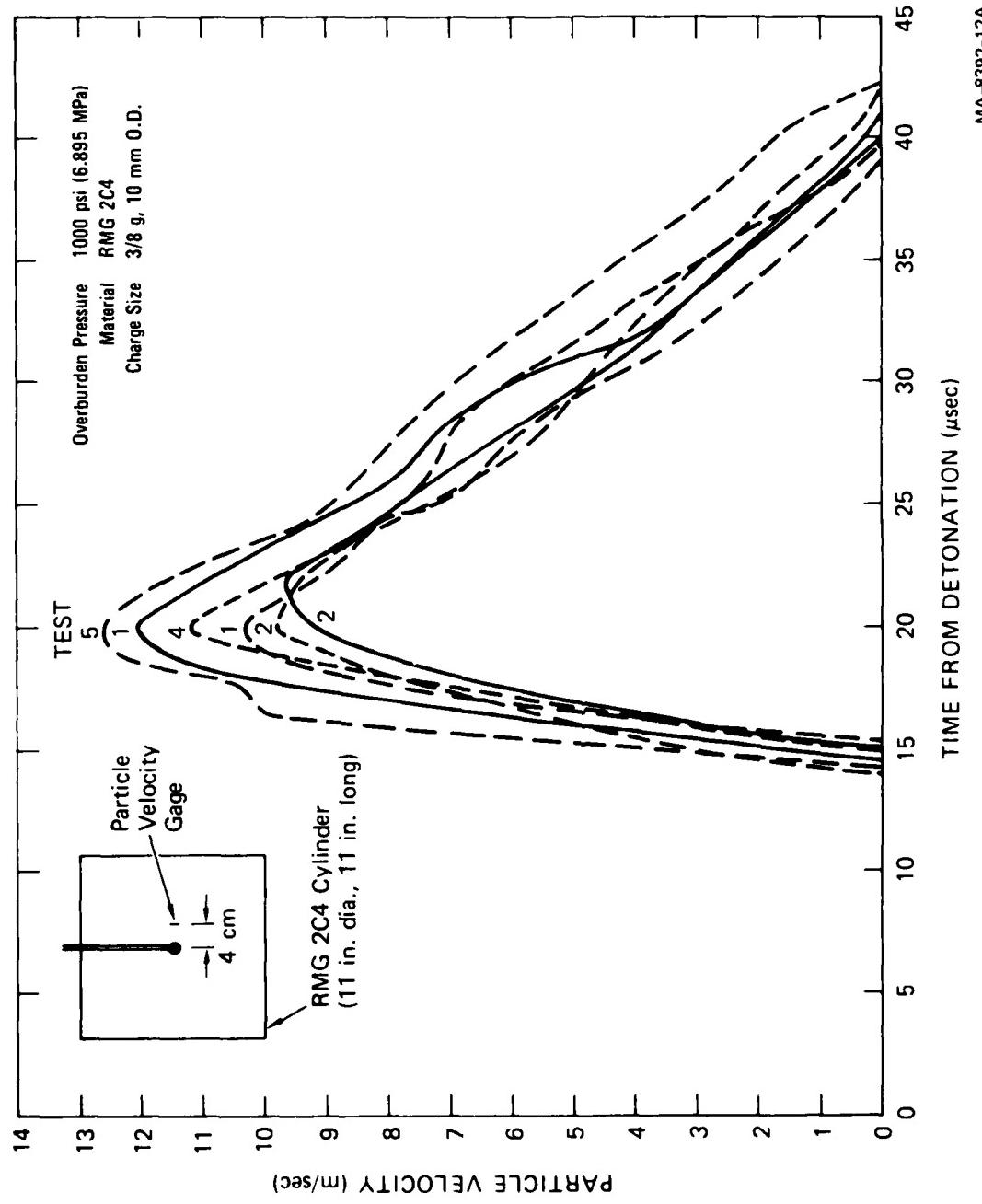
FIGURE 2.11 PARTICLE VELOCITY ASSOCIATED WITH CHARGE DETONATION IN EXPLODED CAVITY TESTS

MA-8392-12A

31

2.4 CHARGE REPRODUCIBILITY

The reproducibility of the explosive source is a basic requirement of exploded cavity tests and has been demonstrated in the past.[6] To continually monitor charge reproducibility, we used quartz gages to measure the reflected pressure pulse generated in the overburden water during exploded cavity tests. Measurements were made at the bottom of the pressure vessel directly below the charge as shown in Figure 2.2. Although the nominal distance from charge center to gage was 6-5/8 inches (17.0 cm), a tolerance of 1/8 inch (0.318 cm) should be allowed.

A summary of the charge reproducibility results is given in Table 2.1, where tests are categorized according to the material cast and the embedded features. Maximum reflected pressure and total reflected impulse are listed for each test.

Typical reflected pressure pulses are shown in Figure 2.12. The corresponding impulse curves are shown in Figure 2.13. The pulses for tests 203 and 204 are associated with charge detonation in rock-matching grout (RMG 2C4) spheres with no embedded features. The average maximum reflected pressure for tests in this category is 834 psi (5.75 MPa). The corresponding average total reflected impulse is 10.1 psi·msec (0.070 MPa·msec). For calculation of total impulse, the pressure pulse was assumed to end when the pressure dropped to the initial value as shown in Figure 2.12. The pulses for tests 215 and 216 are associated with charge detonation in low density rock-matching grout (LD 2C4) spheres with no embedded features. The average maximum reflected pressure for these tests is 250 psi (17.2 MPa), which is 70% lower than the value for the RMG 2C4. The average total reflected impulse for the LD 2C4 is 2.8 psi·msec (0.019 MPa·msec), which is 73% lower than the value for RMG 2C4. Since the materials differ solely in the air void content, crushing of the air voids in LD 2C4 is responsible for the reduction in pressure and impulse.

Table 2.1 shows that the presence of a nearby vertical fault resulted in an average maximum reflected pressure of 1088 psi (7.50 MPa), which is 30% higher than the value found in tests without a fault. Similarly, the

32

Table 2.1

SUMMARY OF CHARGE REPRODUCIBILITY RESULTS

Test No.	OD of Charge holder (mm)	Material	Embedded Feature	Maximum Reflected Pressure (psi)[a]	Total Reflected Impulse (psi·msec)[a]
157	9.5	RMG 2C4	None	887	10.7
162	9.5			818	9.6
163	9.5			965	10.4
203	10.0			767	11.0
204	10.0			733	8.9
215	10.0	LD 2C4	None	285	2.9
216	10.0			216	2.7
210	10.0	RMG 2C4	Vertical fault 1-3/8 inches from center of sphere	996	12.8
221	10.0			1180	14.2
213	10.0	RMG 2C4/ GS3	Material interface 3/4 inch below center of sphere	1115	15.2
209	10.0	RMG 2C4	Nearby tunnel	996	11.6
214	10.0	RMG 2C4	Hollow radial tunnel	1125	10.0

[a]1 psi = 6.895 kPa.

33
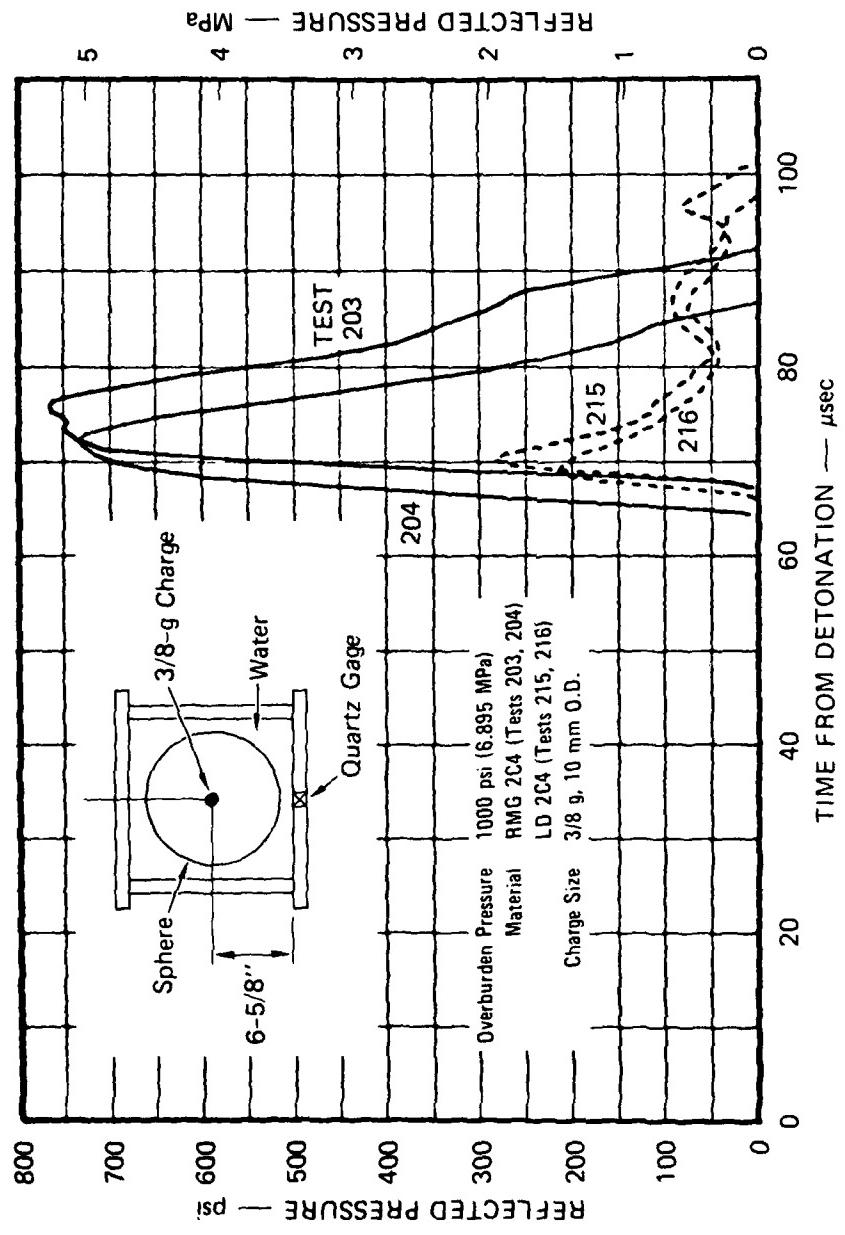
FIGURE 2.12   REFLECTED PRESSURE PULSES GENERATED DURING UNVENTED EXPLODED
CAVITY TESTS 203, 204, 215, AND 216

34
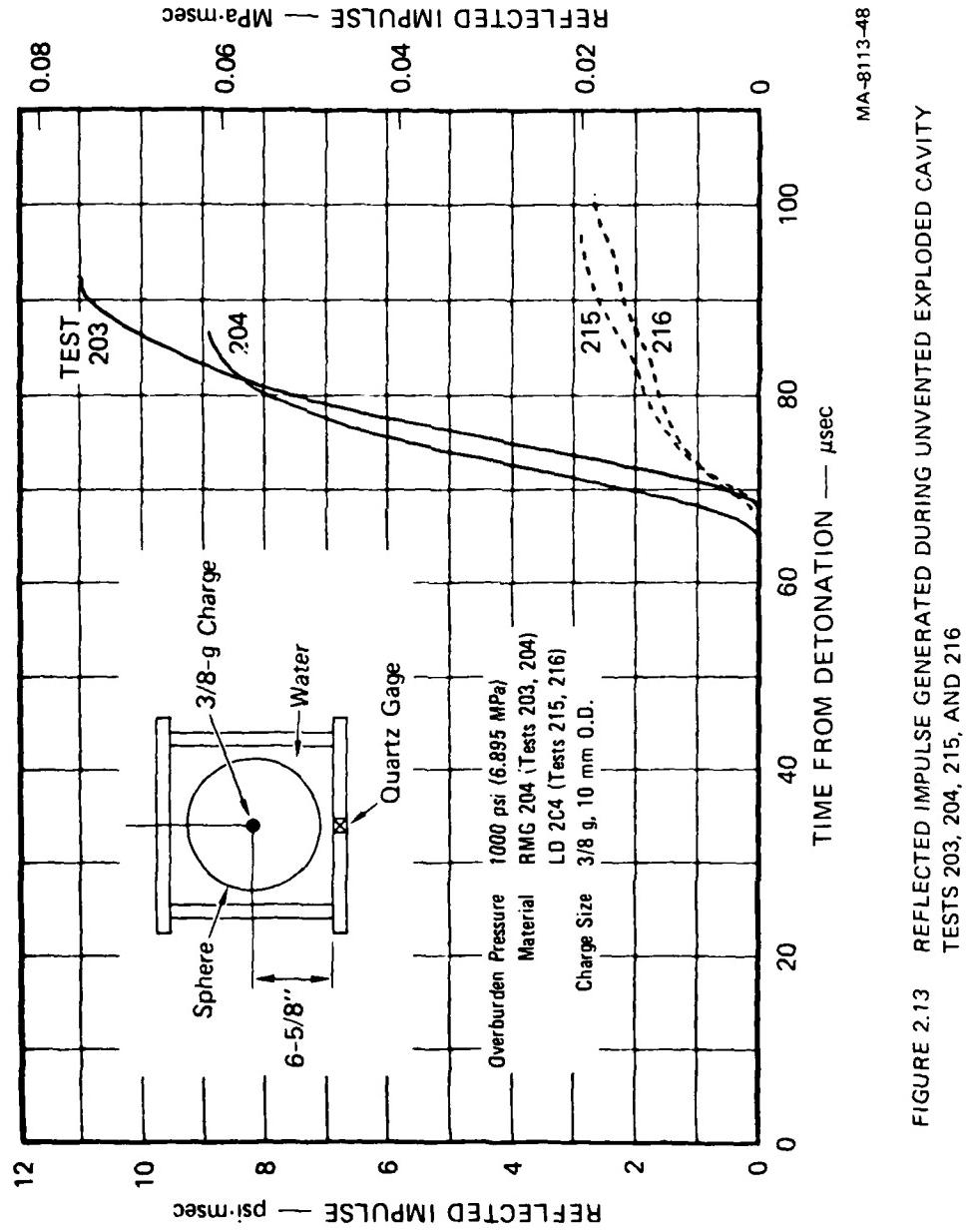
FIGURE 2.13   REFLECTED IMPULSE GENERATED DURING UNVENTED EXPLODED CAVITY
TESTS 203, 204, 215, AND 216

35

average total reflected impulse for the fault plane tests is 13.5 psi•msec (0.093 MPa•msec), an increase of 33%. These increases are attributed to reflection of the pulse from the fault.

In conclusion, Figure 2.12 shows pulse shapes that are strikingly similar for a given material, indicating a reproducible release of energy from the charges.

SECTION 3

HYDROFRACTURE RESULTS

3.1 HYDROFRACTURE TEST SERIES

The experiments were performed to obtain hydrofracture pressures in unexploded and exploded cavities so that by comparison the contribution of the residual stress field to containment may be assessed. They were also performed to provide the influence of various factors on containment such as viscosity, overburden, rock properties, charge coupling, and nearby faults and tunnels. Conclusions based on these results are contained in the summary of Section 1.2.

Results of the hydrofracture experiments are summarized in Table 3.1. Unexploded cavity tests are grouped in series 1 through 6; exploded cavity tests are grouped in series 7 through 17. Reproducibility tests, series 1 and 7, were performed to demonstrate the reliability of the current experimental techniques and to provide comparison data for the following areas of investigation:

- Viscosity (series 2 and 12). Dyed conductive water, with a viscosity of 1 centipoise, was chosen as the standard hydrofracture fluid. To assess the effects on hydrofracture of a more viscous fluid, we chose dyed glycerol, with a viscosity of 660 centipoise, as a substitute for water in several unexploded and exploded cavity tests.

- Overburden (water) (series 3). In unexploded cavity tests, overburden pressure provides a strong parameter for the study of fracture initiation and growth. Simulation of of the in-situ stress state surrounding a typical underground nuclear cavity was achieved by applying a pressure of 1000 psi (6.895 MPa). Pressures of 0, 1000, and 2000 psi (0, 6.895, and 13.79 MPa) were found to be sufficient for a study of overburden.

37

Table 3.1

SUMMARY OF CONTAINMENT INVESTIGATIONS

Series	Purpose or Parameter	Hydrofracture Pressures (Figure)	Overburden Pressure (psi)	Cavity Diameter (in.)	Number of Tests	Observations
Unexploded Cavity Experiments						
1	Reproducibility	3.1	1000	3/4	4	Excellent reproducibility; fracture initiation pressures are within 4.3% of 1870-psi average.
2	Viscosity	3.3	1000	3/4	2	Replacing water with glycerol increases peak fracture pressure to 2680 psi.
3	Overburden (water)	3.4	0 1000 2000	3/4	2 4 2	A line with unit slope fits the fracture initiation versus overburden data for water hydrofracture.
4	Overburden (glycerol)	3.6	0	3/4	1	A line with unit slope fits the fracture initiation versus overburden data for glycerol hydrofracture.
5	Material property	3.7 3.8	1000 0 1000	3/4 3/4	2 2 2	Low density grout reduces fracture initiation pressure to 1580 psi. Granite simulant increases fracture initiation pressure to 2760 psi.
6	Cavity lining	3.9	1000	3/4	2	Partial cavity lining increases hydrofracture pressures and allows for stable crack growth.

Table 3.1 (concluded)

SUMMARY OF CONTAINMENT INVESTIGATIONS

Series	Purpose or Parameter	Hydrofracture Pressures (Figure)	Overburden Pressure (psi)	Cavity Diameter (in.)	Number of Tests	Observations
Exploded Cavity Experiments						
7	Reproducibility	3.10	1000	3/8	4	Good reproducibility; fracture initiation pressures are within 8.5% of 3290-psi average.
8	Vented cavity	3.12	1000	3/8	4	A spectrum of hydrofracture records is generated. Venting reduces average fracture initiation pressure 25%.
9	Charge holder thickness	3.14	1000	3/8	3	Increasing wall thickness of charge holder by 10 mils has no effect on pressure records.
10	Uncoupled charge	3.16	1000	3/8	3	A 3/4-inch-diameter air gap surrounding charge has no effect on hydrofracture pressures.
11	Geometry	3.18	1000	3/8	2	Pressure records for a cylinder have a shape similar to those for spheres; a wider range of pressures is generated.
12	Viscosity	3.20	1000	3/8	3	Replacing water with glycerol increases fracture pressure 18%.
13	Material property	3.21 3.24	1000	3/8	3 2	Air voids reduce fracture initiation pressure to 1770 psi.
14	Material interface	3.25 3.26	1000	3/8	2 2	Boundary conditions along an interface influence hydrofracture pressures.
15	Radial tunnel	3.28	1000	3/8	2	Hollow unlined radial tunnels allow for venting and reduce hydrofracture pressures.
16	Nearby tunnel	3.30	1000	3/8	3	Containment of gases was achieved with embedded tunnel one exploded cavity radius away.
17	Fault plane	3.33 3.35	1000	3/8	3 1	Containment of gases was achieved with fault plane less than three exploded cavity radii away.

- Overburden (glycerol) (series 4). The viscosity and overburden parameters were combined in several unexploded tests. Glycerol hydrofractures were performed on spheres subjected to overburden pressures of 0, 1000, and 2000 psi (0, 6.895, and 13.79 MPa).

- Material property (series 5 and 13). Rock-matching grout (RMG 2C4), which approximates the properties of Nevada Test Site tuff, was chosen as the standard material tested. Effects of material property variations on hydrofracture were studied by testing a slightly weaker low-density grout containing air voids (LD 2C4) and a stronger granite simulant (GS3). Unexploded and exploded cavity spheres were tested. Both water and glycerol hydrofractures were performed.

- Cavity lining (series 6). A flexible cavity lining allows for fracture initiation and propagation without hydro-fracture fluid acting directly on the wall of the cavity or entering the plane of the crack. Changes in the pressures required for fracture initiation and the subsequent stability of crack growth are the major influences of cavity lining on hydrofracture. Testing was limited to unexploded cavities.

- Vented cavity (series 8). Release of the detonation products from an exploded cavity before hydrofracture provides the limiting case of complete unloading for the unvented hydro-fracture tests. Relaxation of the dynamically produced residual stress field surrounding an exploded cavity is enhanced by cavity venting.

- Charge holder thickness (series 9). For increased reliability, the charge holder wall thickness was increased from 16 mils to 26 mils (0.406 mm to 0.660 mm). All charges contained approxi- mately 3/8 gram of explosive pressed to a density of 1 g/cm^3. The thinner-walled charge produced a 0.750-inch (1.905-cm) exploded cavity diameter. Use of the thicker walled charge resulted in a 0.800-inch (2.032-cm) exploded cavity diameter.

- Uncoupled charge (series 10). In standard exploded cavity tests, the explosive source is in direct contact with the surrounding material. In an uncoupled charge test, an annular region of air separates the explosive source from the surrounding material.

- Geometry (series 11). In preparation for future asymmetry tests, several exploded cavity tests were performed on grout cylinders with diameters and lengths equal to the diameter of a sphere (~12 inches).

- Material interface (series 14). An important geological feature at the test site is the presence of layers of different media in the region surrounding a cavity. This feature was simulated in several exploded cavity hydrofracture tests by bonding rock-matching grout to either low density rock-matching grout or granite simulant along a plane interface. The charge was always detonated in the rock-matching grout.

- Radial tunnel (series 15). Spheres containing hollow and filled radial tunnels were tested to provide results for possible tunnel configurations.

- Nearby tunnel (series 16). Spheres containing hollow tunnels embedded at two different distances from the explosive charge were tested. The tunnels allowed for possible venting of detonation products and loss of hydrofracture fluid.

- Fault plane (series 17). Natural fault planes in the vicinity of a nuclear device cavity were simulated by embedding sheets of Mylar in exploded cavity grout spheres. Nearby faults as well as a fault through the explosive source were simulated.

3.2 UNEXPLODED CAVITY TESTS

Series 1 - Reproducibility

Hydrofracture tests were performed on unexploded cavity rock-matching grout (RMG 2C4) spheres to demonstrate the reliability of the current experimental techniques and to provide comparison data for parameter studies. The smooth unlined cavity configuration shown in Figure 2.9 was used in these tests. A cavity diameter of 3/4 inch (1.90 cm) was chosen because it corresponds to the exploded cavity diameter generated by the thinner-walled 3/8-gram charge. The external pressure applied to each sphere was fixed at 1000 psi (6.895 MPa) to simulate the hydrostatic pressure in nuclear tests typically conducted at a depth of 1100 feet (335 m) in tuff with a density of 2.1 g/cm^3. Dyed conductive water was pumped into each cavity at a rate of 4.26 cm^3/min. The above parameters were arbitrarily chosen as standard. The sensitivity of hydrofracture pressures to variations in these parameters was investigated in the following series of tests.

Hydrofracture records for tests 93, 94, 160, and 161 are shown in Figure 3.1. Tests 93 and 94 are previously reported tests in which the access tube was not modified by the addition of the copper cone shown in

41
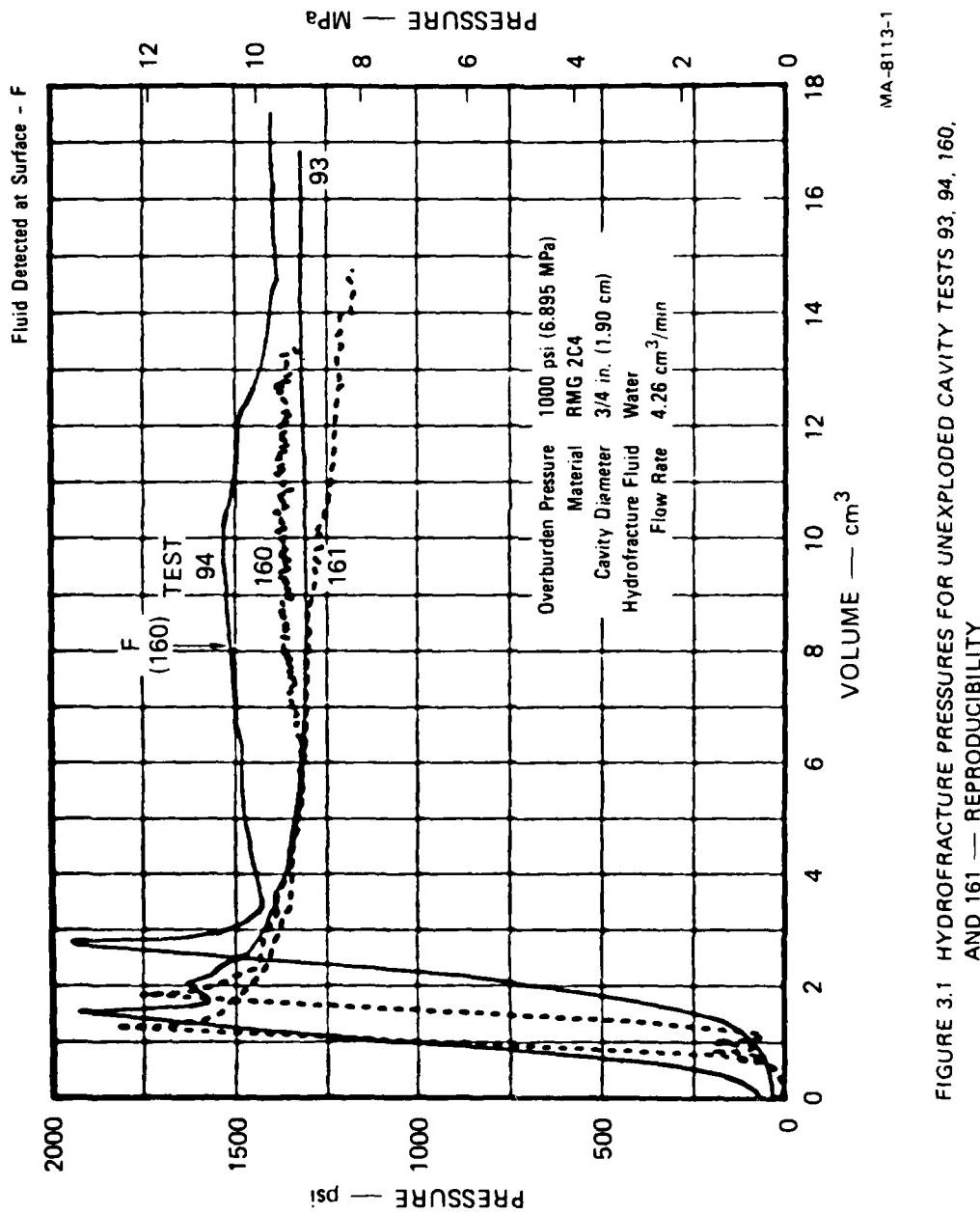
FIGURE 3.1 HYDROFRACTURE PRESSURES FOR UNEXPLODED CAVITY TESTS 93, 94, 160, AND 161 — REPRODUCIBILITY

42

Figure 2.9. The similarity of the four pressure records suggests that this modification has a negligible effect on hydrofracture pressures. The results shown in Figure 3.1 are representative of unexploded cavity tests in that a smooth increase in pressure is followed by a sharp drop to form a well-defined peak. Previous fracture initiation studies[5] have shown that the pronounced spike represents the initiation of a crack in the wall of the cavity. Calibration tests, in which the cavity was replaced by a rigid vessel of equivalent volume, resulted in pressure records with an initial slope comparable to those in a hydrofracture test. Hence the fluid volume apparently required to initiate fracture can be attributed to a combination of fluid compressibility and system compliance. Loss of fluid due to porous flow is negligible.

Fracture initiation pressures, which provide the primary measure of reproducibility, were 1950, 1940, 1820, and 1770 psi (13.44, 13.38, 12.55, and 12.20 MPa). Reproducibility is seen to be excellent, with a maximum deviation of only 4.3% from the 1870-psi (12.89-MPa) average.

Following fracture initiation, a crack continues to grow as cavity pressure decays slowly to a plateau that is 200 to 400 psi (1.38 to 2.76 MPa) above the overburden pressure. As shown in Figure 3.1, hydrofracture fluid advancing behind the crack tip was detected at the surface of the sphere in test 160 after 6.8 cm^3 of flow. This volume, measured from the point of fracture initiation, provides an upper bound estimate of the flow required to generate a surface fracture. The subsequent steady-state cavity pressure provides a measure of the flow resistance along the fracture plane.

Figure 3.2 shows a typical fracture surface associated with an unexploded cavity test. The uniformity of the dyed region suggests that the fracture initially propagated symmetrically from the cavity. Sectioning of the unexploded cavity spheres showed that a single planar fracture surface was produced by hydrofracture in each test. Figure 3.2 also shows a section taken through the access tube in test 160. The presence of the copper cone prevented flow along the tube and resulted in a horizontal fracture plane. In general, the cone allows for a random orientation of the fracture plane in unexploded cavity tests.
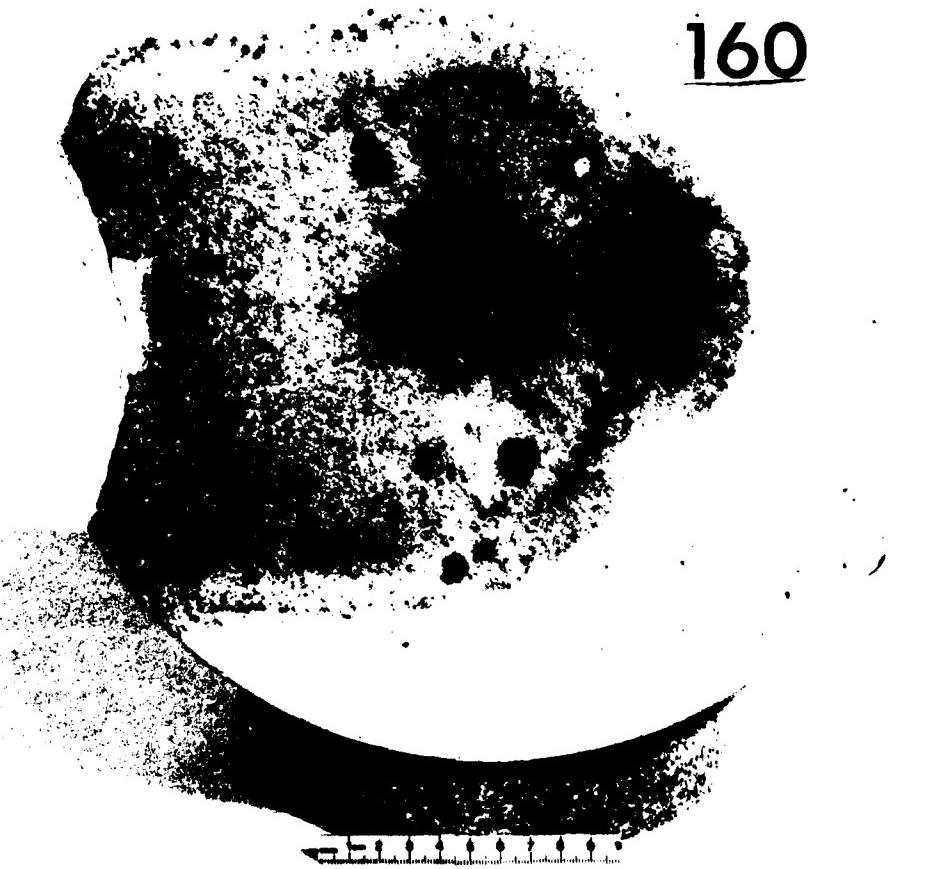
160

MP 8113

FIGURE 3.2 HYDROFRACTURE FROM UNEXPLODED CAVITY
TEST 160   REPRODUCIBILITY

MP 8113 3

FIGURE 3.2 HYDROFRACTURE FROM UNEXPLODED CAVITY
TEST 160 REPRODUCIBILITY (Concluded)

The initially erratic rise in cavity pressure in test 161 is attributed to the presence of an air void adjacent to the cavity. Although hydrofracture pressures were not significantly affected by the imperfection, the fracture plane did intersect this region. Previous tests with notched cavities[5] also showed that imperfections control fracture orientation.

Series 2 - Viscosity

The effects of a change in fluid viscosity on the pressure records are shown in Figure 3.3. Tests 160 and 161 are typical water hydrofracture results selected from the reproducibility series. Viscosity of the dyed water was 1 centipoise. The spheres in tests 154 and 155 are representative of those hydrofractured with dyed glycerol, which has a viscosity of 660 centipoise. Use of the more viscous fluid increased the average fracture initiation pressure from 1870 psi to 2680 psi (12.89 MPa to 18.48 MPa). For a perfectly smooth cavity and a completely impermeable sphere, changes in fluid viscosity would have no effect on fracture initiation. However, as fracture commences and fluid flows into the crack, the higher viscosity of the glycerol causes a spatial pressure decay from the cavity to the crack tip. Thus higher cavity pressures are required to continue the crack propagation. A theoretical treatment of this process is detailed in Appendix A.

Figure 3.3 shows that the volume of fluid required to establish a steady-state flow along a fracture plane increases with fluid viscosity. However, the lower steady-state pressures for the glycerol tests suggest less resistance to flow. Since flow resistance along the planar crack is controlled by crack width, use of a more viscous hydrofracture fluid apparently produces larger separation of the fractured surfaces.

Series 3 - Overburden (Water)

The effects of a change in overburden pressure on water hydrofracture are shown in Figure 3.4. Tests 165 and 166, performed without external pressure, resulted in an average fracture initiation pressure of 860 psi (5.929 MPa). Tests 160 and 161, which are typical results of 1000-psi (6.895 MPa) overburden, were selected from the reproducibility series.
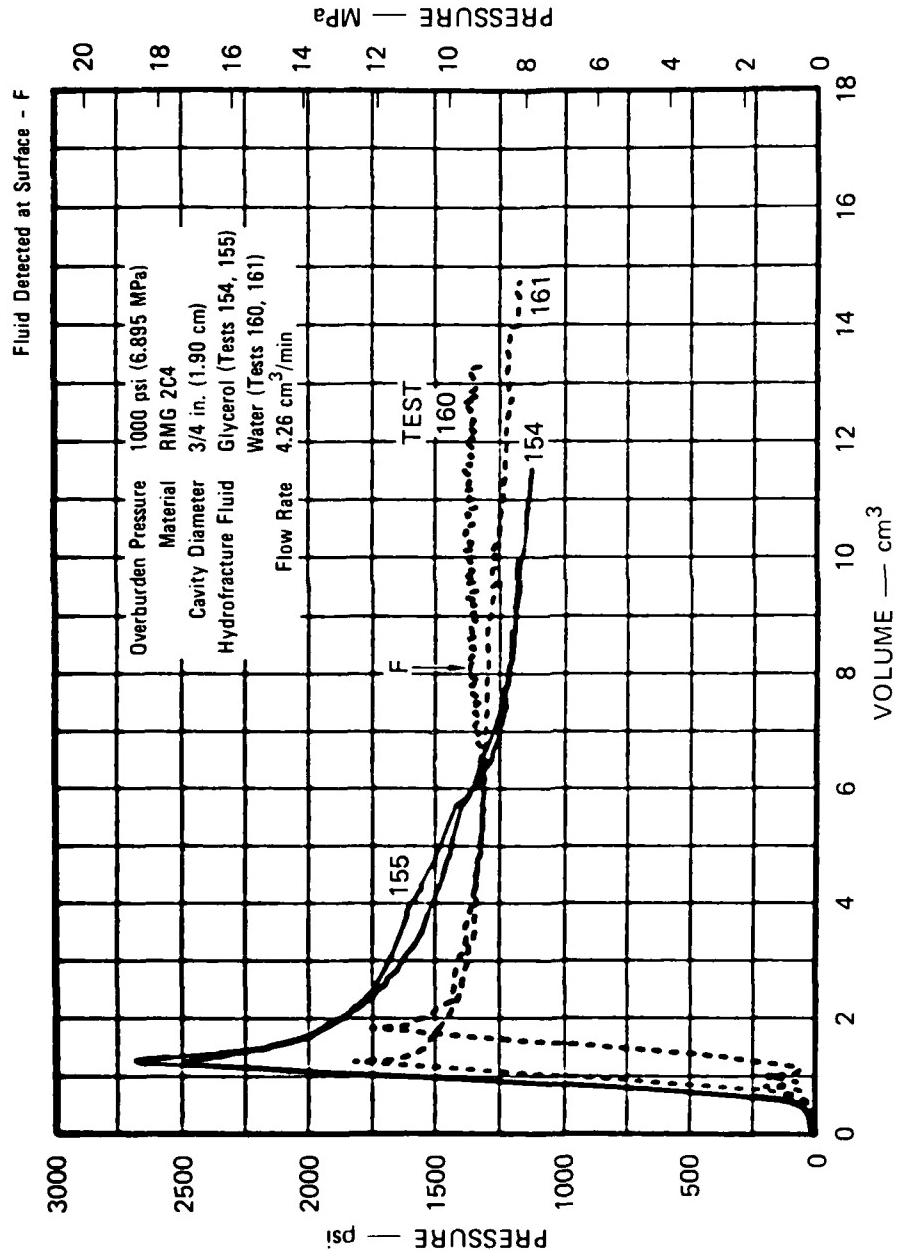
FIGURE 3.3 HYDROFRACTURE PRESSURES FOR UNEXPLODED CAVITY TESTS 154, 155, 160, AND 161 — VISCOSITY

47
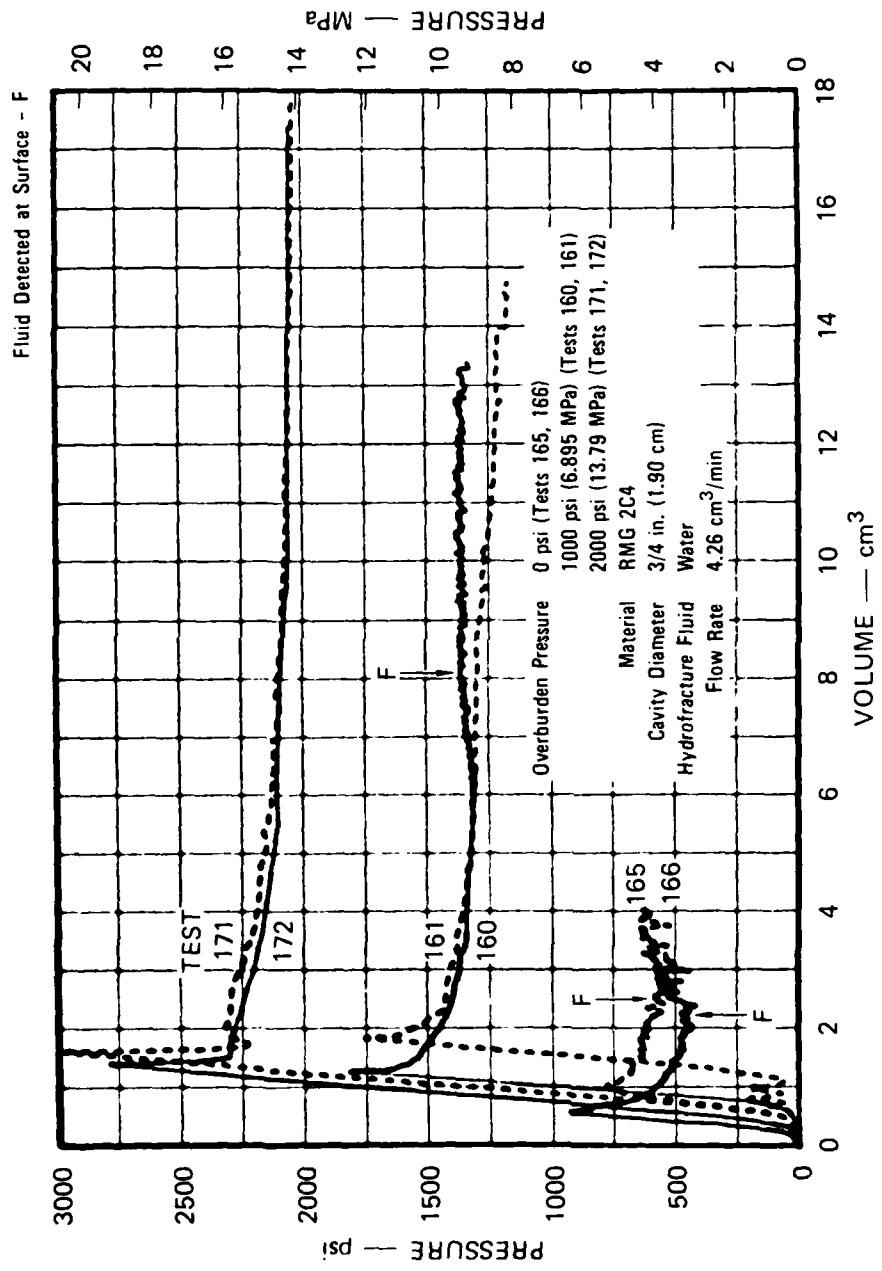
FIGURE 3.4 HYDROFRACTURE PRESSURES FOR UNEXPLODED CAVITY TESTS 160, 161, 165, 166, 171, AND 172 — OVERBURDEN (WATER)

48

Average fracture initiation pressure for all these tests was 1870 psi (12.89 MPa). Tests 171 and 172, performed at 2000-psi (13.79-MPa) overburden, resulted in an average fracture initiation pressure of 2870 psi (19.79 MPa). Results are summarized in Figure 3.5. For water hydro-fracture of RMG 2C4 spheres, the slope of the curve showing fracture initiation pressure versus overburden is one. The result is consistent with the fracture mechanics analysis presented in Appendix A, where fracture initiation pressure is related to overburden by means of fracture toughness.

Figure 3.4 shows that an increase in overburden reduces the overall rate of crack growth. With no external pressure applied, fluid was detected at the surface of a sphere after 1.6 cm^3 of flow. With 1000-psi (6.895-MPa) external pressure, 6.8 cm^3 of flow was required before fluid was detected at the surface. Hence overburden serves to increase fracture initiation pressure and slow crack growth.

Series 4 – Overburden (Glycerol)

A series of overburden tests was performed with glycerol as the hydrofracture fluid to provide additional data for the study of fracture initiation and growth. The pressure records are shown in Figure 3.6. Test 195, conducted with no overburden, resulted in a fracture initiation pressure of 1760 psi (12.13 MPa). Average fracture initiation pressure for tests 154 and 155, conducted at 1000-psi (6.895-MPa) overburden, was 2580 psi (17.79 MPa). Finally, test 178, conducted with 2000-psi (13.79-MPa) overburden, resulted in cavity fracture at 3610 psi (24.89 MPa). A summary of these results is shown in Figure 3.5. For glycerol hydrofracture of RMG 2C4 spheres, the slope of the curve showing fracture initiation pressure versus overburden is one. The result, which was also obtained for water hydrofracture, is consistent with the fracture mechanics analysis presented in Appendix A.

The effect of hydrofracture fluid viscosity on crack growth and fluid motion is shown by a comparison of the zero overburden tests for water and glycerol. In these tests visual detection of surface cracking and fluid arrival was convenient. For glycerol hydrofracture, Figure 3.6 shows that 2.1 cm^3 of flow was required to produce surface cracking,
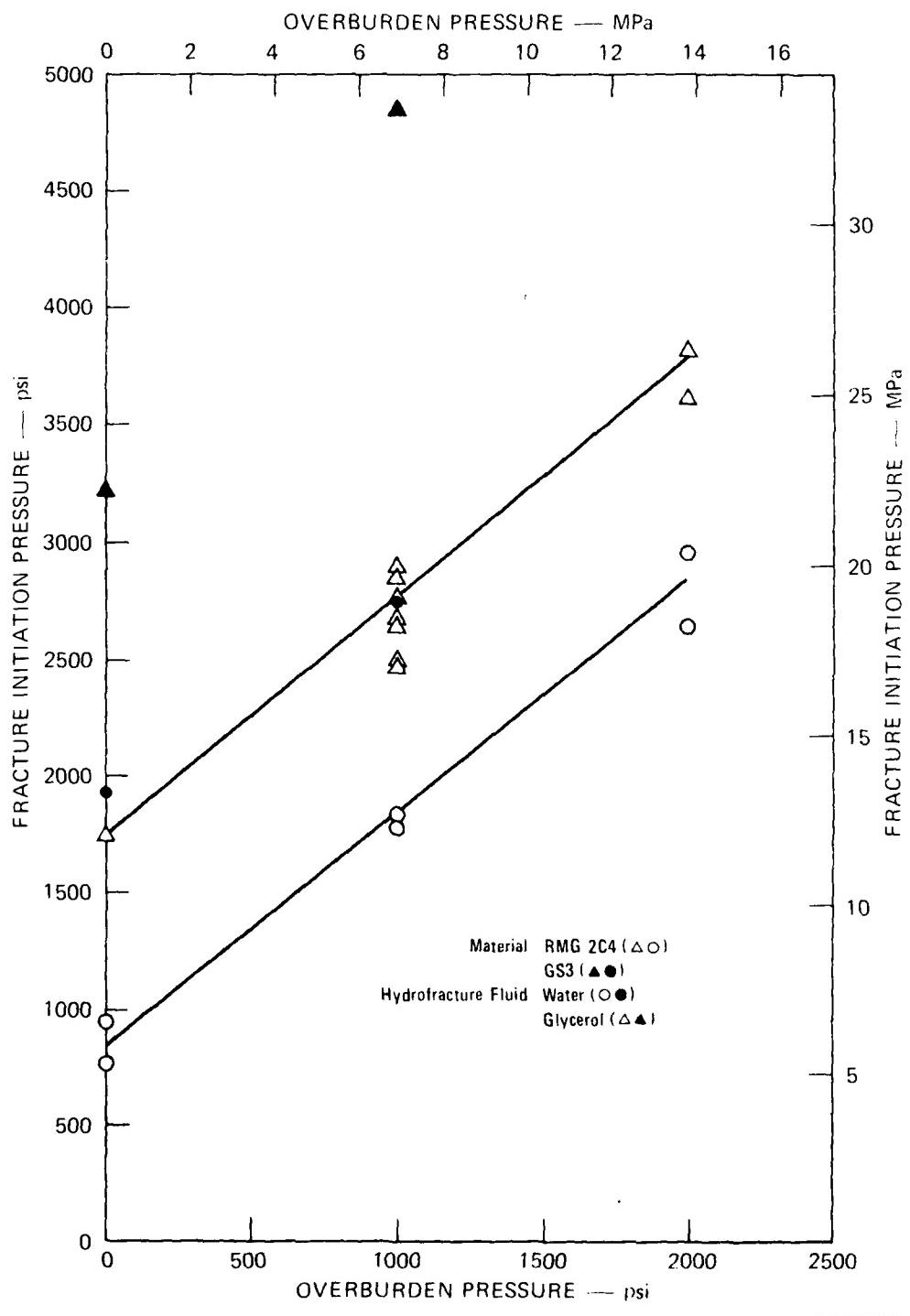
FIGURE 3.5   FRACTURE INITIATION PRESSURE VERSUS OVERBURDEN FOR UNEXPLODED
CAVITY TESTS

FIGURE 3.6 HYDROFRACTURE PRESSURES FOR UNEXPLODED CAVITY TESTS 154, 155, 178, AND 195 — OVERBURDEN (GLYCEROL)
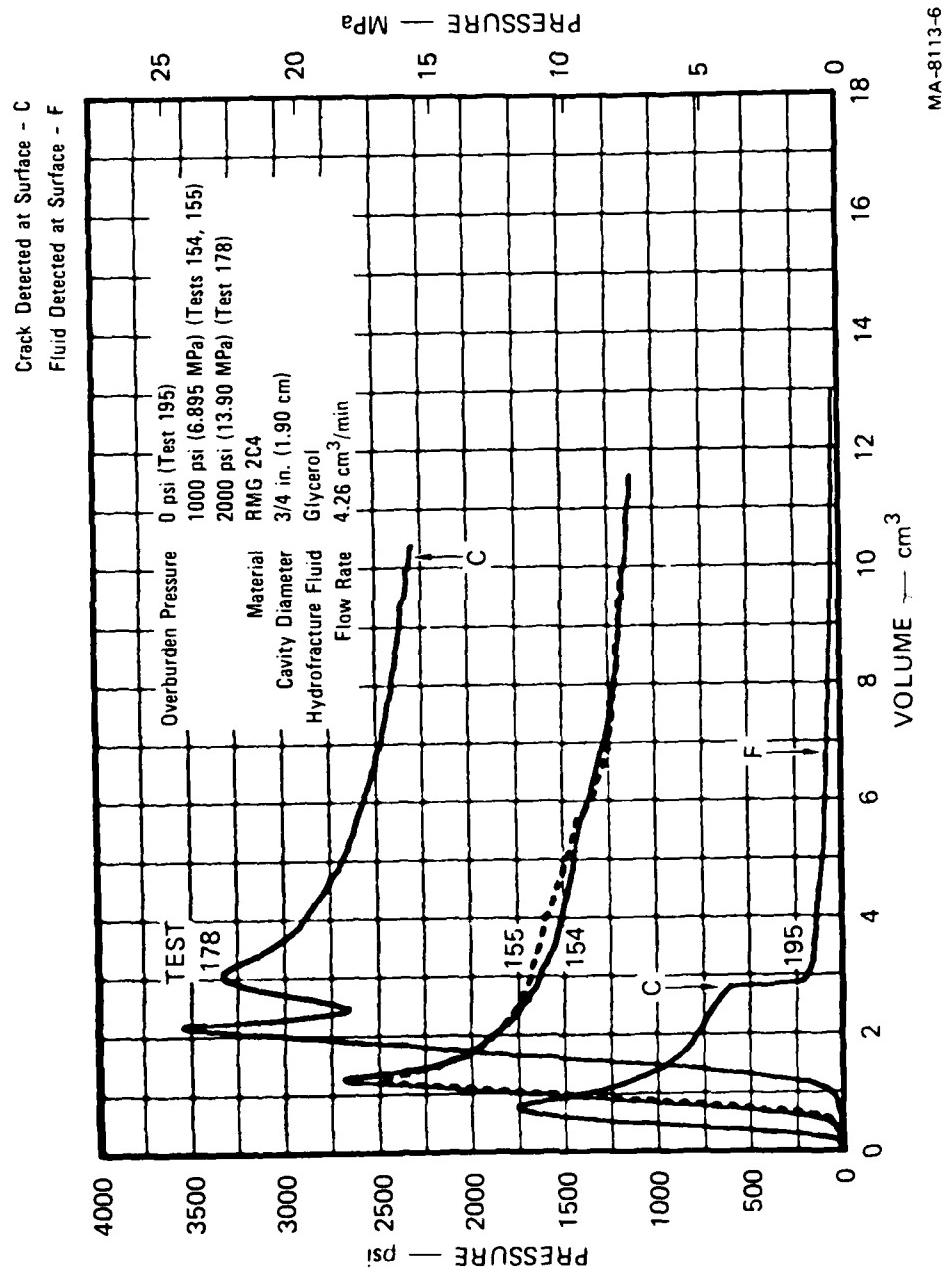
and 6.1 cm^3 of flow was required to drive fluid to the surface. Volume measurements are made relative to the point of fracture initiation. For water hydrofracture, Figure 3.4 shows that an average flow of 1.5 cm^3 was required to drive fluid to the surface. Cracking of the surface was not detected before fluid arrival because of the initially small crack width. The conclusion drawn from the data is that lower viscosity fluid flows nearer the crack tip and generates increased rates of crack growth and fluid motion.

Series 5 - Material Property

Effects of material properties on containment were studied by comparing hydrofracture records for rock-matching grout (RMG 2C4), low density rock-matching grout (LD 2C4), and granite simulant (GS3) spheres. Properties of these materials are given in Appendix C.

Hydrofracture pressures for LD 2C4 tests 193 and 194 are shown in Figure 3.7. The records have overall features typical of unexploded cavity tests, but differ in detail. For example, the rise in pressure immediately following cavity fracture indicates a temporarily stable crack growth. The feature is atypical of unexploded cavity tests but has been observed in tests on RMG 2C4 and GS3. The average fracture initiation pressure is 1580 psi (10.89 MPa). Hydrofracture records for tests 160 and 161 were selected from the reproducibility series and are also shown in Figure 3.7 for comparison. The average fracture initiation pressure for RMG 2C4 tests is 1870 psi (12.89 MPa). Hence the average fracture initiation pressure for LD 2C4 is 15% less than the value for RMG 2C4. A decrease is expected since the tensile strength of LD 2C4 [460 psi (3.172 MPa)] is 13% less than the tensile strength of RMG 2C4 [530 psi (3.654 MPa)], which implies a lower fracture toughness.

Pressure records for tests on GS3 spheres are shown in Figure 3.8. These results show the effects of overburden and fluid viscosity on hydrofracture. Tests 224 and 222 are water hydrofractures conducted at 0-psi and 1000-psi (6.895-MPa) overburden, respectively. The corresponding fracture initiation pressures are 1940 psi (13.36 MPa) and 2760 psi (19.03 MPa). Tests 196 and 218 are glycerol hydrofractures
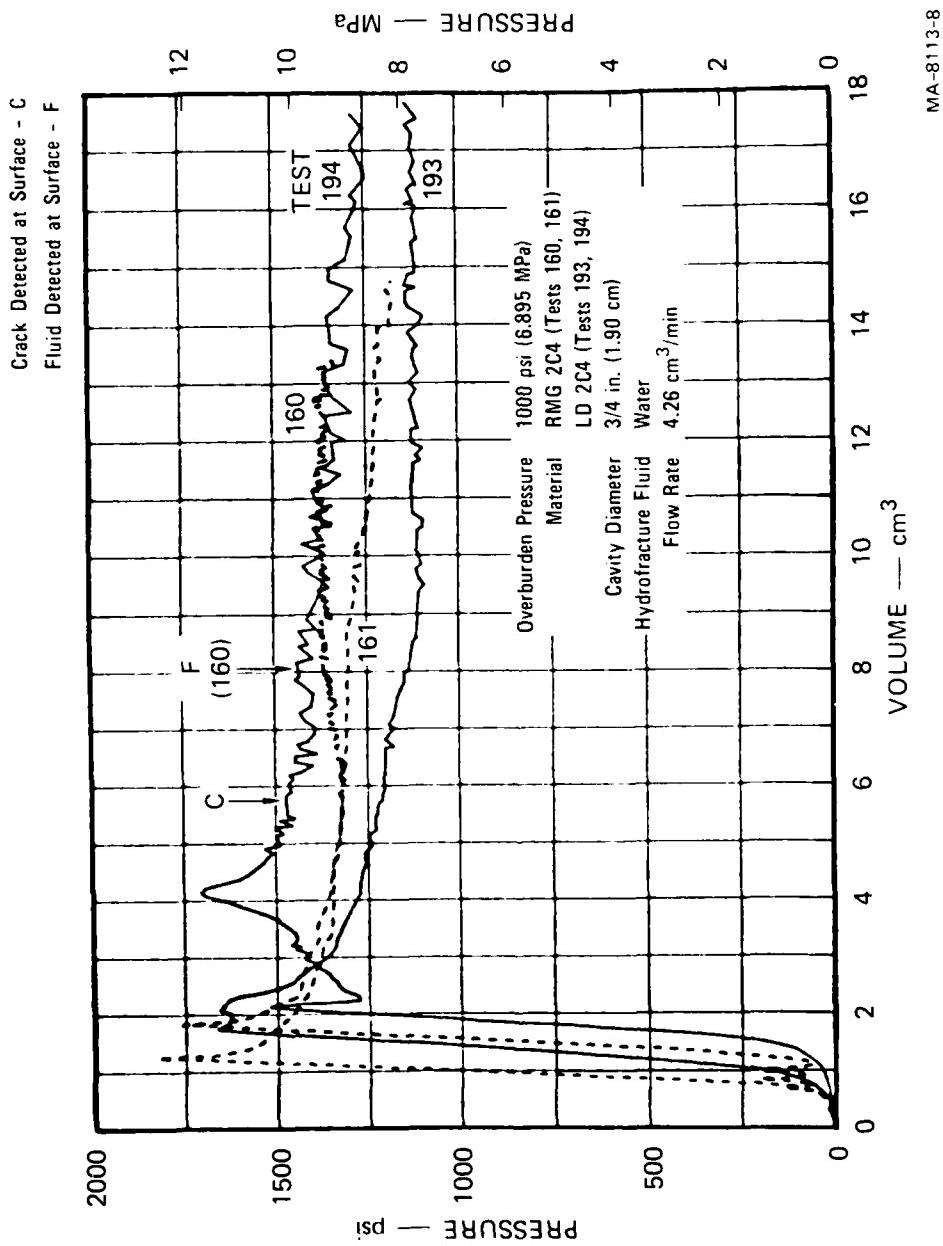
FIGURE 3.7 HYDROFRACTURE PRESSURES FOR UNEXPLODED CAVITY TESTS 160, 161, 193,
AND 194 — MATERIAL PROPERTY (LD 2C4)
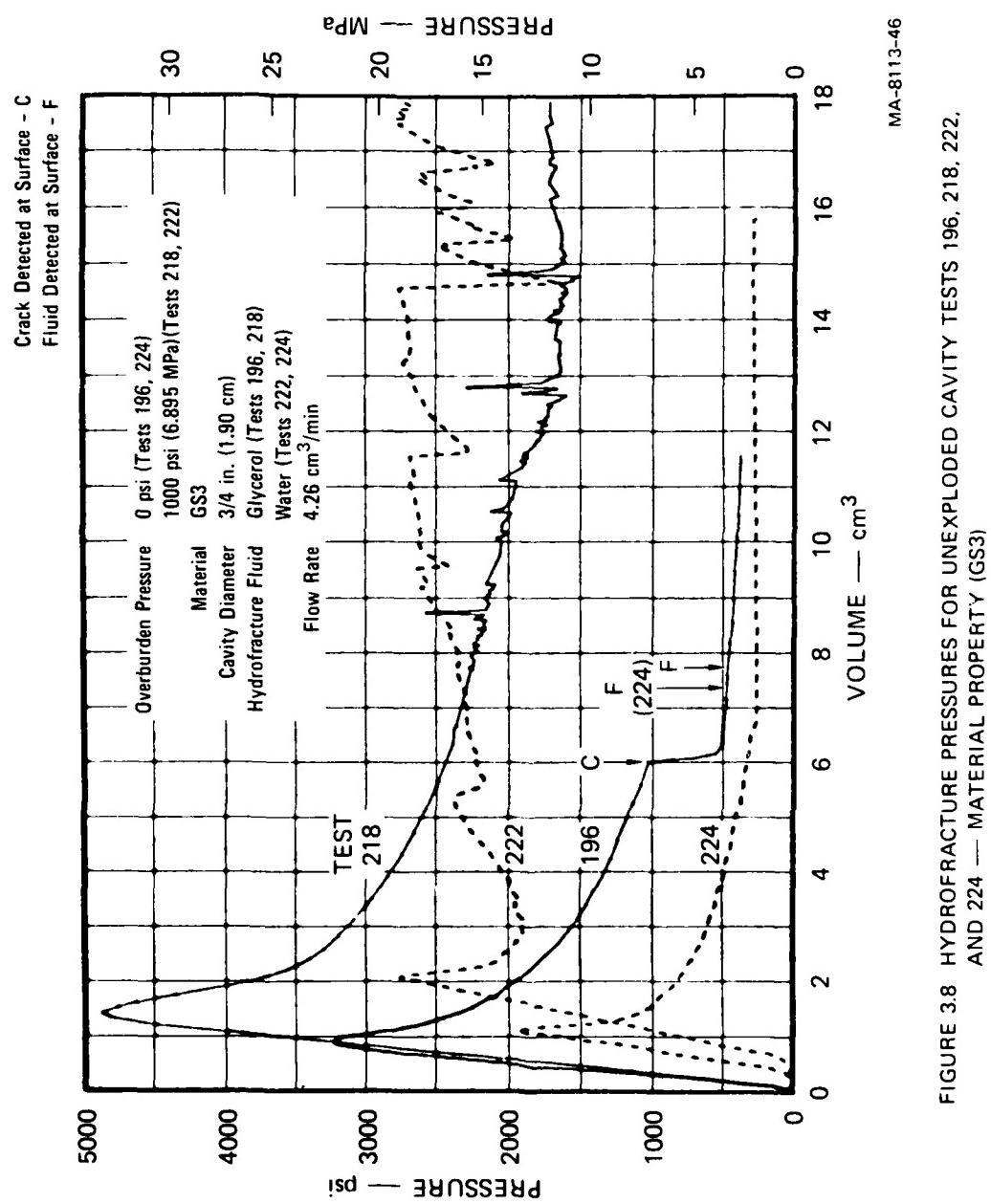
FIGURE 3.8 HYDROFRACTURE PRESSURES FOR UNEXPLODED CAVITY TESTS 196, 218, 222, AND 224 — MATERIAL PROPERTY (GS3)

54

conducted at 0-psi and 1000-psi (6.895-MPa) overburden, respectively.
The corresponding fracture initiation pressures are 3230 psi (22.27 MPa)
and 4840 psi (33.37 MPa). These values are shown in Figure 3.5. For
water hydrofracture, the slope of the curve showing fracture initiation
versus overburden is one. This result, which agrees with the results of
water and glycerol hydrofracture tests on RMG 2C4, supports the conclusion
of Appendix A regarding the dependence of fracture initiation pressure on
overburden. For glycerol hydrofracture of the two GS3 spheres, the slope
of the curve showing fracture initiation pressure versus overburden is
greater than one. However, if a typical scatter of unexploded cavity
results is considered, the data points can be fitted to a line with unit
slope. Since the tensile strength of GS3 [920 psi (6.343 MPa)] is 74%
greater than the tensile strength of RMG 2C4 [530 psi (3.654 MPa)], implying
greater fracture toughness, the increased fracture initiation pressures
associated with GS3 are expected.

Series 6 - Cavity Lining

Unexploded cavities were lined with an impermeable membrane using
the technique described in Section 2.2. The lining is intended to
prevent hydrofracture fluid from acting directly on the cavity wall
and from entering the fracture plane following cavity fracture. A
comparison of pressure records for lined and unlined cavities then
allows assessment of the effects of hydrofracture fluid on fracture
initiation pressure and stability of subsequent crack growth. Crack
growth is stable if increasing cavity pressure is required to propagate
the crack.

Water hydrofracture records for lined cavity tests 179 and 180 are
shown in Figure 3.9. In each test a small leak path developed around
the access tube before fracture initiation that allowed fluid to escape.
Loss of fluid from the cavity lining is indicated by the small pressure
spikes on the hydrofracture record below 2000 psi (13.79 MPa). With the
restricted flow, an average fracture initiation pressure of 2520 psi
(17.37 MPa) was developed. Fracture initiation is indicated by the
pronounced pressure spikes. In each test stable crack growth followed
fracture initiation. In test 180, a cavity pressure of 5090 psi (35.09 MPa)
was applied without generating a surface crack. Pumping was then stopped.
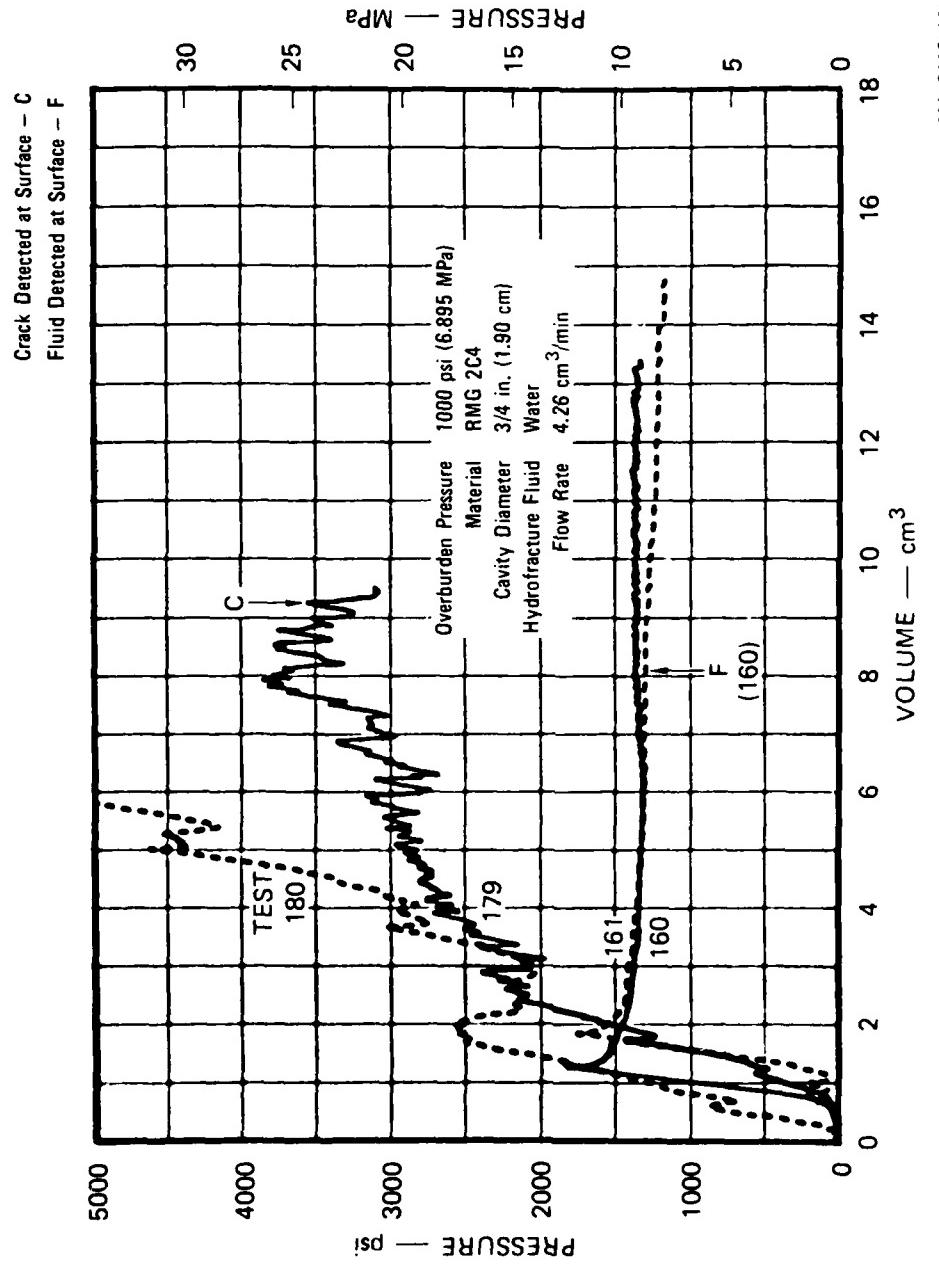
FIGURE 3.9 HYDROFRACTURE PRESSURES FOR UNEXPLODED CAVITY TESTS 160, 161, 179, AND 180 — CAVITY LINING

MA-8113-10

56

Subsequent inspection of the sphere revealed that hydrofracture fluid flowed 5 inches (12.7 cm) from the center of the sphere. In test 179, cavity pressure reached 3910 psi (26.96 MPa) before crack growth became unstable. Surface cracking was detected after 6.5 cm^3 of flow. Hydrofracture records for equivalent unlined cavity tests 160 and 161 are shown in Figure 3.9 for comparison. These tests were selected from the reproducibility series where the average fracture initiation pressure was 1870 psi (12.89 MPa). Hence the partial cavity lining increased the average fracture initiation pressure by 35%.

3.3 EXPLODED CAVITY TESTS

Series 7 - Reproducibility

Unvented exploded cavity hydrofracture tests were performed to assess the reproducibility of the experimental techniques and to provide reference data for the parameter studies. The configuration and procedure for conducting these tests were described in Section 2.2. With this configuration the cavity gas pressure resulting from charge detonation was measured. Also, pumping was started at the time of charge detonation so that stress relaxation due to loss of cavity pressure and creep could be minimized. The compliance of the system was reduced by prepressurizing the hydrofracture fluid to a nominal value of 300 psi (2.068 MPa).

Hydrofracture records for tests 158, 159, 169, and 170 are shown in Figure 3.10. Not shown are the initially high cavity gas pressures that prohibited the immediate lowering of the steel ball at the end of the access tube (Figure 2.7). As the gas cooled, the pressure decayed and allowed the access tube to be opened. The cavity gases then reached a state of equilibrium with the hydrofracture fluid. This process, which required approximately four seconds to complete, precedes the hydrofracture records shown in Figure 3.10. A theoretical estimate of the gas pressure in a dynamically expanding cavity is shown in Figure 3.11. The curve was derived from the pressure-volume data listed in Table 3.2. The explosive source used in the calculations was assumed to be a mixture of the PETN and Lucite composing the charge shown in Figure 2.5. The assumption is based on the experimental observation that the Lucite
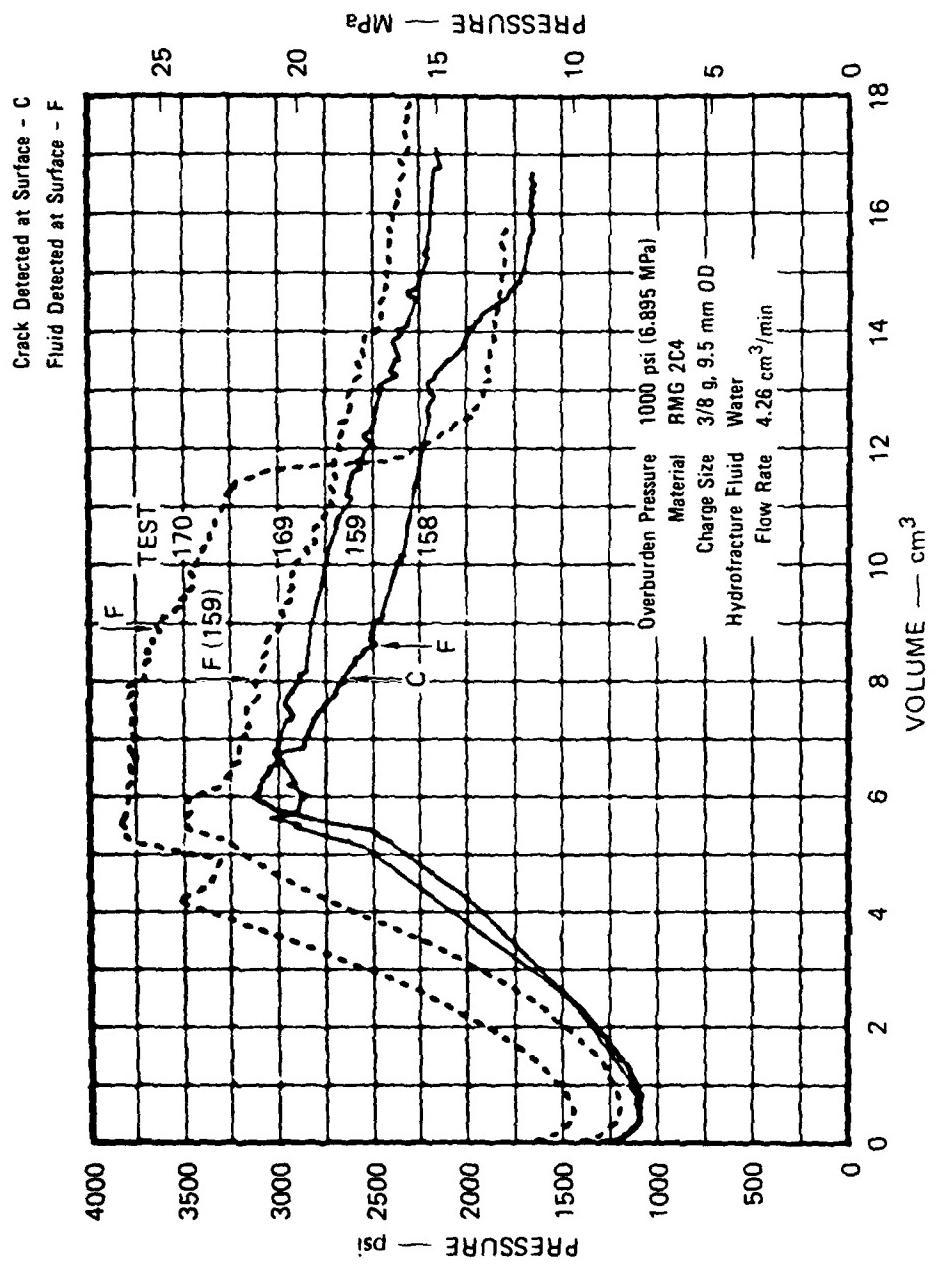
FIGURE 3.10   HYDROFRACTURE PRESSURES FOR UNVENTED EXPLODED CAVITY TESTS
158, 159, 169, AND 170 — REPRODUCIBILITY

58
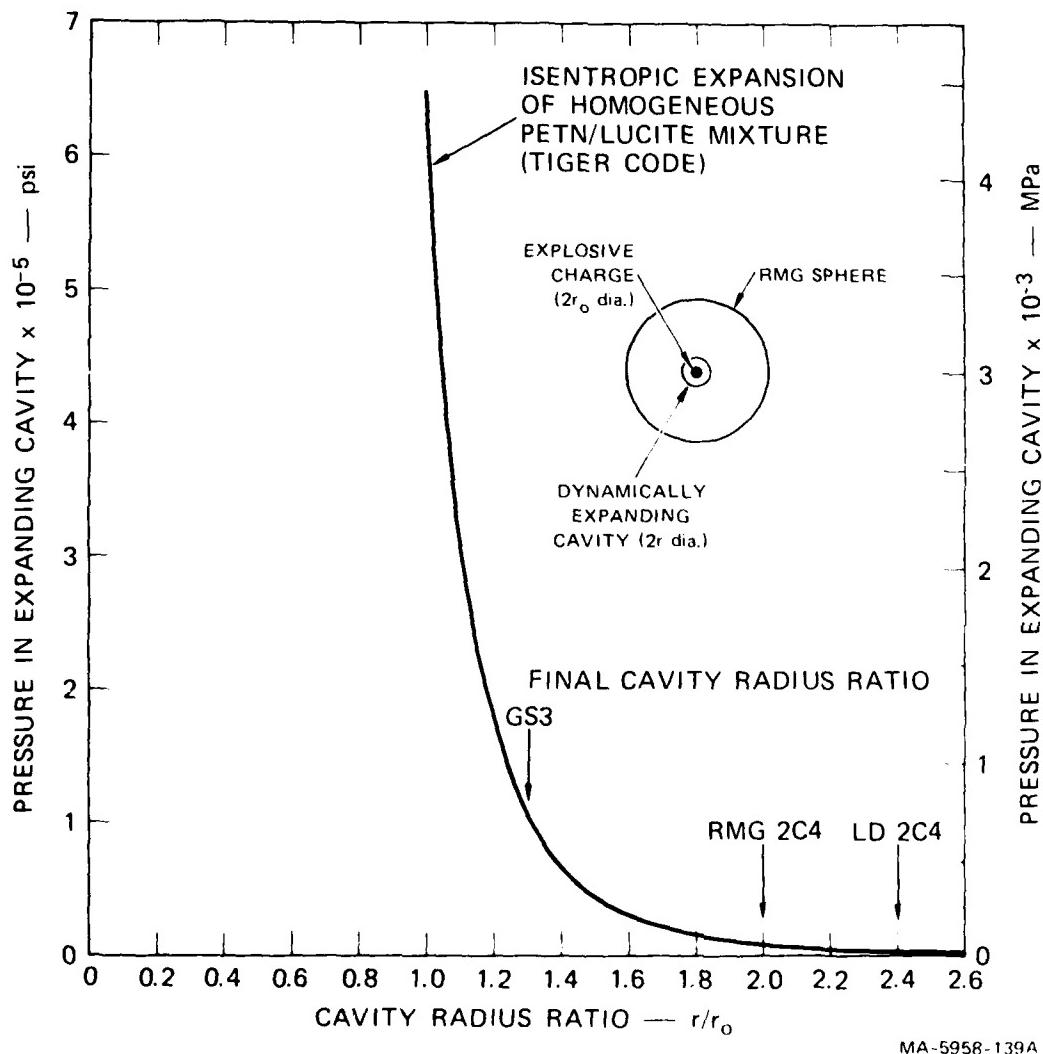
FIGURE 3.11   CALCULATED CAVITY GAS PRESSURE FOR A DYNAMICALLY
EXPANDING CAVITY

Table 3.2

PRESSURE AND VOLUME FOR EXPLOSIVE PRODUCTS
OF PETN/LUCITE MIXTURE[a]

Pressure		Specific Volume	Radius Ratio
psi x 10^{-3}	MPa x 10^{-2}	$(cm^3/gram)$	(r/r_o)
643.0	44.38	0.9589	1.00
356.2	24.57	1.2246	1.08
203.8	13.99	1.5639	1.18
119.0	8.20	1.9972	1.28
97.4	6.72	2.2488	1.33[b]
71.5	4.93	2.5507	1.39
44.2	3.05	3.2574	1.50
28.0	1.93	4.1601	1.63
18.2	1.25	5.3128	1.77
12.0	0.83	6.7849	1.92
10.1	0.70	7.6712	2.00[c]
8.2	0.56	8.6650	2.08
5.6	0.39	11.0660	2.23
4.3	0.30	13.4355	2.40d
3.9	0.27	14.1324	2.45
2.0	0.19	18.0484	2.66

[a]Pressure-Volume data from SRI TIGER code (PETN density 1 gram/cm^3, BKW equation of state).

[b]Final cavity radius ratio for GS3 (interpolated).

[c]Final cavity radius ratio for RMG 2C4.

[d]Final cavity radius ratio for LD 2C4 (interpolated).

charge holder is completely consumed in the explosion. Since the exploded cavity diameter is twice the initial cavity diameter, the theoretical estimate of cavity pressure immediately following detonation is found to be 10,100 psi (75.84 MPa). This is the pressure that initially holds the steel ball against the end of the access tube.

Figure 3.10 shows that hydrofracture pressures for unvented exploded cavity tests are related to the unloading of cavity pressure. In test 158, pressure decayed to 1110 psi (7.653 MPa), and the subsequent pressure required to initiate cavity fracture was 3140 psi (21.65 MPa). In test 170, a minimum cavity pressure of 1460 psi (10.07 MPa) resulted in a fracture initiation pressure of 3530 psi (24.34 MPa). Despite these differences, reproducibility is good. The maximum deviation from the 3290-psi (22.68-MPa) average fracture initiation pressure is 8.5%. This average is 76% higher than the corresponding 1870-psi (12.89-MPa) average for equivalent unexploded cavity tests.

The existence of a compressive residual stress field surrounding an exploded cavity is indicated by the high hydrofracture pressures and the general stability of early crack growth shown in Figure 3.10. In addition, Figure 3.12 shows an undyed region in the neighborhood of the cavity in test 170. Hydrofracture fluid appears to have flowed from the cavity along isolated paths and spread around an annular region of compressive residual stress.

Series 8 - Vented Cavity

Vented exploded cavity tests were performed to assess the effect on containment of complete unloading of cavity gas pressure. The configuration and procedure for conducting these tests were described in Section 2.2. In each test, water hydrofracture was started 20 to 40 minutes following charge detonation. The analysis presented in Appendix B indicates that relaxation of the explosively generated stress field during this time interval caused by pore water migration may be negligible. However, creep may give rise to different residual stress fields by the time pumping begins.

170

FIGURE 3-12 HYDROFRACTURE FROM UNVENTED EXPLODED CAVITY
TEST 170 — REPRODUCIBILITY

MP 8113-12

67

170

FIGURE 3.12   HYDROFRACTURE FROM UNVENTED EXPLODED CAVITY
TEST 170   REPRODUCIBILITY (Continued)

Hydrofracture records for tests 162, 163, 164, and 177 are shown in Figure 3.13. In test 164, cavity pressure increased smoothly to a fracture initiation spike and then decreased monotonically to a steady state. In the remaining tests, fracture initiation was followed by a small increase in pressure before the monotonic decay to steady state. Stability of crack growth thus appears to be marginal. However, compared with the initially rapid decay in cavity pressure for unexploded cavity tests, the initially slow decay in cavity pressure for the exploded cavity tests indicates that compressive stresses are tending to stabilize crack growth. In addition, the average steady-state cavity pressure for the exploded cavity tests is 500 psi (3.45 MPa) higher than the value for the corresponding unexploded cavity tests. Since steady-state pressure is a measure of flow-resistance along a fracture plane, a higher value suggests compressive stresses restricting crack growth. Figure 3.14, which shows the major fracture surface for test 164, reveals that hydrofracture fluid escaped from the cavity along a fracture plane of small sectorial extent and then spread around the annular region of residual compressive stress.

Fracture initiation pressures for the vented exploded cavity tests ranged from 2080 to 2930 psi (14.34 to 20.20 MPa). Values at the lower end of the range are slightly higher than those for the corresponding unexploded cavity tests. Values at the upper end of the range are slightly lower than the minimum fracture initiation pressure for the corresponding unvented exploded cavity tests.

Series 9 - Charge Holder Thickness

Consistent detonation of the explosive source cast in a sphere requires that the Lucite charge holder carry the stresses associated with overburden. Although the design shown in Figure 2.5 is generally adequate, reliability was improved by increasing the outside diameter of the spherical charge holder from 0.375 inch (0.952 cm) to 0.400 inch (1.016 cm). The improved charge design, shown in Figure 2.6, was incorporated in all exploded cavity tests numbered 199 and higher.
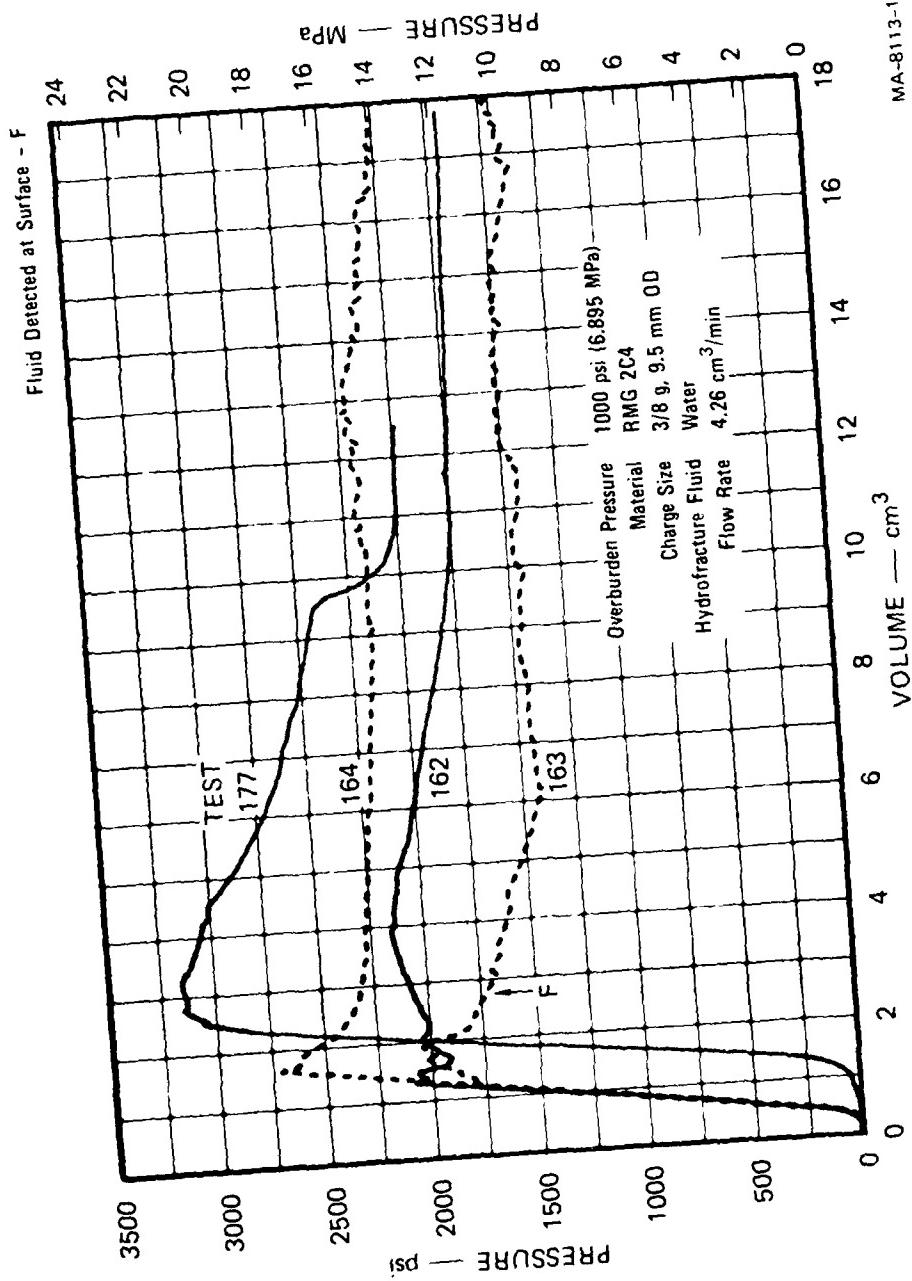
FIGURE 3.13   HYDROFRACTURE PRESSURES FOR VENTED EXPLODED CAVITY TESTS
162, 163, 164, AND 177 — VENTED CAVITY

65
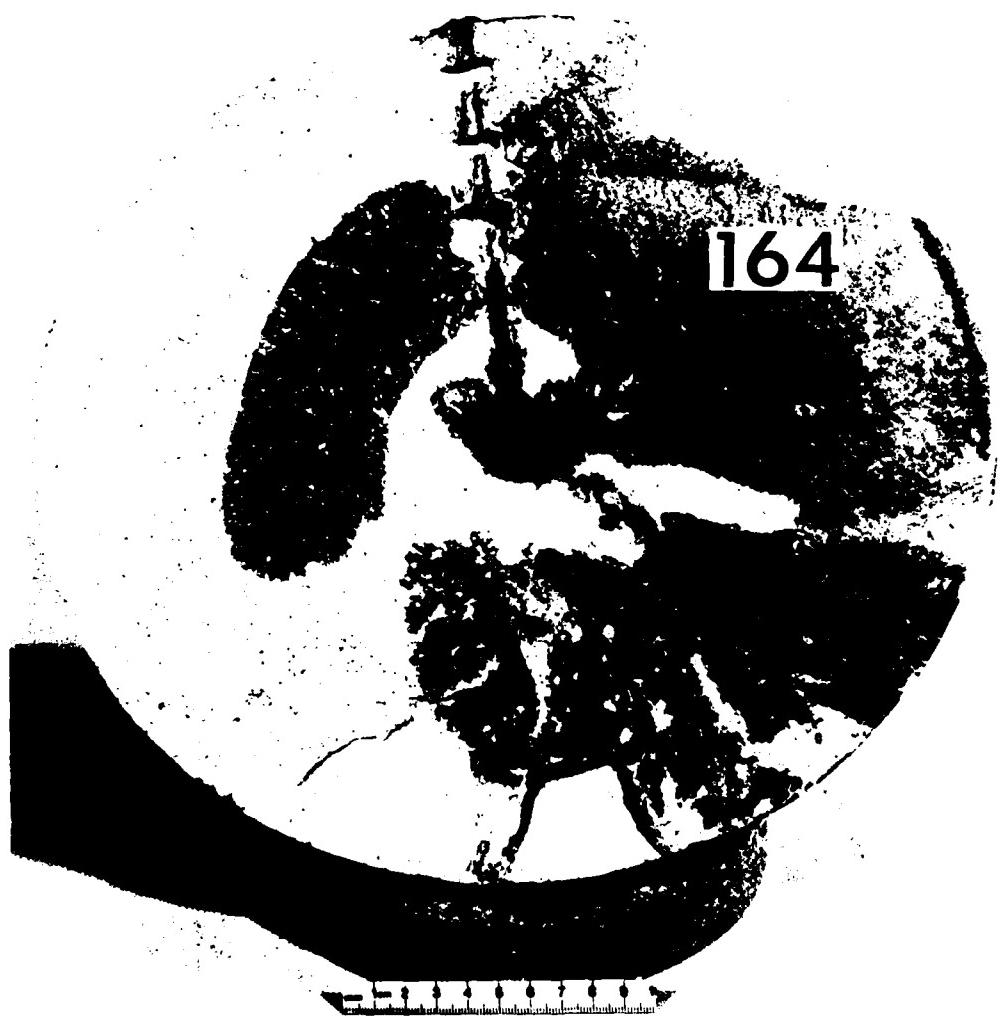
MP-8113-15

FIGURE 3.14   HYDROFRACTURE FROM VENTED EXPLODED CAVITY
TEST 164   VENTED CAVITY

FIGURE 3-11 HYDROFRACTURE FROM VENTED EXPLODED CAVITY
TEST 164 VENTED CAVITY (Concluded)

Figure 3.15 shows hydrofracture records for unvented exploded cavity tests 199, 200, and 204 performed with the improved charge. Shown in the figure for comparison are records from the reproducibility series (tests 159 and 170) obtained with the thinner-walled charge. Hydrofracture tests conducted with the new design yielded pressures within the range of pressures from tests with the thinner-walled charge. Although the new charge results in a slightly larger exploded cavity diameter [0.800 inch (2.032 cm) compared with 0.750 inch (1.905 cm)], the ratio of exploded cavity diameter to charge diameter remains a factor of two. Figure 3.16 shows the major fracture surface associated with test 200. The dyed pattern is typical of unvented exploded cavity tests. Fluid escaped from the cavity along an area of small sectorial extent and then spread around an annular region of compressive residual stress.

The pressure record for test 199 reflects the importance of adequately pressurizing the hydrofracture system before charge detonation. In this test the nominal 300-psi (2.068-MPa) prepressure was eliminated. System compliance with no prepressure required 15 seconds of pumping to open the access tube. For a prepressure of 300 psi (2.068 MPa), only 3 to 5 seconds of pumping is normally required. Hence the hydrofracture record for test 199 begins 15 seconds after detonation with an initial cavity pressure of 970 psi (6.688 MPa). The subsequent fracture initiation pressure, 3080 psi (21.24 MPa), is at the low end of the range for unvented exploded cavity tests.

Series 10 - Uncoupled Charge

Water hydrofracture tests were performed on unvented exploded cavity spheres in which a 3/16-inch (0.476-cm) annular air space separated the charge from the surrounding grout before detonation. This configuration, shown schematically in Figure 3.17, simulates an uncoupled nuclear cavity detonation. The initial 3/4-inch-diameter (1.90-cm) cavity was cast around a spherical glass shell with an 8-mil (0.203-mm) wall thickness. The shell shattered upon charge detonation.
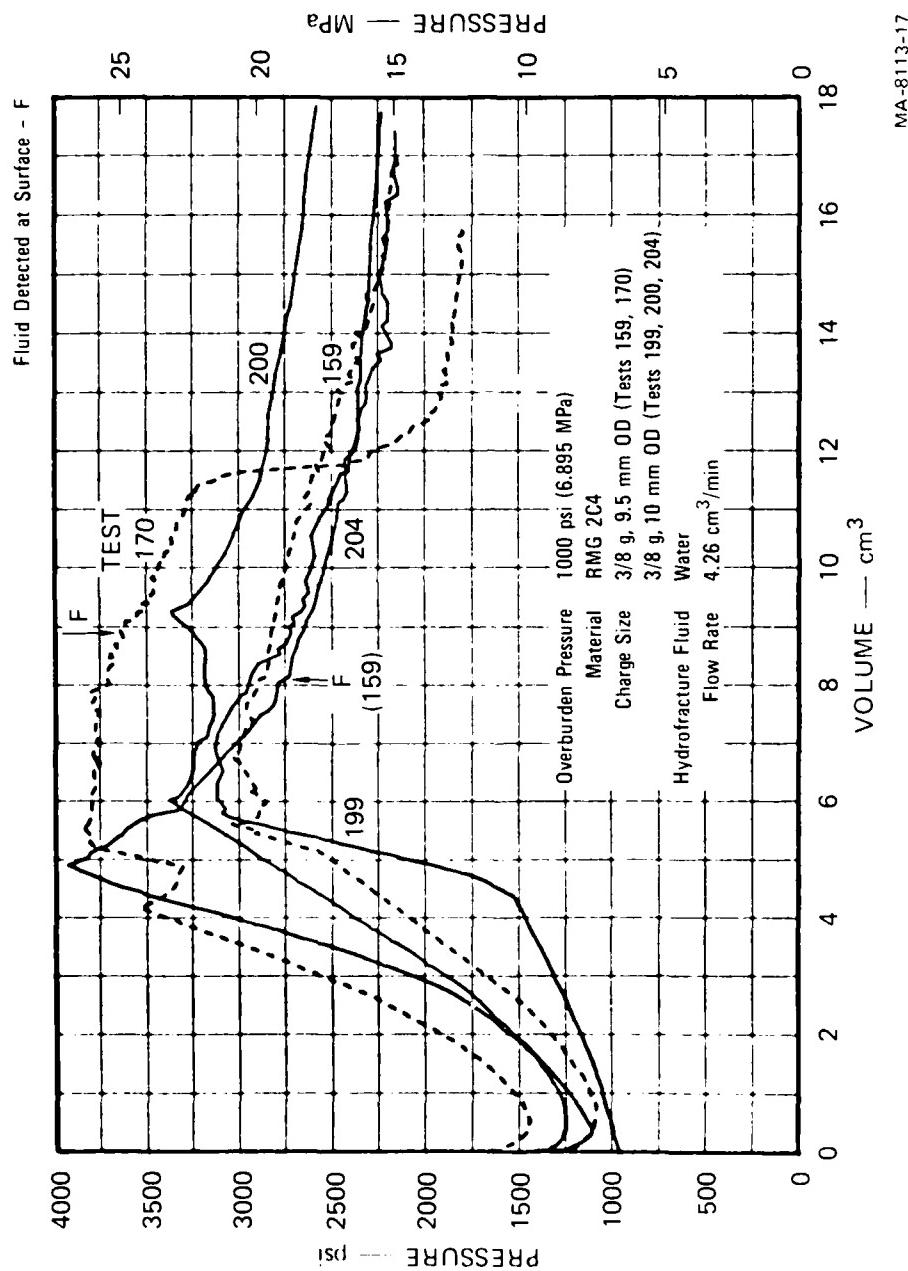
FIGURE 3.15   HYDROFRACTURE PRESSURES FOR UNVENTED EXPLODED CAVITY
TESTS 159, 170, 199, 200, AND 204 — CHARGE HOLDER THICKNESS
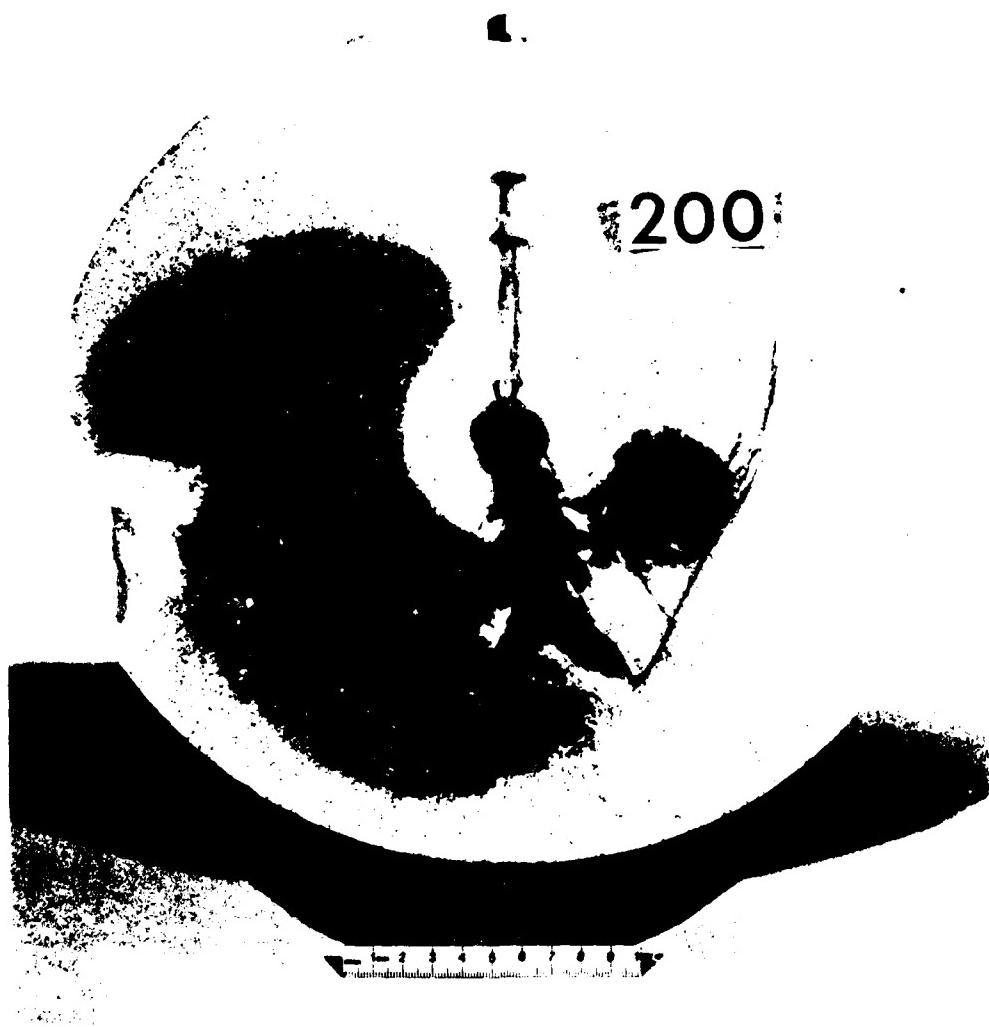
69

FIGURE 3-16. HYDROFRACTURE FROM UNVENTED EXPLODED CAVITY
TEST 200 — CHARGE HOLDER THICKNESS

200
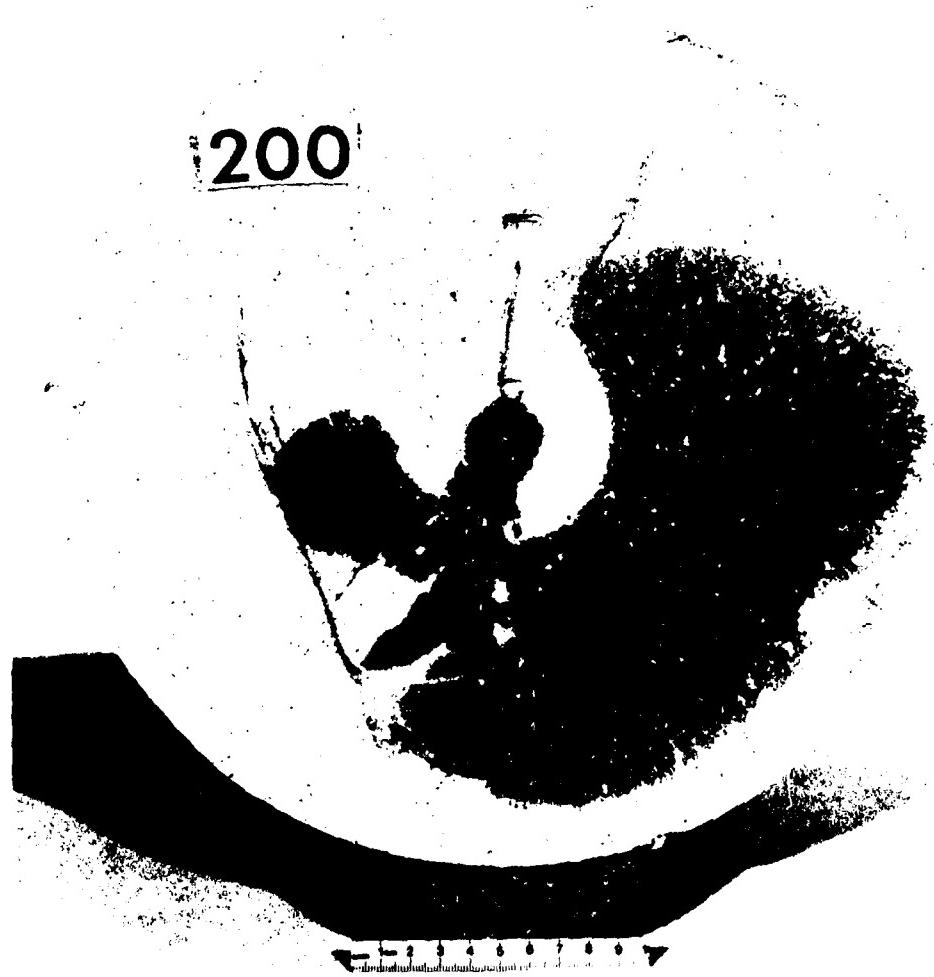
MP 8113 19

FIGURE 3.16   HYDROFRACTURE FROM UNVENTED EXPLODED CAVITY
TEST 200   CHARGE HOLDER THICKNESS (Concluded)

Hydrofracture records for uncoupled charge tests 174, 175, and 176 are shown in Figure 3.17. For comparison, tests 159 and 170 from the reproducibility series are also shown. Uncoupling the charge allows the detonation products to expand into a larger volume. Hence unloading of cavity gas pressure is more pronounced in the uncoupled charge configuration. The exploded cavity diameters in tests 174, 175, and 176 were 54/64, 61/64, and 62/64 inch (2.14, 2.42, and 2.46 cm), respectively. Expansion of cavity diameters thus ranged from a minimum of 6/64 to a maximum of 14/64 inch (0.238 to 0.556 cm). The highest residual cavity gas pressure, 1020 psi (7.033 MPa), and the highest fracture initiation pressure, 3720 psi (26.65 MPa), for the uncoupled charge experiments were developed during test 174, where cavity expansion was the smallest.

In tests 175 and 176, embedded fluid arrival gages detected hydro-fracture fluid 1 inch (2.54 cm) from the center of the sphere after 0.92 cm^3 and 2.18 cm^3 of flow, respectively. Since cavity pressure was increasing at this time, crack growth was stable. In test 174, fluid was detected 2 inches (5.08 cm) from the center of the sphere after 0.97 cm^3 of flow. Since cavity pressure was unchanging at this time, crack growth was neutral.

Figure 3.18 shows the multiple fracture planes that developed during hydrofracture in test 176. A complex pattern of fracture surfaces is a general characteristic of exploded cavity tests.

Series 11 - Geometry

To study the influence of different external geometries on hydro-fracture pressures and for use in future asymmetry tests, we performed water hydrofracture tests 181 and 182 on cylinders with unvented exploded cavities. The cylinders measured 12 inches (30.48 cm) in diameter and 12 inches (30.48 cm) in length. Hydrofracture records are shown in Figure 3.19, where a comparison is made with typical tests conducted on 12-inch-diameter (30.48-cm) spheres. Although the records for the cylinder exhibited no new features, the change in geometry reoriented the major fracture plane. For a sphere, surface cracking generally appears in a plane inclined to the access tube. For a cylinder, a vertical fracture plane was developed as shown in Figure 3.20.
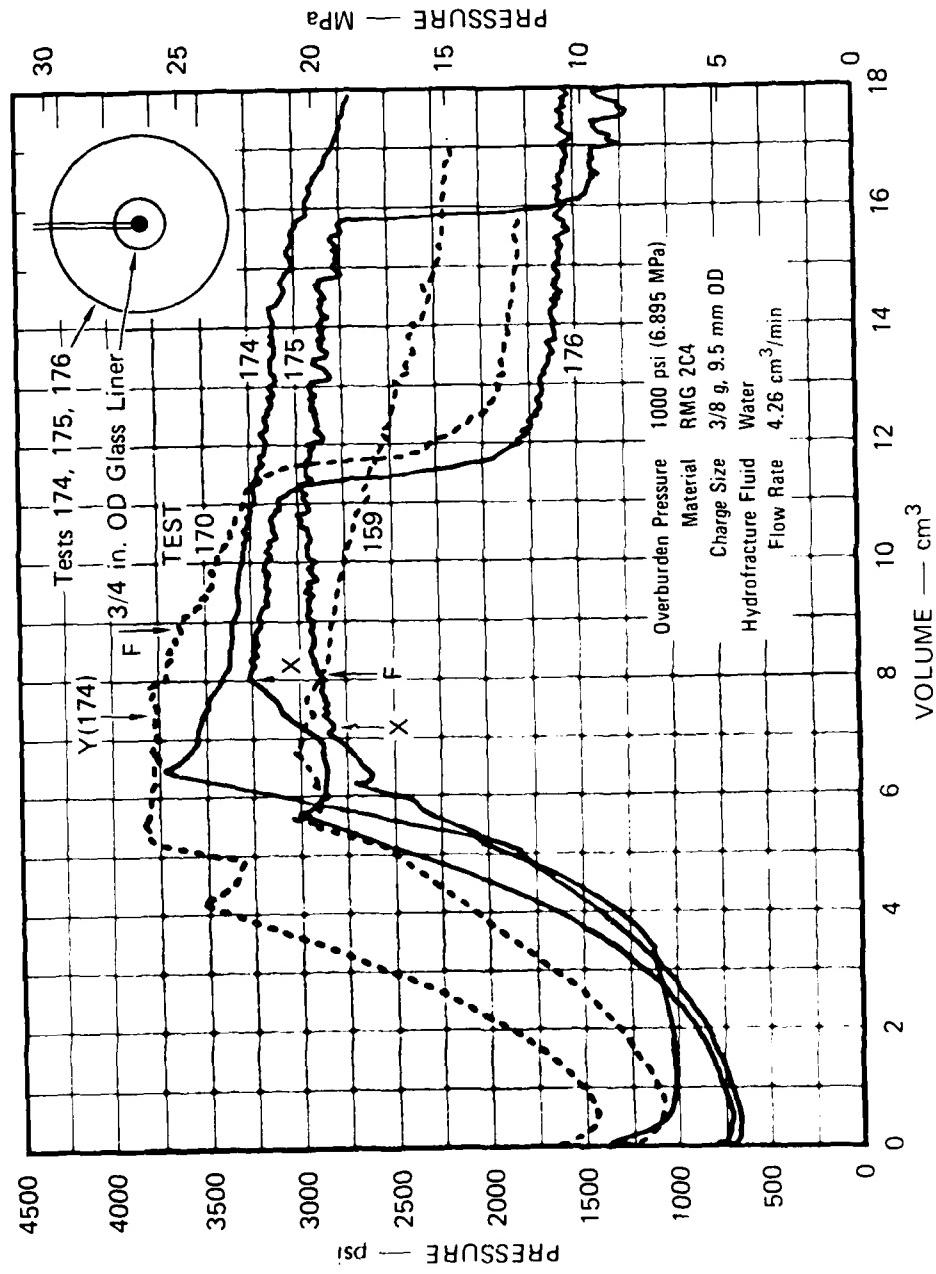
FIGURE 3.17   HYDROFRACTURE PRESSURES FOR UNVENTED EXPLODED CAVITY TESTS
159, 170, 174, 175, AND 176 -- UNCOUPLED CHARGE
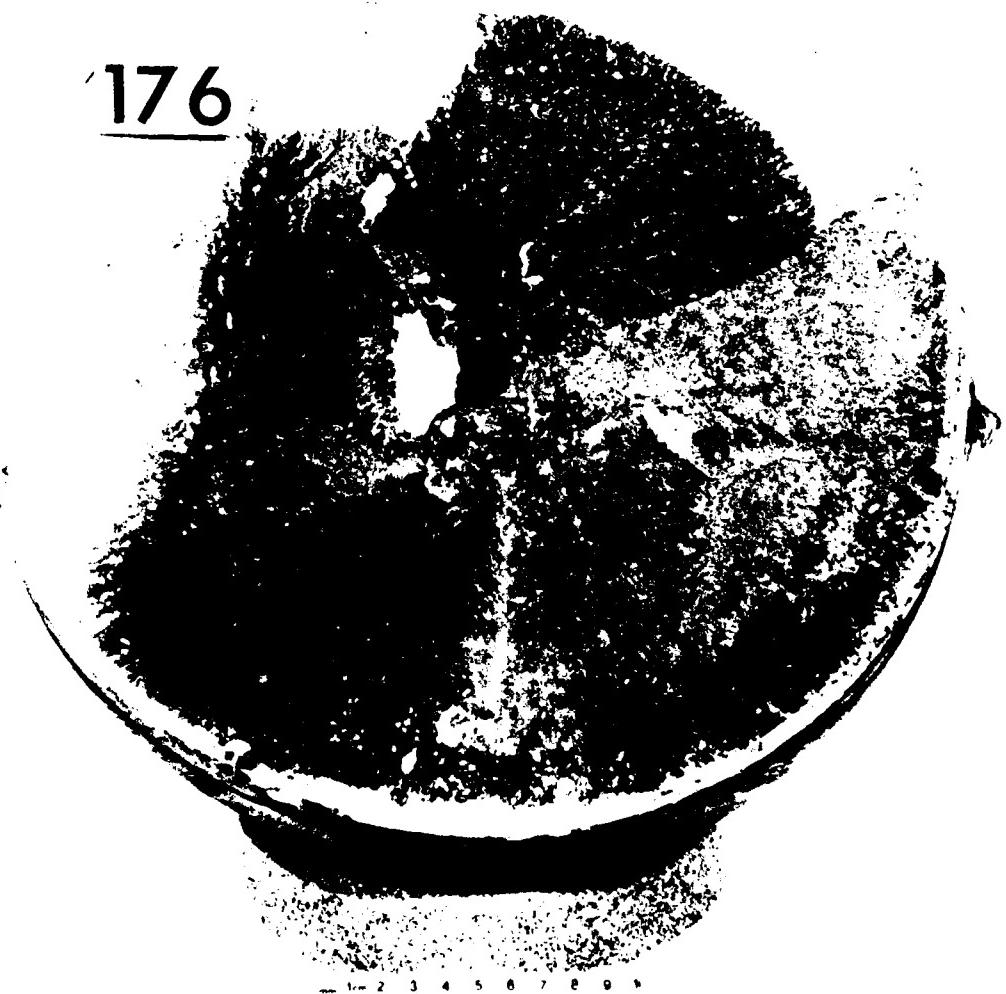
73

FIGURE 3.18 HYDROFRACTURE FROM CEMENTED EXPLODED CAVITY
TEST 176 — UNCOUPLED CHARGE

FIGURE 3-18   HYDROFRACTURE FROM UNVENTED EXPLODED CAVITY
TEST 176   UNCOUPLED CHARGE
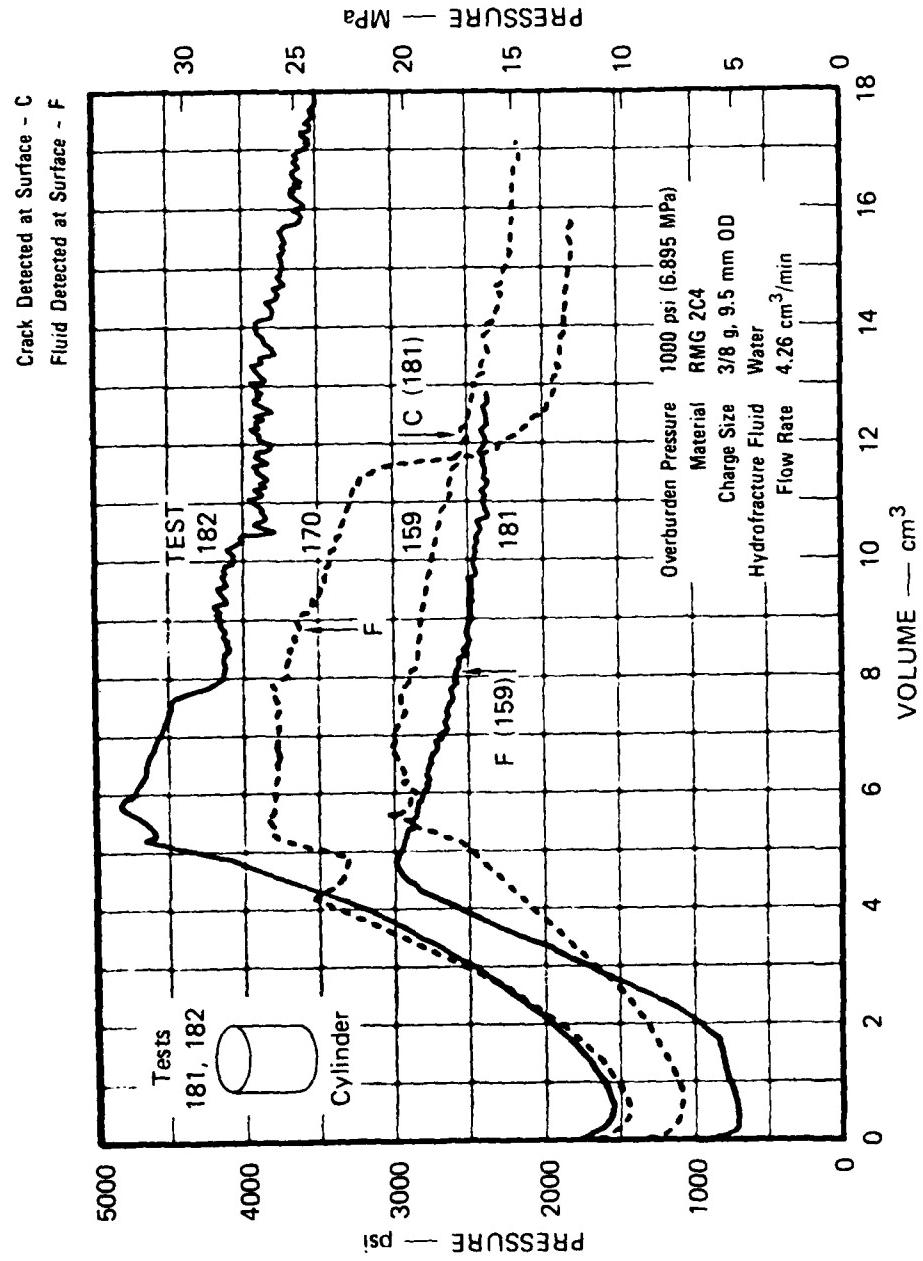
FIGURE 3.19   HYDROFRACTURE PRESSURES FOR UNVENTED EXPLODED CAVITY TESTS
159, 170, 181, AND 182 — GEOMETRY

76

FIGURE 3-20   [illegible] EXPLODED CAVITY
[illegible]

Series 12- Viscosity

Glycerol hydrofracture of unvented exploded cavity spheres was performed to study the influence of fluid viscosity on hydrofracture. Pressure records for tests 135, 142, and 157 are shown in Figure 3.21. For comparison, typical water hydrofracture tests 159 and 170 are also shown. Tests 135 and 142 are previously reported experiments[6] in which cavity gas pressure was allowed to decay to near steady state before fluid was pumped into the cavity. Test 157 was performed during the developmental stage of unvented cavity testing when the delay from charge detonation to measurement of cavity gas pressure was longer than the nominal 4-second delay in later tests. Hence the full effect of a change in fluid viscosity on hydrofracture is not indicated in Figure 3.21. A comparison of the hydrofracture pressures for tests 157 and 159 does indicate the trend, however. Unloading of cavity gas pressure was the same in both tests. For water hydrofracture, the fracture initiation pressure was 3010 psi (20.75 MPa). For glycerol hydrofracture, the fracture initiation pressure was 3540 psi (24.41 MPa), an increase of 18%.

Series 13 - Material Property

Effects of a change in material properties on containment were evaluated by comparing unvented exploded cavity hydrofracture records for rock-matching grout (RMG 2C4), low density rock-matching grout (LD 2C4), and granite simulant (GS3) spheres. Properties of these materials are presented in Appendix C.

Figure 3.22 shows the water hydrofracture records for unvented exploded cavity tests 189, 215, and 216 performed on LD 2C4 spheres. For comparison, results of tests 159 and 170 performed on RMG 2C4 spheres are also shown. An important feature of the low density material in exploded cavity tests is the 13.4% air void content. This property accounts for the formation of an exploded cavity with a final-to-initial radius ratio of 2.4. Figure 3.11 shows that the corresponding theoretical estimate of initial gas pressure in the expanded cavity is 4300 psi (29.65 MPa). For a RMG 2C4 sphere, the radius ratio is 2.0 and the theoretical initial pressure is 10,100 psi (69.64 MPa). As shown in Figure 3.22, these values

78

Crack Detected at Surface - C

Fluid Detected at Surface - F
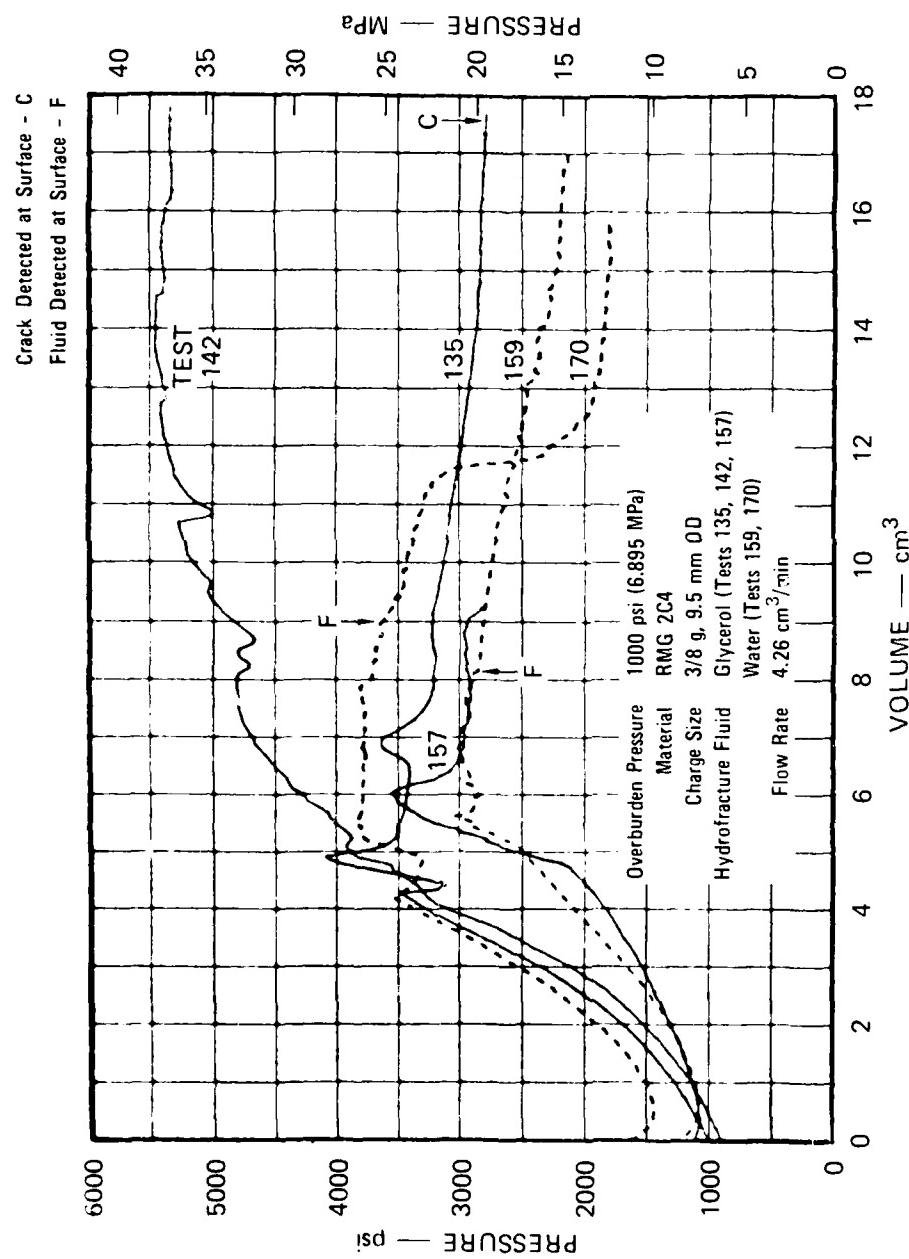
FIGURE 3.21   HYDROFRACTURE PRESSURES FOR UNVENTED EXPLODED CAVITY TESTS
135, 142, 157, 159, AND 170 — VISCOSITY

MA-8113-25

Overburden Pressure	1000 psi (6.895 MPa)
Material	RMG 2C4
Charge Size	3/8 g, 9.5 mm OD
Hydrofracture Fluid	Glycerol (Tests 135, 142, 157)
	Water (Tests 159, 170)
Flow Rate	4.26 cm³/min

79
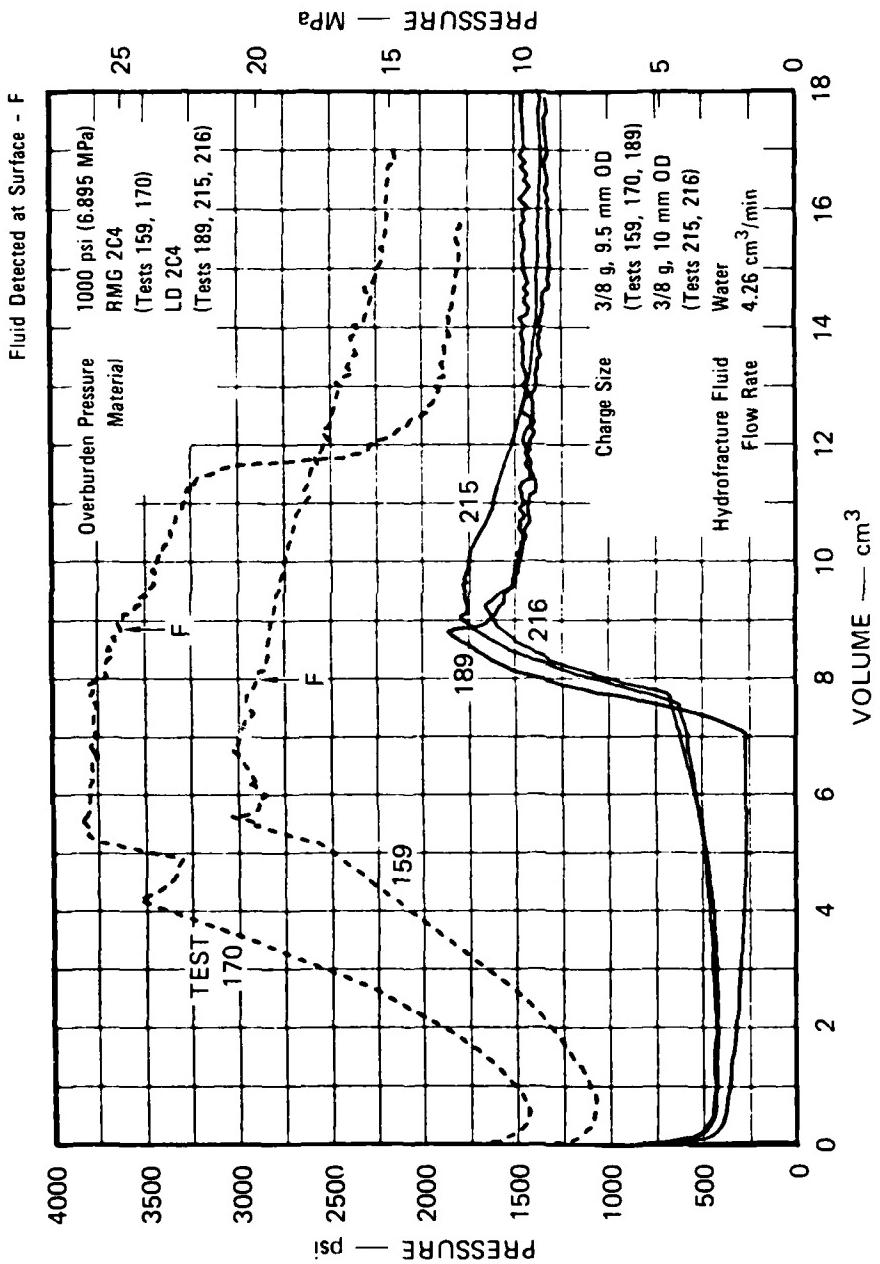
FIGURE 3.22   HYDROFRACTURE PRESSURES FOR UNVENTED EXPLODED CAVITY TESTS 159,
170, 189, 215, AND 216 — MATERIAL PROPERTY (LD 2C4)

are reflected in the initial cavity pressures and the volumes of fluid required to fill the cavities. The average fracture initiation pressure for the LD 2C4 spheres, 1770 psi (12.20 MPa), is considerably less than the 3290-psi (22.68-MPa) average for RMG 2C4 spheres, but is comparable to the 1580-psi (10.89-MPa) average for unexploded cavity low density spheres. Hence, the residual stress field developed around an LD 2C4 exploded cavity is weak. Figure 3.23 shows the fracture surface for test 216. The absence of a clearly defined undyed region surrounding the cavity is further evidence of weak residual stresses.

Dynamic pressure pulses measured at the bottom of the containment vessel were shown in Figure 2.12. For LD 2C4 the average reflected peak pressure is 250 psi (1.72 MPa), and the average total reflected impulse is 2.8 psi·msec (0.019 MPa·msec). The corresponding values for RMG 2C4 tests are 834 psi (5.75 MPa) and 10.1 psi·msec (0.070 MPa·msec). Hence attenuation of the stress wave associated with charge detonation is more pronounced in the low density material. Explosive crushing of the air voids contained in LD 2C4 is the process by which energy is absorbed without the generation of significant residual stresses.

The results of additional tests on materials containing air voids are shown in Figure 3.24. Tests 201 and 202 were unvented exploded cavity water hydrofractures performed on a medium density rock-matching grout (MD 2C4) containing approximately 6% air voids. For comparison, results for the fully saturated RMG 2C4 and the LD 2C4 with 13.4% air voids are also shown. The values for exploded cavity diameter and fracture initiation pressure obtained in the MD 2C4 tests lie between the corresponding values obtained in the RMG 2C4 and LD 2C4 tests. Hence the air void content of a material represents a significant containment parameter.

A final series of material property hydrofracture tests was performed on granite simulant (GS3) spheres. Charge detonation resulted in a final-to-initial cavity radius ratio of 1.3. Figure 3.11 shows that the corresponding theoretical estimate of initial cavity pressure is 97,400 psi (67.15 MPa). In the tests, high gas pressures resulted in fracture initiation before fluid was pumped into the cavity.

FIGURE 3.23   HYDROFRACTURE FROM DEVELOPED EXPLODED CAVITY
TEST 216   MATERIAL PROPERTY (LD 2G)

FIGURE 3.23   HYDROFRAC TURE EFFECT ON CLAY TEST 216
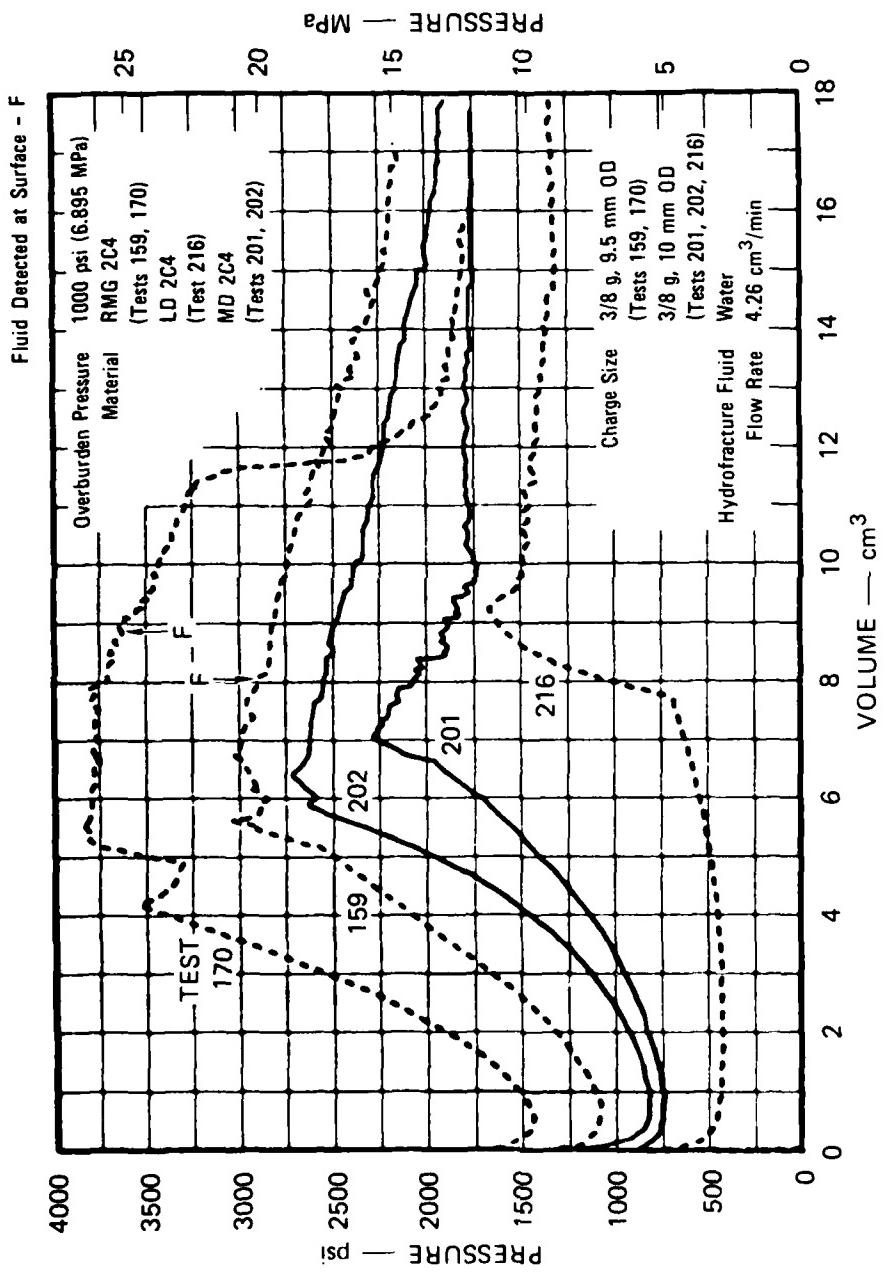
FIGURE 3.24 HYDROFRACTURE PRESSURES FOR UNVENTED EXPLODED CAVITY TESTS 159,
170, 201, 202, AND 216 — MATERIAL PROPERTY (MD 2C4)

MA-8113-29

84

Series 14 - Material Interface

Potential sites for underground nuclear testing include areas near
a surface of discontinuity that separates regions of different materials.
The effect of this geological feature on containment was simulated by
conducting unvented exploded cavity tests on spheres containing a
material interface.

The case of a weaker nearby material was examined by testing composite
spheres of rock-matching grout (RMG 2C4) and low density rock-matching
grout (LD 2C4). In each test the plane horizontal interface passed within
3/4 inch (1.905 cm), or approximately one exploded cavity diameter, of
the center of the sphere. The locations of the interface and the resulting
hydrofracture records for tests 205 and 208 are shown in Figure 3.25. Charge
detonation occurred in the RMG 2C4, and the resulting exploded cavity
diameter, 0.800 inch (2.032 cm), was the same as that found in tests on
LMG 2C4 spheres. Hydrofracture produced a fracture plane that propagated
across the interface without changing direction. Figure 3.25 shows that
hydrofracture pressures for the composite spheres are similar to those
for standard RMG 2C4 tests. Hence the influence of the nearby low-density
material appears to be negligible.

The case of a stronger nearby material was examined by testing composite
spheres of RMG 2C4 and granite simulant (GS3). The distance of the inter-
face from the center of the sphere was 2 inches (5.080 cm) in test 188 and
3/4 inch (1.905 cm) in test 213, as shown in Figure 3.26. Charge detonation
again occurred in RMG 2C4 and resulted in an exploded cavity diameter the
same as that found in tests on 2C4 spheres. The pressure record for test
188 is typical of a test on a 2C4 sphere, with fracture initiation at
3540 psi (24.41 MPa). The pressure record for test 213, however, indicates
fracture initiation at 1750 psi (12.7 MPa). The low fracture initiation
pressure suggests low adherence of RMG 2C4 to GS3. In fact, the hydrofracture-
driven crack propagated along the interface. Bonding in test 188 appeared
to be adequate, however. Hence boundary conditions along an interface
appear to control hydrofracture pressures in the composite spheres tested.
Future composite sphere experiments with GS3 require development of a
technique for producing a reliable interface bond.
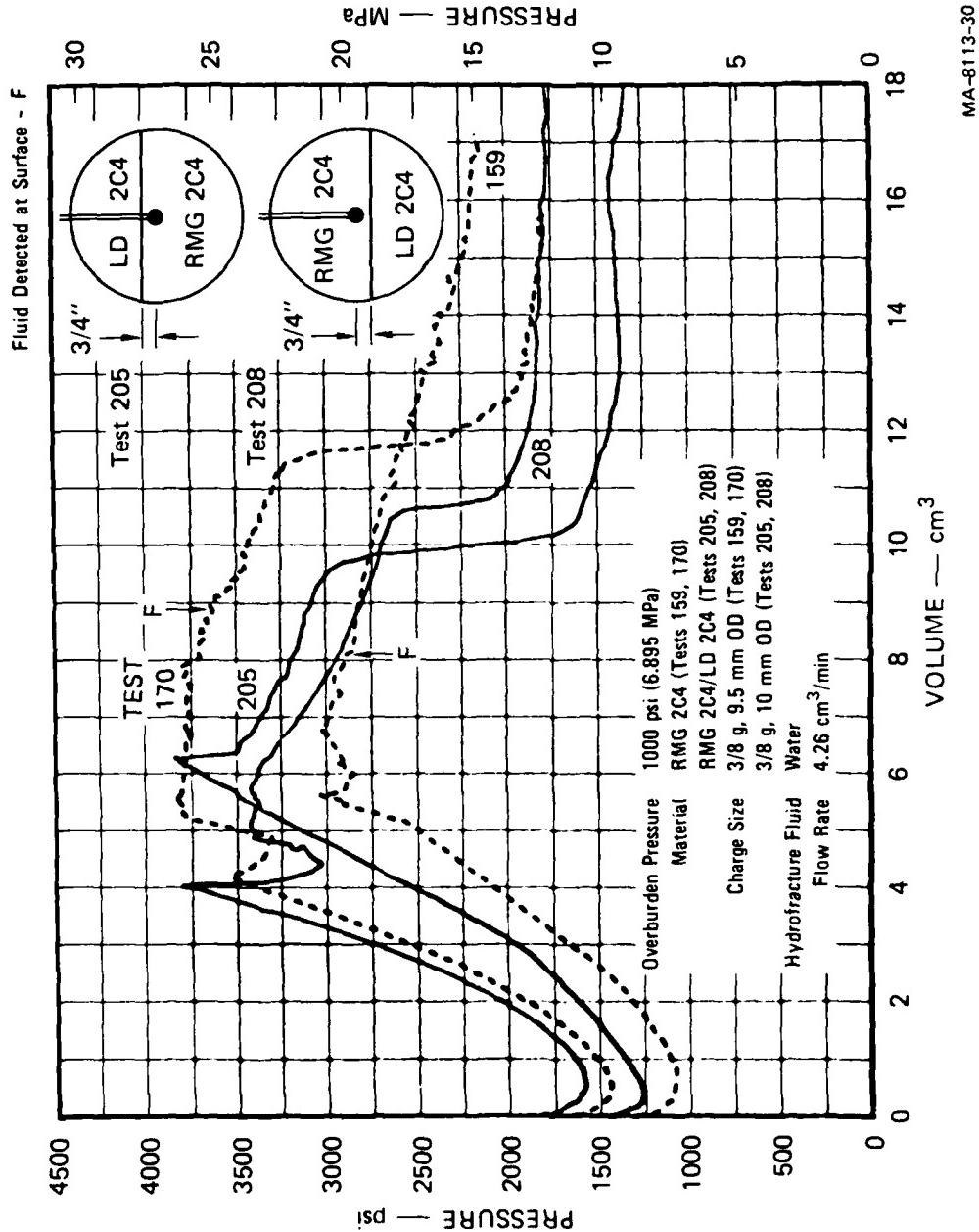
FIGURE 3.25   HYDROFRACTURE PRESSURES FOR UNVENTED EXPLODED CAVITY TESTS 159, 170, 205, AND 208 — MATERIAL INTERFACE (RMG 2C4/LD 2C4)
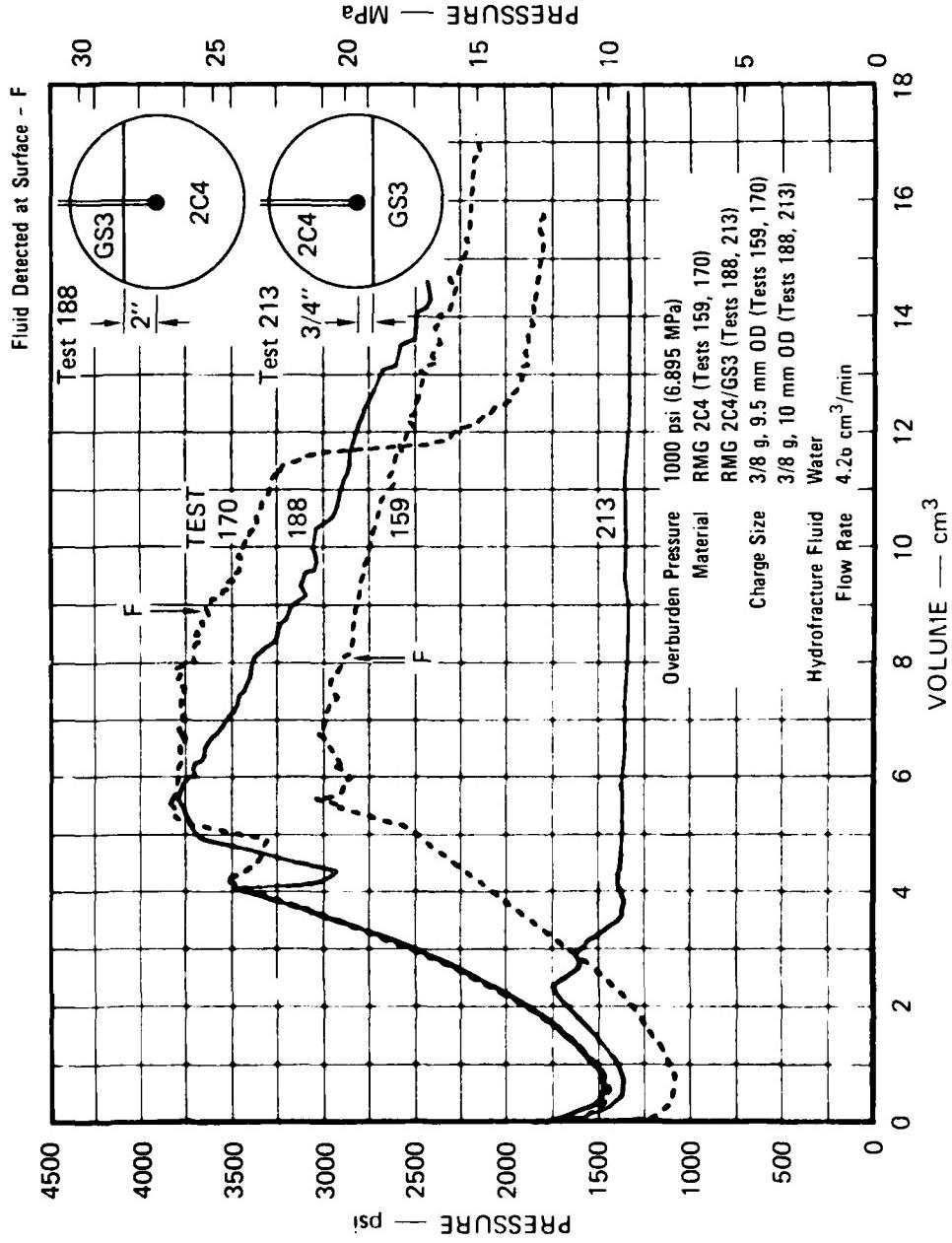
FIGURE 3.26 HYDROFRACTURE PRESSURES FOR UNVENTED EXPLODED CAVITY TESTS
159, 170, 188, AND 213 — MATERIAL INTERFACE (RMG 2C4/GS3)

87

Series 15 - Radial Tunnel

An underground nuclear test has a tunnel extending from the device cavity. The effects of tunnels on containment were studied by conducting unvented exploded cavity tests on spheres containing different radial tunnel configurations.

Simulation of a radial tunnel filled over most of its length was provided by the configuration shown in Figure 3.27(a). A solid Lucite rod filled the entire length of tunnel except for a 1/8-inch (0.318-cm) air gap at the end opposite the charge. The resulting hydrofracture record for test 185 is shown in Figure 3.28. The cavity pressure and maximum hydrofracture pressure were consistent with those in tests 159 and 170 without a tunnel. Examination of the sphere following the test revealed that the Lucite rod had been extruded to the end of the tunnel. However, the fracture plane reaching the surface did not intersect the tunnel. Surface cracking was detected after 3.8 cm^3 of flow, with volume measured from the point of fracture initiation. The associated sudden loss of cavity pressure shown in Figure 3.28 indicates development of widespread surface cracking.

Simulation of a hollow radial tunnel was provided by the configuration shown in Figure 3.27(b). The 2-1/2-inch-long (6.35-cm) tunnel extending from the charge was cast around a thin-walled glass tube, which shattered upon charge detonation. Hence, the pressure record for test 214, shown in Figure 3.28, is the hydrofracture associated with a hollow unlined tunnel. For comparison, results of tests without a tunnel, 159 and 170, are also shown. Since venting of the cavity gases to the open tunnel reduced the initial cavity gas pressure, the subsequent hydrofracture pressures were also reduced. Fracture initiated from the end of the tunnel when the cavity pressure reached 1560 psi (10.76 MPa). Examination of the sphere following the test showed no signs of stemming along the tunnel.

(a) SOLID TUNNEL

DETONATOR WIRES

STEEL TUBE

3/8 g PETN CHARGE

0.005-in.-THICK MYLAR COVER

12-in.-O.D. RMG 2C4 SPHERE

PLASTIC TUBE
0.153 in. O.D.,
0.139 in. I.D.,
1/4 in. LONG
EPOXIED TO CHARGE

LUCITE ROD
0.129 in. O.D.,
1 7/8 in. LONG
EPOXIED TO CHARGE

(b) HOLLOW TUNNEL

DETONATOR WIRES

STEEL TUBE

3/8 g PETN CHARGE

0.005-in.-THICK MYLAR COVER

12-in.-O.D. RMG 2C4 SPHERE

GLASS TUBE
0.187 in. O.D.,
0.153 in. I.D.,
2 1/2 in. LONG
EPOXIED TO CHARGE
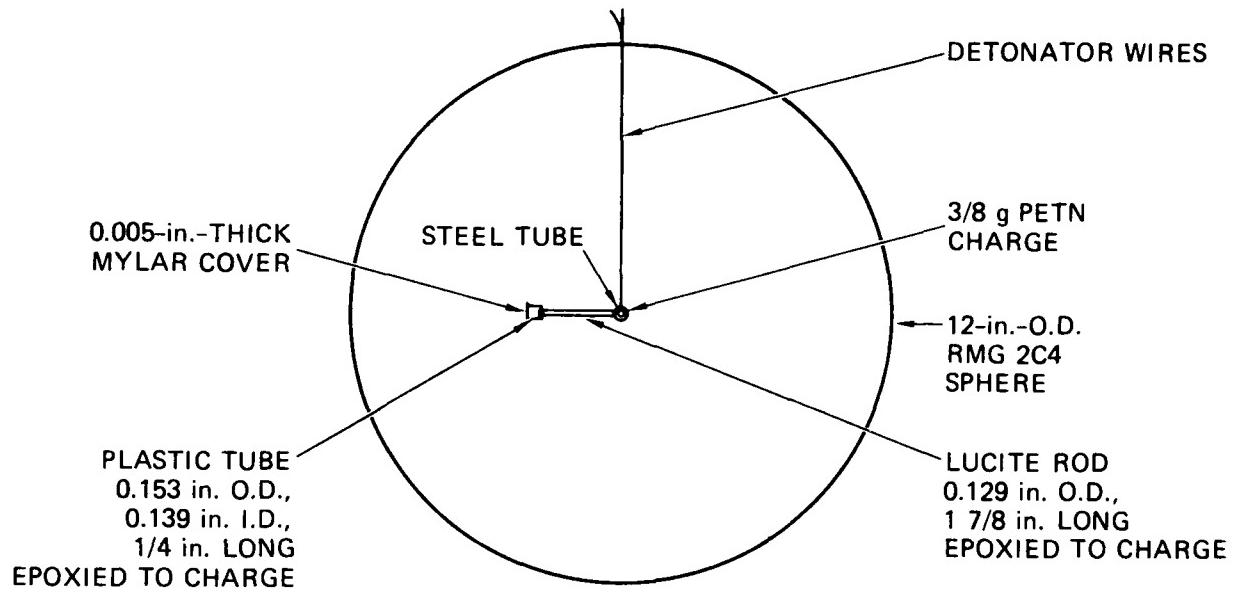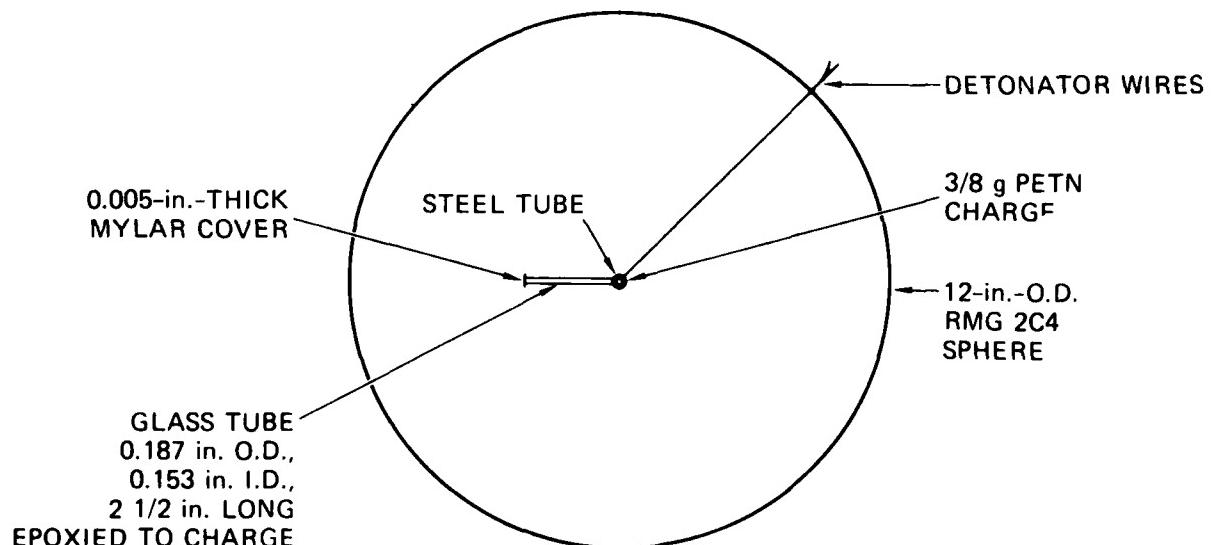
MA-8113-32

FIGURE 3.27   CONFIGURATIONS FOR RADIAL TUNNEL TESTS

89
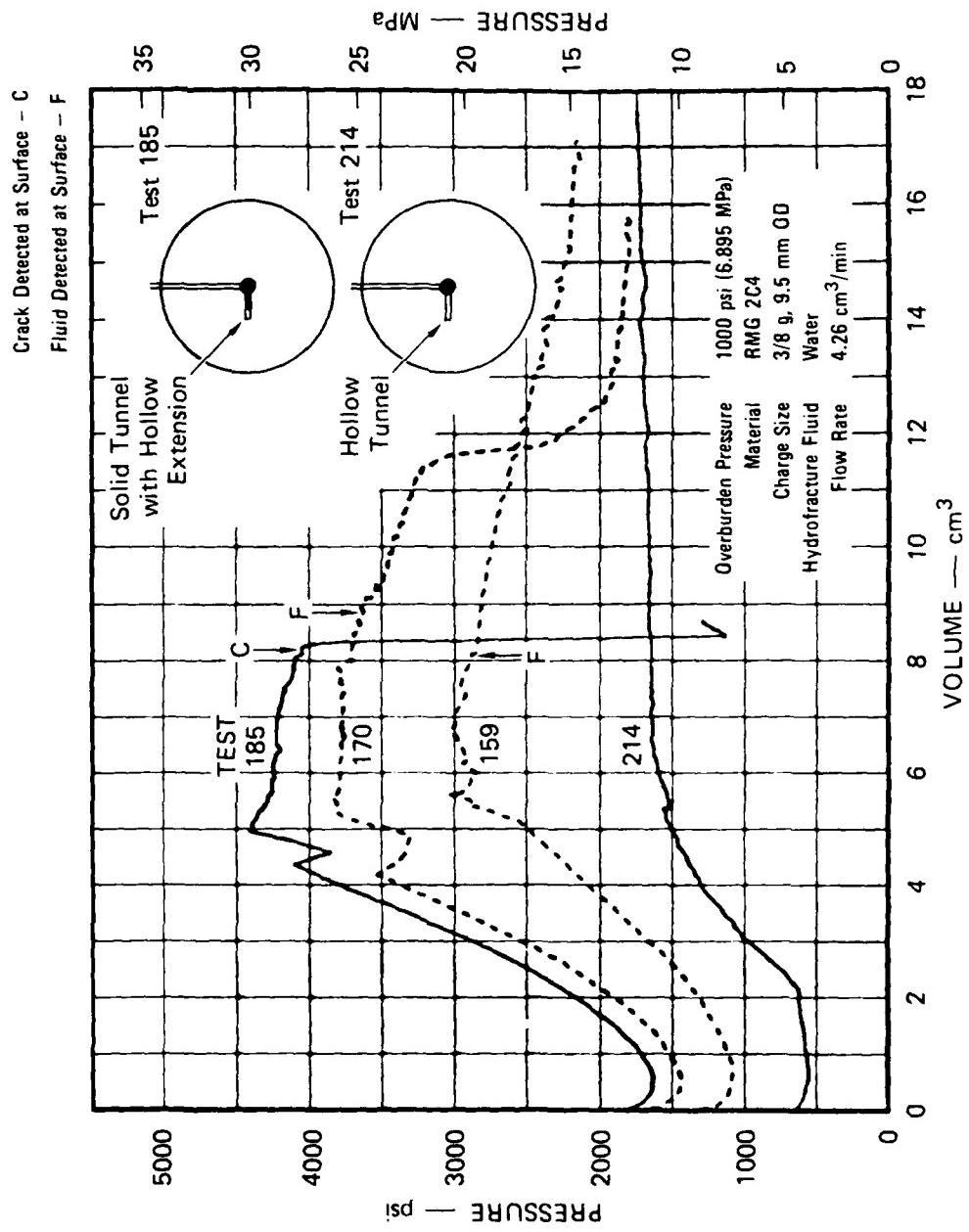
FIGURE 3.28 HYDROFRACTURE PRESSURES FOR UNVENTED EXPLODED CAVITY TESTS 159, 170, 185, AND 214 — RADIAL TUNNEL

MA-8113-33

90

Series 16 – Nearby Tunnel

Nearby tunnels associated with past nuclear tests represent a possible path for the venting of detonation products in future tests. The effects of these test site features on containment were examined by testing unvented exploded cavity spheres containing nearby tunnels.

The configuration for simulating a nearby tunnel is shown in Figure 3.29. A thin-walled plastic tube serves as a lining for the 6-inch-long (15.2-cm) tunnel. The distance d from the center of the tunnel to the center of the charge provides a parameter for locating the tunnel.

In test 186 the distance d was 1/2 inch (1.27 cm). Venting of the explosive gases into the tunnel upon charge detonation resulted in the low residual cavity gas pressure measurement shown in Figure 3.30. Subsequent hydrofracture pressures were also low relative to those for tests 159 and 170 without a tunnel. Hydrofracture resulted in fluid flowing from the cavity into the tunnel along the explosively formed crack. Fluid then flowed along the tunnel and was discharged along a 1-1/2-inch-long (3.81-cm) section at one end of the tunnel. As shown in Figure 3.31, a 3-inch-diameter (7.62-cm) region surrounding the cavity was left undyed. This undyed region is further evidence of the residual stress field surrounding an exploded cavity. The absence of a pronounced fracture initiation spike in the pressure record for test 186 confirms that the cavity ruptured as a result of charge detonation.

In tests 209 and 223, the distance d was 3/4 inch (1.90 cm), or approximately one exploded cavity diameter. The detonation products were contained in the cavity and generated hydrofracture records typical of tests without a tunnel (Figure 3.30). In both tests the crack extending to the surface of the sphere intersected the tunnel but did not rupture the plastic liner. Hence the tunnels appeared to have no influence on hydro-fracture. The sudden drop in cavity pressure shown in Figure 3.30 for test 223 corresponds to the detection of a surface crack.

DETONATOR WIRES

12-in.-O.D.
RMG 2C4 SPHERE

0.153-in.-O.D.
PLASTIC TUBE

STEEL
TUBE

3/8 g PETN
CHARGE

d

6 in.

0.005-in.-THICK
MYLAR DIAPHRAGM
EPOXIED TO BOTH
ENDS OF TUBE

THREAD
SUPPORT

TOP VIEW
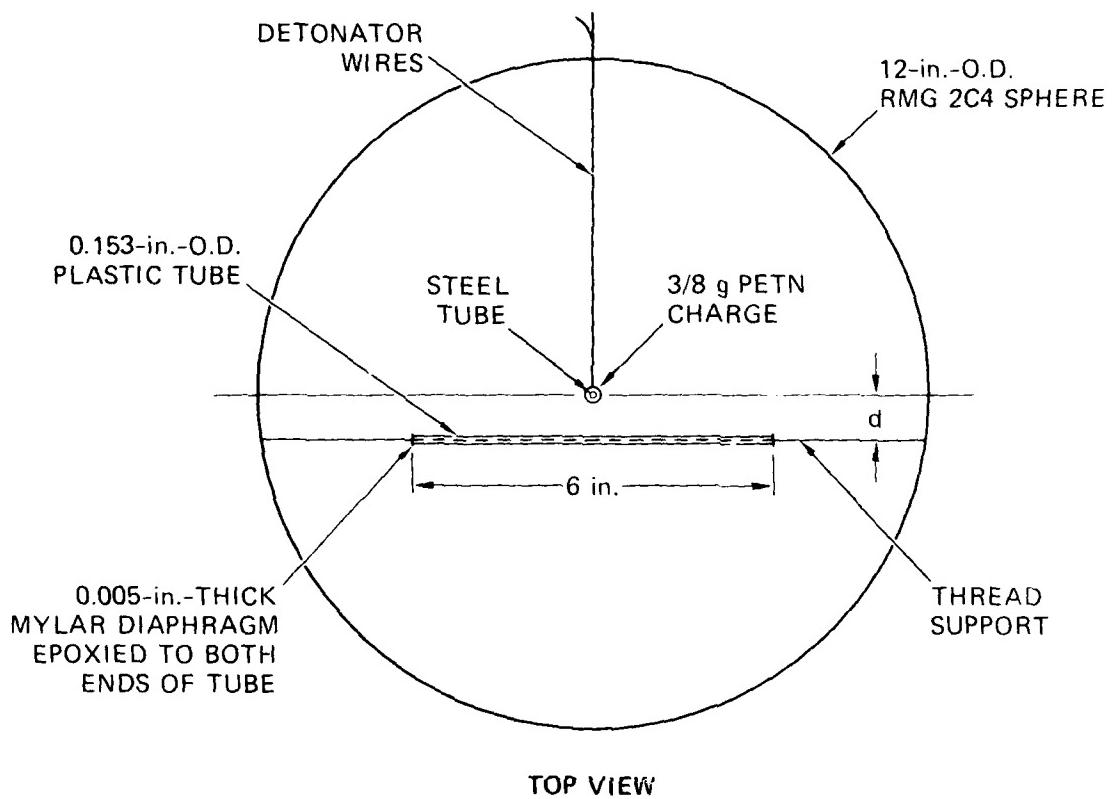
MA-8113-34

FIGURE 3.29   CONFIGURATION FOR NEARBY TUNNEL TESTS
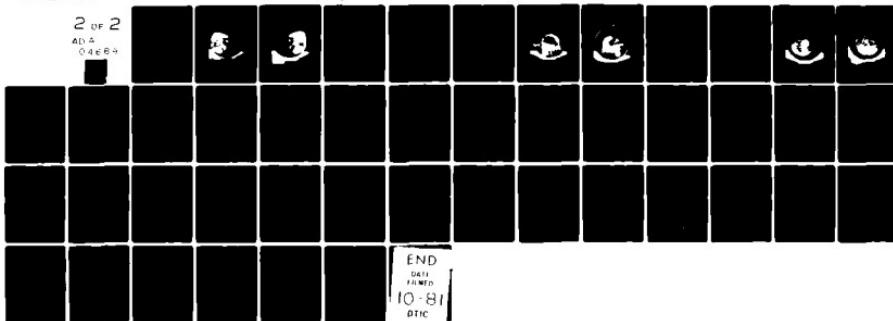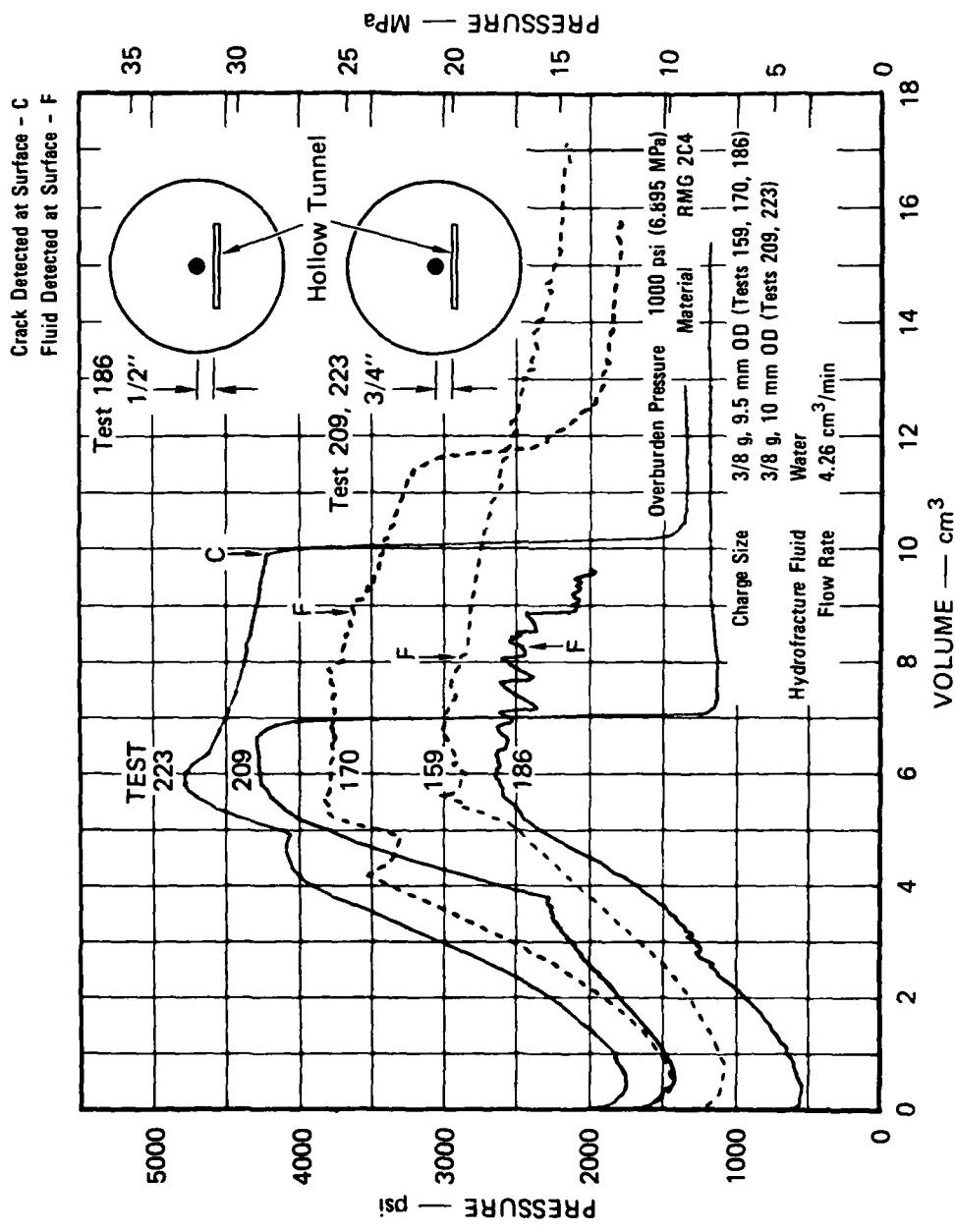
FIGURE 3.30   HYDROFRACTURE PRESSURES FOR UNVENTED EXPLODED CAVITY TESTS 159, 170, 186, 209, AND 223 — NEARBY TUNNEL

93
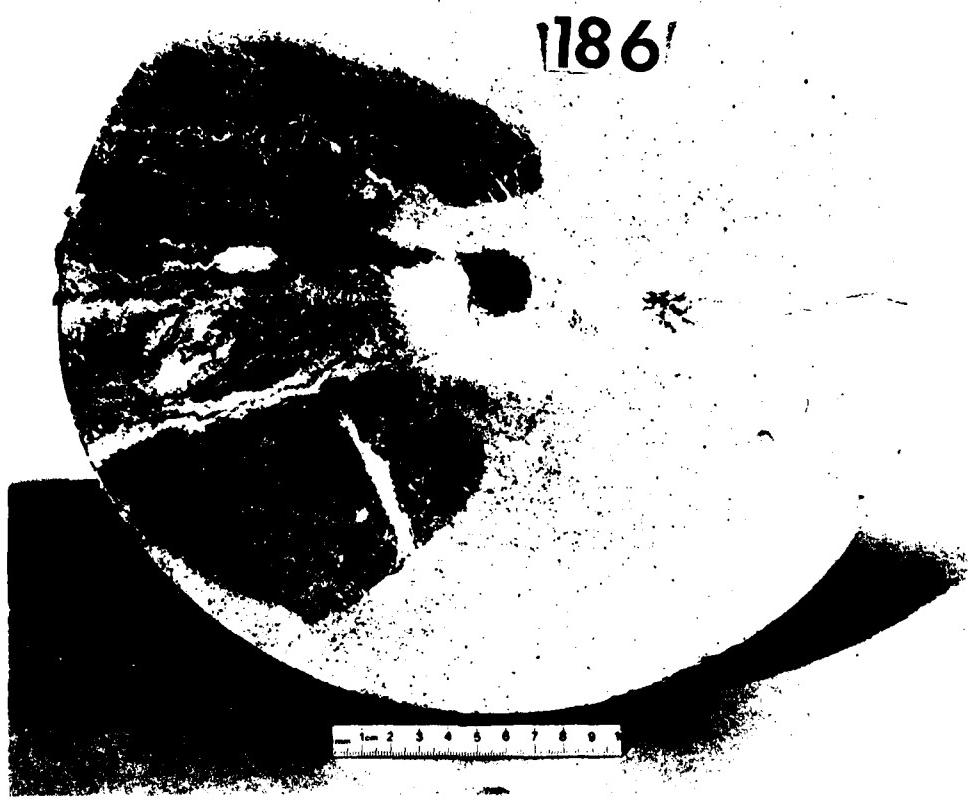
MP-8113-3C

FIGURE 3.31   HYDROFRACTURE FROM UNVENTED EXPLODED CAVITY
TEST 186   NEARBY TUNNEL
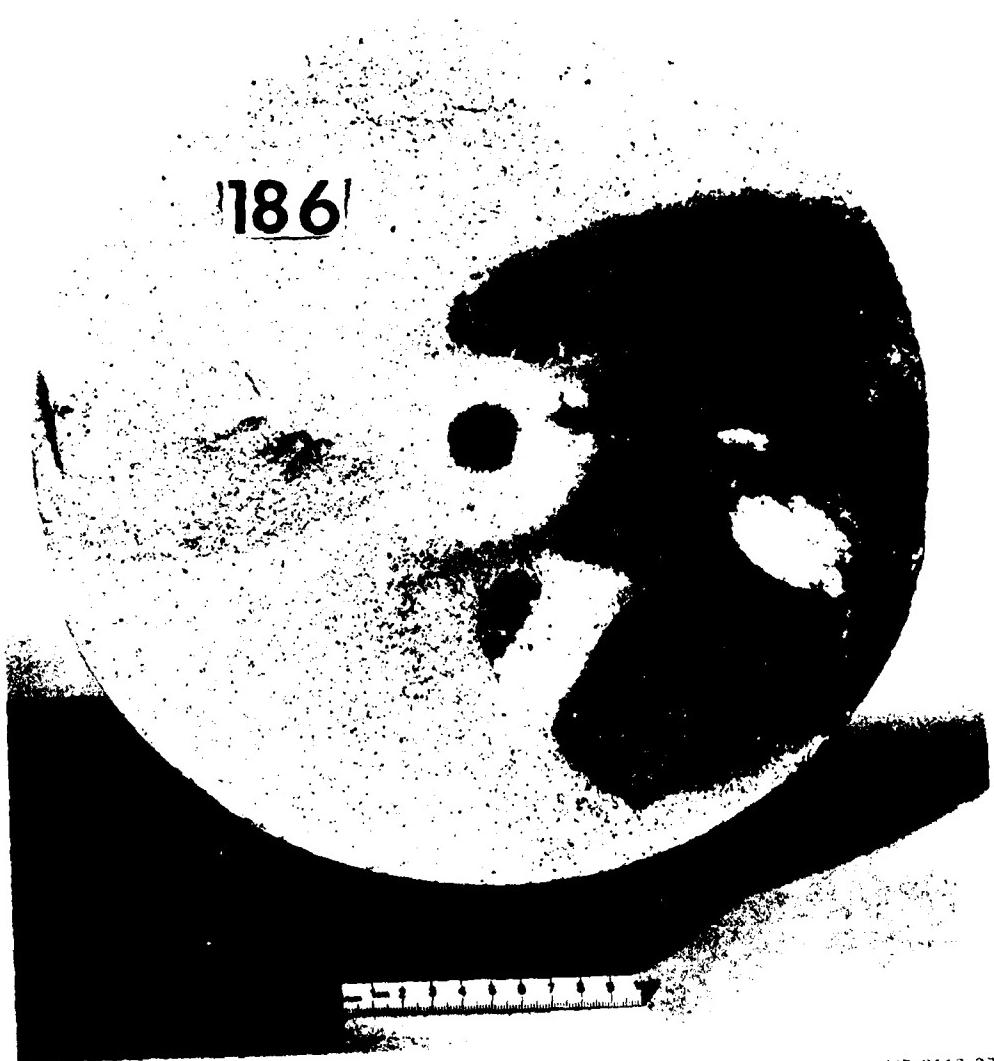
MP-8113-37

FIGURE 3.31   HYDROFRACTURE FROM UNVENTED EXPLODED CAVITY
TEST 186   NEARBY TUNNEL (Concluded)

Series 17 - Fault Plane

Fault planes in the vicinity of a nuclear device cavity represent paths along which the detonation products may escape to the atmosphere. The effects of these geological features on containment were examined by testing unvented exploded cavity spheres containing a fault plane.

The configuration for simulating a vertical fault plane is shown in Figure 3.32(a). The 6-inch-diameter (15.2-cm) fault consists of three layers of low friction material that allow for slipping along the plane. In each test, the fault plane passed within 1-3/8 inch (3.49 cm), or approximately 1.8 exploded cavity diameters, of the center of the sphere.

The hydrofracture record for test 192 is shown in Figure 3.33. The initially low cavity pressure indicates that charge detonation resulted in venting of the detonation products. The subsequent increase in pressure to a maximum of 2660 psi (18.34 MPa) was erratic and suggests that fluid was escaping from the cavity. Examination of the sphere following the test revealed that the crack shown in Figure 3.34 extended from the cavity to the fault plane.

The hydrofracture records for fault plane tests 210 and 221 are also shown in Figure 3.33. The similarity of these records to those of tests 159 and 170 from the reproducibility series suggests that the fault plane was not a factor in these hydrofractures. Cavity gases were not vented upon charge detonation. Furthermore, examination of each sphere following the tests revealed that fluid escaped from the side of the cavity opposite the fault. Fluid then flowed around the annular region of residual stress and eventually reached the fault later in the hydrofracture process.

Simulation of a fault plane intersecting a cavity was provided by the configuration shown in Figure 3.32(b). The 3-inch-diameter (7.62-cm) fault allows for slipping along the plane. The resulting hydrofracture record for test 217 is shown in Figure 3.35. For comparison, tests 159 and 170 from the reproducibility series are also shown. Initial cavity gas pressure for the fault test is in the range of pressures for tests without the fault. Hence cavity gas appeared to be contained as hydrofracture began. As hydrofracture continued, however, cavity pressure

96

6-in.-DIA. FAULT
0.005 in. MYLAR
WAX PAPER
0.005 in. MYLAR

DETONATOR
WIRES

12-in.-O.D.
RMG 2C4 SPHERE

3/8 g PETN
CHARGE

1-3/8 in.

THREAD SUPPORT

(a) NEARBY FAULT

12-in.-O.D.
RMG 2C4 SPHERE

DETONATOR
WIRES

3-in.-DIA. FAULT
0.005 in. MYLAR
WAX PAPER
0.005 in. MYLAR
FAULT EPOXIED
TO CHARGE

3/8 g PETN
CHARGE

45°

(b) FAULT THROUGH CHARGE
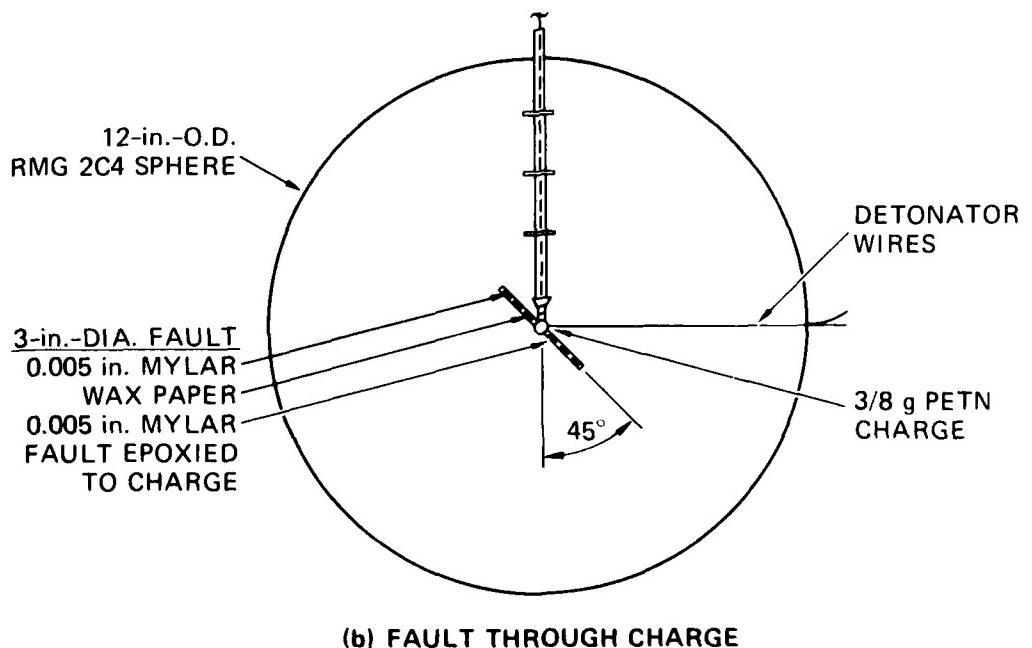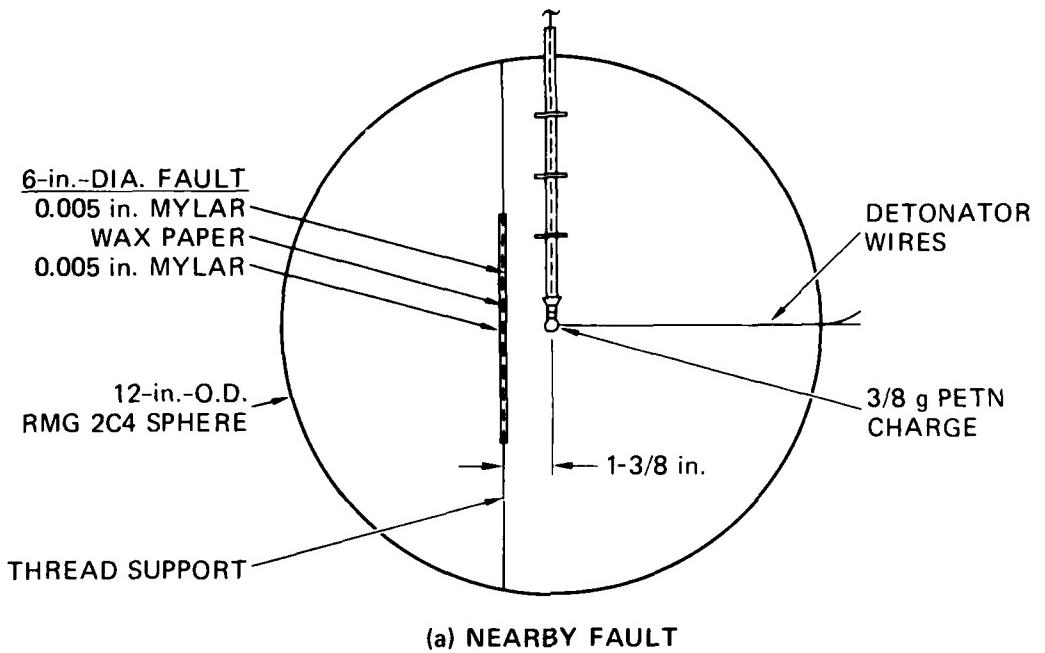
MA-8113-38

FIGURE 3.32   CONFIGURATIONS FOR FAULT PLANE TESTS

97
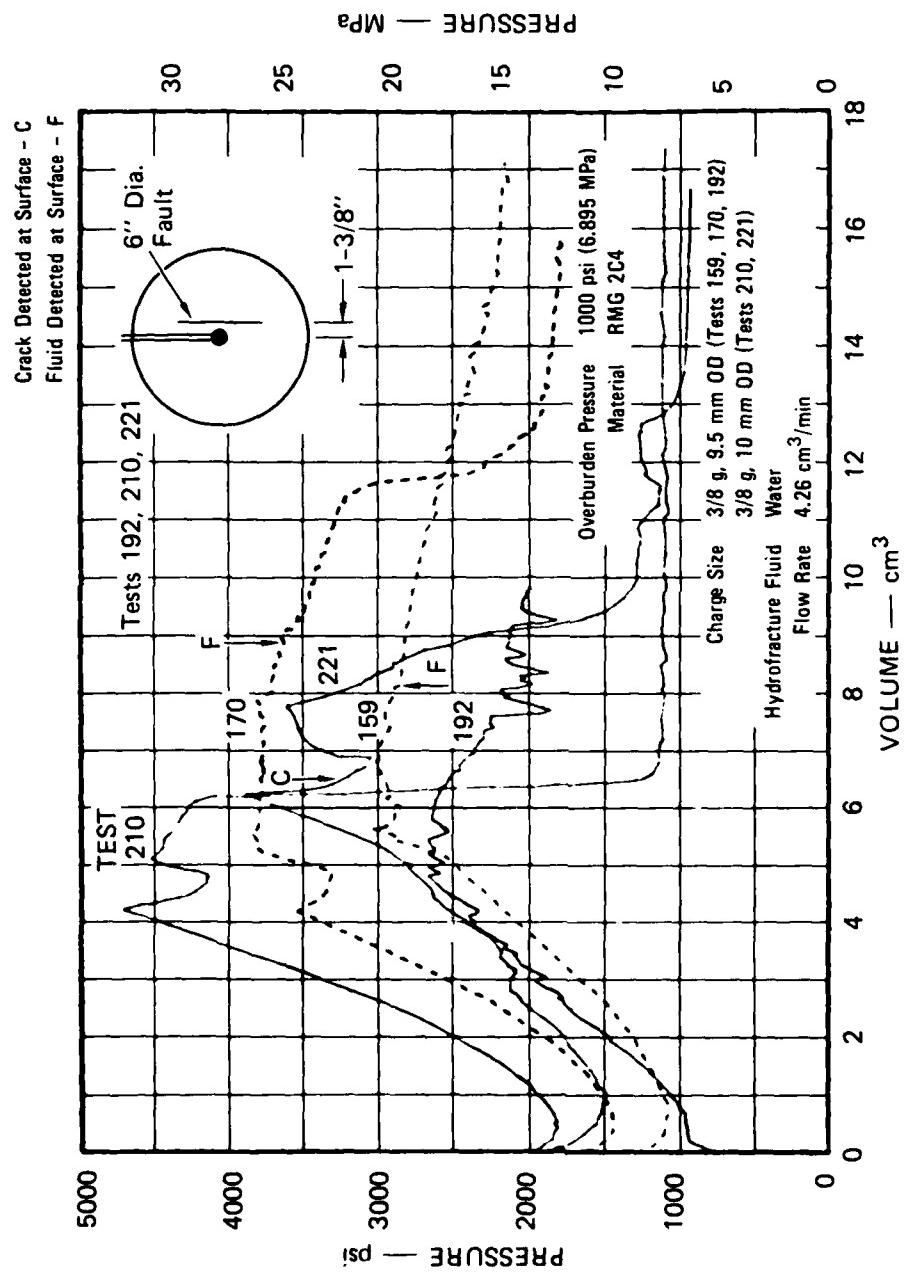
FIGURE 3.33 HYDROFRACTURE PRESSURES FOR UNVENTED EXPLODED CAVITY TESTS 159, 170, 192, 210, AND 221 — NEARBY VERTICAL FAULT

98

MP-8113-40

FIGURE 3.34   HYDROFRACTURE FROM UNVENTED EXPLODED CAVITY
TEST 192   NEARBY VERTICAL FAULT
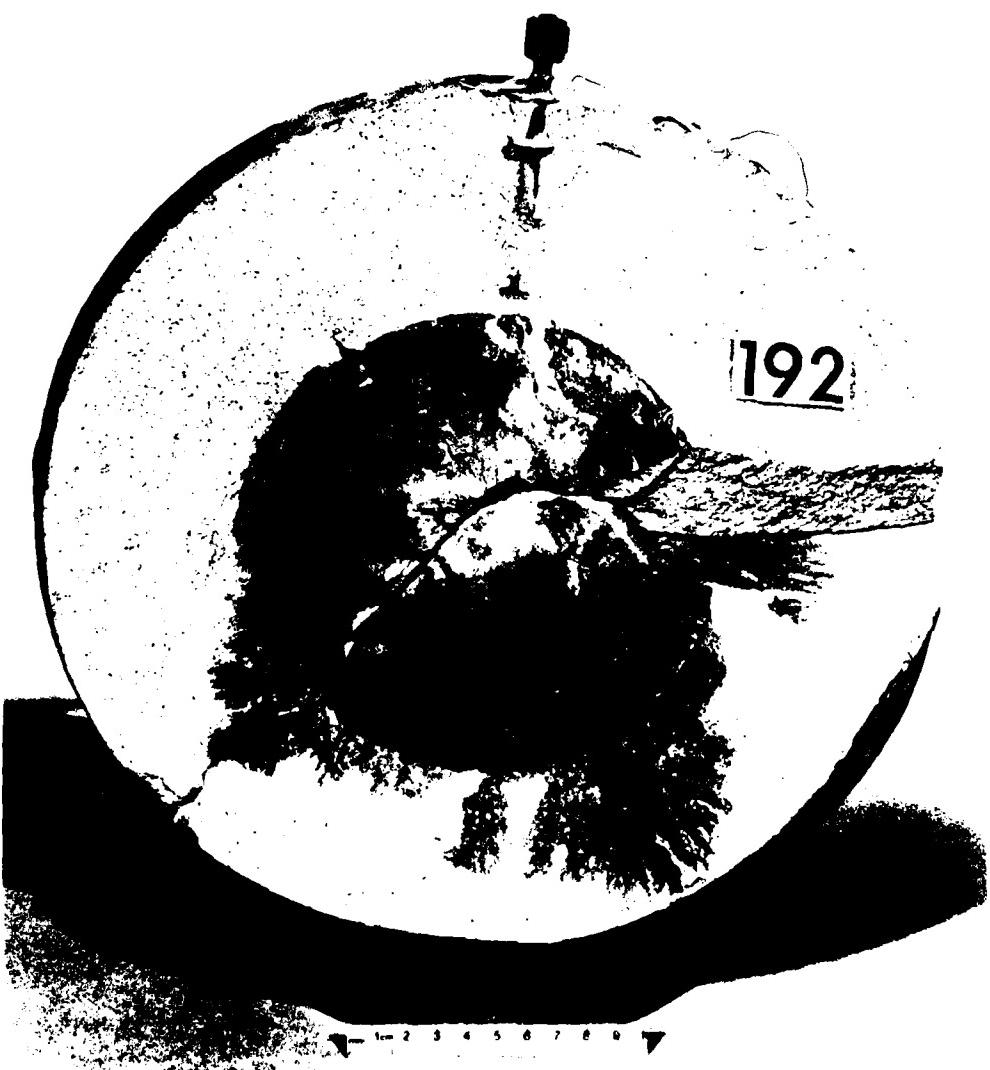
MP 8113-41

FIGURE 3.34 HYDROFRACTURE FROM UNVENTED EXPLODED CAVITY
TEST 192 NEARBY VERTICAL FAULT (Concluded)
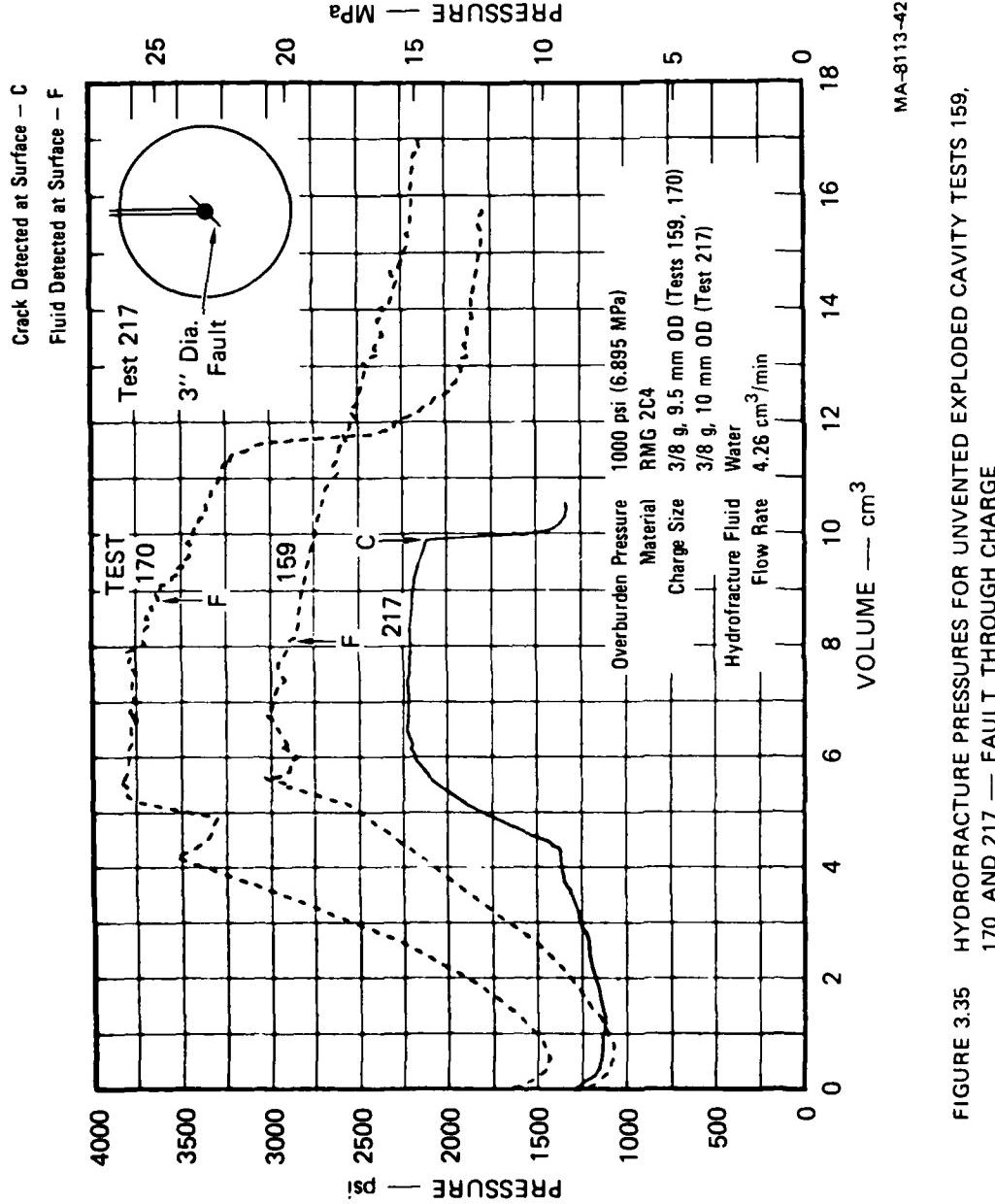
FIGURE 3.35   HYDROFRACTURE PRESSURES FOR UNVENTED EXPLODED CAVITY TESTS 159, 170, AND 217 — FAULT THROUGH CHARGE

increased slowly and erratically to a plateau at 2230 psi (15.38 MPa), indicating a continual loss of fluid. The sudden loss of cavity pressure at the end of the plateau corresponds to the detection of a surface crack. The absence of a distinct fracture initiation spike in the pressure record suggests that fluid loss occurred along the fault. Figure 3.36 shows that a fracture extended to the surface of the sphere along the plane of the fault.

217
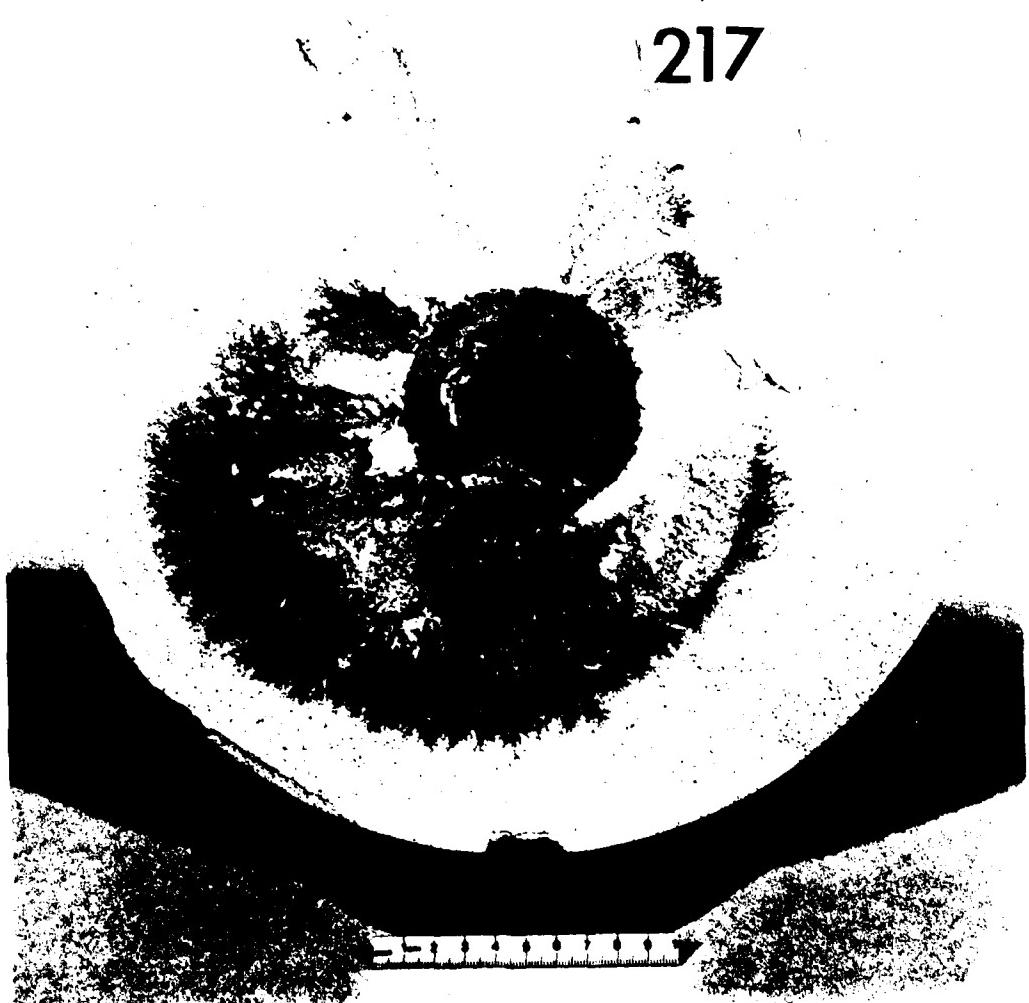
MP-8113-43

FIGURE 3 36   HYDROFRACTURE FROM UNVENTED EXPLODED CAVITY
TEST 217   FAULT THROUGH CHARGE

MP 8113-44

FIGURE 3.36   HYDROFRACTURE FROM UNVENTED EXPLODED CAVITY
TEST 217   FAULT THROUGH CHARGE (Concluded)

Appendix A

FRACTURE MECHANICS ANALYSIS

A fracture mechanics analysis is presented here as an aid to inter-
preting the hydrofracture records of the unexploded cavity tests. The
analytical results are formulas for the pressure in a penny-shaped crack
that will cause crack propagation in an infinite elastic medium. The
formulas are used to show the relationship between pressure distribution
and crack stability. The pressure is taken as uniform over a constant
central circular area that represents the unexploded cavity, and different
pressure distributions are considered in the surrounding annular region
that represents a crack propagating from a spherical cavity. Pressures
required to start expansion of the circular crack from the constant cen-
tral circular region are modified by predictions of the plate edge notch
formulas that are presented.

The stress intensity factor K_I for a penny-shaped crack of radius a,
subjected to an axisymmetric pressure distribution $p(r)$ inside the crack
is[11]

$$K_I = \frac{2}{(\pi a)^{1/2}} \int_0^a \frac{r p(r) dr}{(a^2 - r^2)^{1/2}} \qquad \text{(A-1)}$$

A concentric region of radius b equal to that of the spherical cavity
in the experiments is taken to be loaded by a uniform pressure distri-
bution. The outer annular region is subjected to one of two loadings:
(1) the same pressure as the central region so that the pressure is
uniform throughout the crack or (2) a pressure that decreases linearly
from the central region pressure to zero at the crack tip. Expressed
mathematically, these two cases are

$$p(r) = P \qquad\qquad 0 < r < a \qquad\qquad\qquad (A\text{-}2)$$

$$p(r) = \begin{cases} P & 0 < r < b \\[2mm] P\,\dfrac{a-r}{a-b} & b < r < a \end{cases} \qquad\qquad (A\text{-}3)$$

Substituting pressure distributions (A-2) and (A-3) into the integral in formula (A-1) and integrating provides the corresponding stress intensity factors. As the pressure P is increased in each case, the stress intensity factor is increased. When the pressure reaches the critical value P_c that makes the stress intensity factor equal to the fracture toughness, K_{Ic}, a material property, the crack is about to grow. If an incremental increase in P_c results in an incremental increase in the crack radius a, while imposing the same pressure distribution, the crack growth is stable. If an incrementally larger crack radius requires an incrementally smaller pressure to maintain $K_I = K_{Ic}$, the crack growth is unstable. For the above two loading cases substitution in (A-1), integration, and use of $K_I = K_{Ic}$ gives the critical pressures P_c in the form

$$\frac{2P_c}{K_{Ic}}\left(\frac{b}{\pi}\right)^{\!1/2} = \begin{cases} \dfrac{1}{F_1(\alpha)} & \text{(case 1-uniform)} & (A\text{-}4) \\[4mm] \dfrac{1}{F_2(\alpha)} & \text{(case 2-linear)} & (A\text{-}5) \end{cases}$$

In (A-4) and (A-5),

$$F_1(\alpha) = \alpha^{1/2} \qquad\qquad\qquad\qquad\qquad\qquad\qquad (A\text{-}6)$$

$$F_2(\alpha) = \frac{\alpha^{1/2}}{2\left(1 - \frac{1}{\alpha}\right)}\left[\left(2 - \frac{1}{\alpha}\right)\left(1 - \frac{1}{\alpha^2}\right)^{\!1/2} - \frac{\pi}{2} + \sin^{-1}\!\left(\frac{1}{\alpha}\right)\right] + F_3(\alpha) \qquad (A\text{-}7)$$

where α = a/b. According to the model, b is a constant equal to the spherical cavity radius, so an increase of α from its initial value of unity means an increase of the crack radius a. When a = b, that is, when α = 1, the crack has a radius b and is subjected to a uniform pressure over its entire surface, so the starting critical pressure is given by the classical result

$$\frac{2P_c}{K_{Ic}} \left(\frac{b}{\pi}\right)^{\frac{1}{2}} = 1 \tag{A-8}$$

When α = 1, the functions (A-6) and (A-7) each have the value unity, which makes formulas (A-4) and (A-5) initially consistent with formula (A-8).

Figure A.1 shows the variation of critical pressure with crack radius. In case 1, a uniform pressure always acts over the entire crack surface. Such a condition may be realized approximately by pressurizing fluid of very low viscosity or by using a very slow pumping rate. The crack growth is unstable in that larger cracks require less pressure just to keep them stationary. In case 2, the pressure applied in the crack decreases linearly from the uniform pressure in the initial penny-shape to zero at the crack tip. Such a condition may be realized approximately by pressurizing a very viscous fluid. The crack growth is initially stable until the crack radius is about 2-1/2 times the initial radius. Further growth is unstable.

It has been shown[11] that the displacement normal to the face of a penny-shaped crack that is internally pressurized is

$$v(r) = \frac{4(1 - \nu^2)a}{\pi E} \int_{r/a}^{1} \frac{\mu d\mu}{(\mu^2 - r^2/a^2)} \int_{o}^{1} \frac{xp(\mu ax)dx}{(1 - x^2)} \tag{A-9}$$
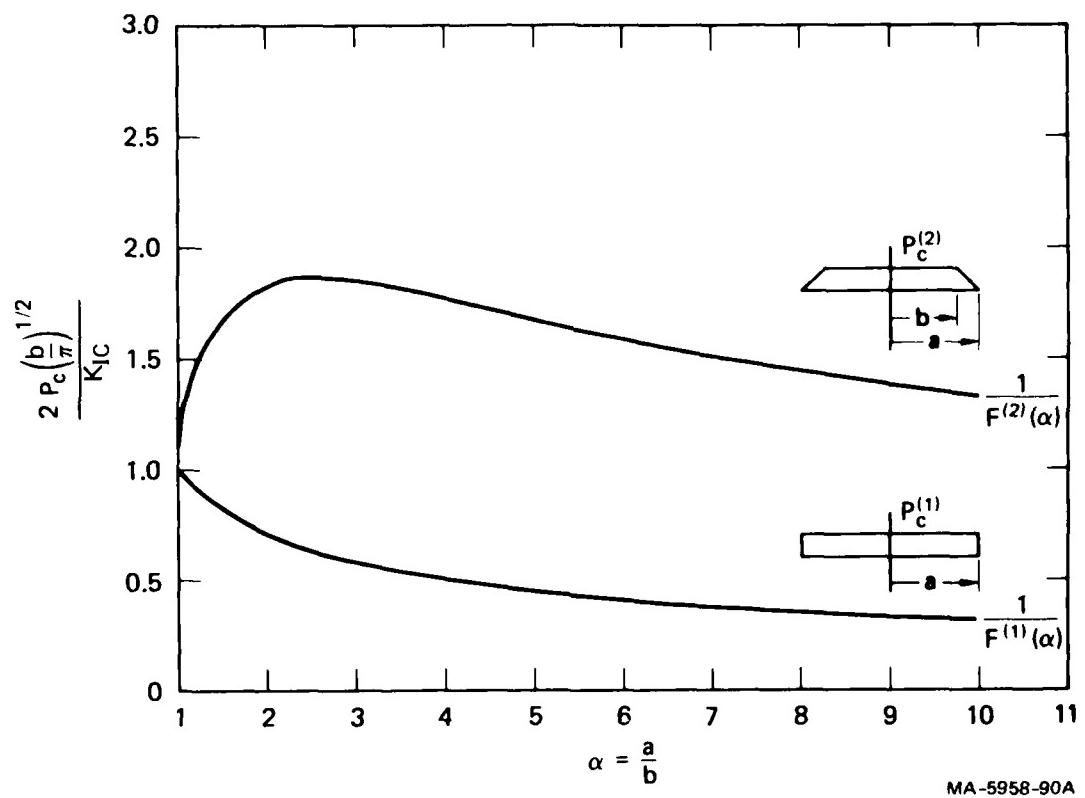
FIGURE A.1 CRITICAL PRESSURE CURVES FOR A PRESSURIZED PENNY-SHAPED CRACK

where E and ν are Young's modulus and Poisson's ratio for the elastic medium. For a uniform pressure of case 1, formula (A-9) reduces to

$$w(r) = \frac{4(1 - \nu^2)aP}{\pi E} \left(1 - \frac{r^2}{a^2}\right)^{\frac{1}{2}} \tag{A-10}$$

which gives a crack volume of

$$V = 16(1 - \nu^2)a^3 P/3E \tag{A-11}$$

The critical pressure-crack radius relationship is given by (A-4) and (A-6), so elimination of the radius in (A-11) leads to the pressure-volume relationship

$$V = \frac{(1 - \nu^2)\pi^3 K_{Ic}^6}{12EP_c^5} \tag{A-12}$$

This relationship is shown in Figure A.2 for K_{Ic} = 400 psi $\sqrt{in.}$ (0.44 MPa $\sqrt{m}$). For comparison, the water hydrofracture record for test 165 conducted at zero overburden is also shown. Theoretical and experimental data both indicate a monotonic decay of cavity pressure following fracture initiation. Closer agreement between the curves would be realized if pore fluid migration were included in the fracture mechanics analysis.

A determination of fracture initiation pressure requires an assumption on the initial size of the crack, that is, the initial flaw size inherent in the material or caused by the manufacturing process. If the flaw is idealized to a circular notch around the cavity and if the depth of the notch is small relative to the cavity radius, an approximation to the stress intensity factor may be taken as that for an edge notch. The tensile stress acting on the notch is the circumferential stress at the cavity caused by internal and external pressures, p_a and p_b. As shown in Figure A.3(a), this stress is $p_a/2 - 3p_b/2$, and the stress intensity factor is[12]
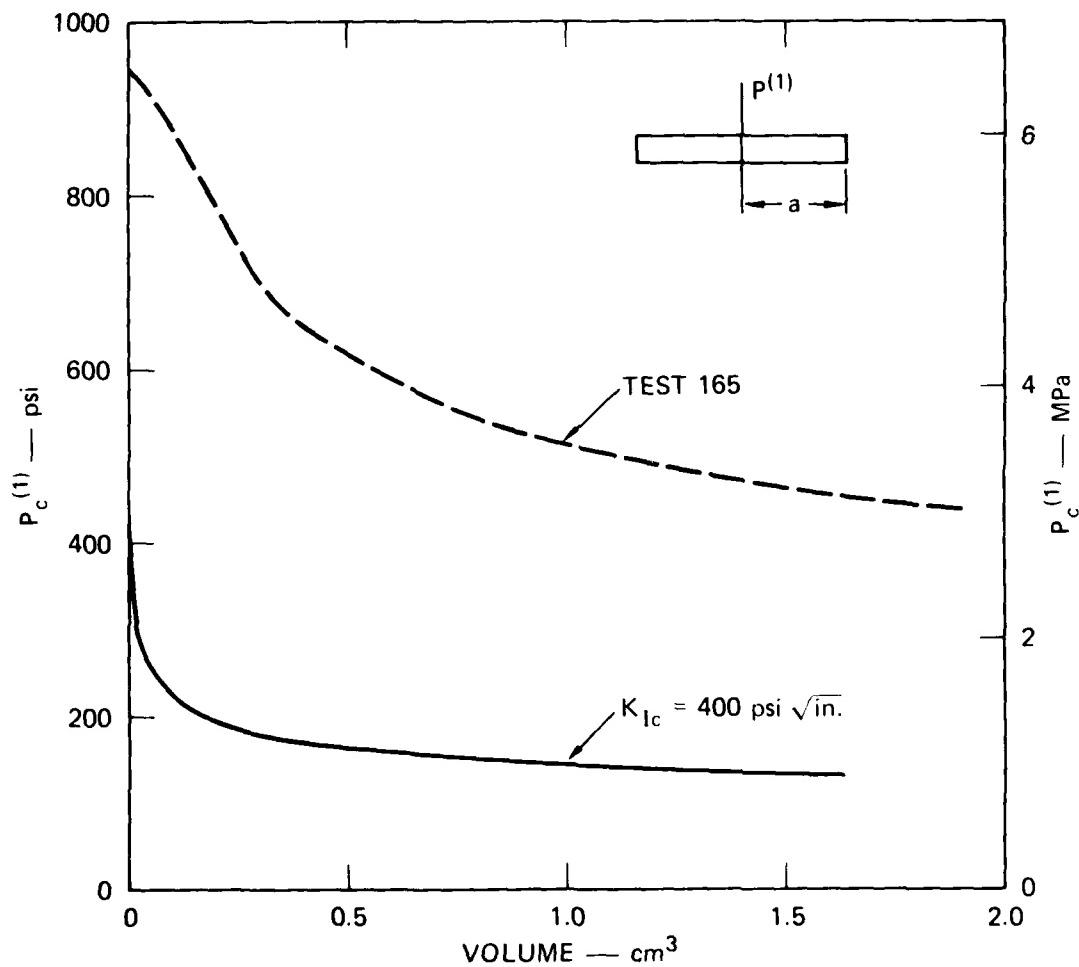
FIGURE A.2 PRESSURE-VOLUME RELATIONSHIP FOR A UNIFORMLY PRESSURIZED CRACK

MA-8113-53

A-6
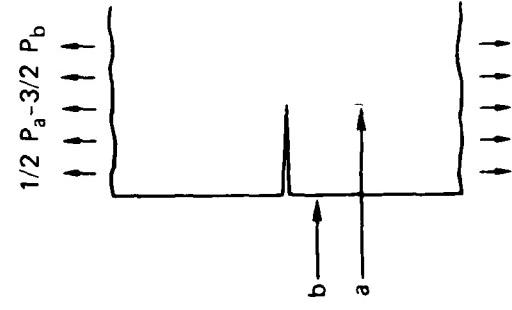
(a) $K_1 = 1.12 (1/2\ P_a - 3/2\ P_b)[\pi(a-b)]^{1/2}$
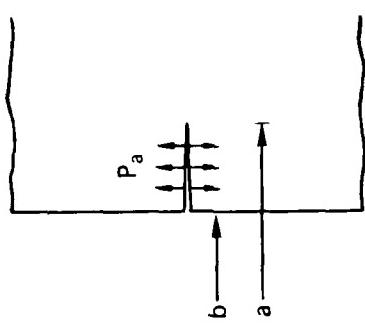
(b) $K_1 = 1.12\ P_a [\pi(a-b)]^{1/2}$
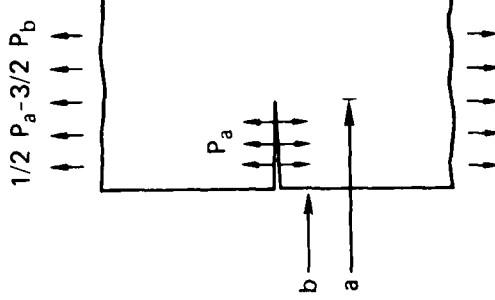
(c) $K_1 = 1.12 \times 3/2\ (P_a - P_b)[\pi(a-b)]^{1/2}$

MA-5958-147

FIGURE A.3   STRESS INTENSITY FACTORS FOR EDGE NOTCH

$$K_I = 1.12 \left[\frac{1}{2} p_a - \frac{3}{2} p_b \right] [\pi(a - b)]^{\frac{1}{2}} \qquad (A-13)$$

For a constant fluid pressure p_a in an edge notch, as shown in Figure A.3(b) the stress intensity factor is[12]

$$K_I = 1.12 \, p_a \, [\pi(a - b)]^{\frac{1}{2}} \qquad (A-14)$$

Superposition of the loading states, as shown in Figure A.3(c) gives the stress intensity factor that is the sum of (A-13) and (A-14), namely,

$$K_I = 1.12 \left\{ \frac{3}{2} (p_a - p_b)[\pi(a - b)]^{\frac{1}{2}} \right\} \qquad (A-15)$$

The critical pressure difference is therefore, from (A-15),

$$p_a - p_b = \frac{K_{1c}}{1.68[\pi(a - b)]^{\frac{1}{2}}} \qquad (A-16)$$

The above analysis is now used to explain the dependence of fracture initiation pressure on hydrofracture fluid viscosity and overburden as shown in Figure 3.5 of the main text of this report.

All tests were performed with a constant flow rate of 4.26 cm^3/min into 3/4-inch-diameter (1.90-cm) smooth cavities. The fracture initiation pressures for glycerol are well above those for water. We postulate that at the cavity wall an edge notch exists that is subjected to a uniform internal pressure, which is the pressure in the hydrofracture fluid. If the overburden and cavity pressures are p_b and p_a and the notch length is c, the stress intensity factor K_I is

$$K_I = 1.68 \, (p_a - p_b)(\pi c)^{\frac{1}{2}} \qquad (A-17)$$

From the results for water in Figure 3.5, $p_a - p_b$ = 800 psi (5.52 MPa) and from fracture tests on 2C4 the fracture toughness is K_{Ic} = 400 psi $\sqrt{in.}$ (0.44 MPa$\sqrt{m}$). If we set $K_I = K_{Ic}$ and use the experimentally determined pressure difference, equation (A-17) gives a constant crack length of c = 28 mils (0.71 mm).

There is no reason to assume that the inherent initial crack length is different in the 2C4 grout spheres that were hydrofractured with glycerol. The hydrostatic fracture mechanism just outlined leads to the same fracture initiation pressure in glycerol as that in water. It is postulated, therefore, that glycerol initiates fracture at the same uniform pressure as water, but immediately after the crack tip moves and allows the glycerol to commence flow in the crack, the viscosity causes a substantial redistribution of pressure in the crack. The pressure falls to a low value near the crack tip and, because of the constant pumping rate, it rises in the cavity. This pressure redistribution creates a lower stress intensity factor. As an example, we approximate the pressure distribution by a linear decrease from p_a in the cavity to p_c near the crack tip. The stress intensity factor is then

$$K_I = [1.68 \, (p_a - p_b) - 0.68 \, (p_a - p_c)](\pi c)^{\frac{1}{2}} \qquad \text{(A-18)}$$

Assuming that the crack has moved only a small amount to start flow along the crack, we see that when the experimental values of p_a = 2700 psi (18.62 MPa) and p_b = 1000 psi (6.90 MPa) again initiate crack growth we have p_c = 483 psi (3.33 MPa) near the crack tip. If the crack were 49 mils (1.24 mm) long at this stage instead of 28 mils (0.71 mm) long, we would have p_c = 0 near the crack tip when crack growth was restarted by p_a = 2700 psi and p_b = 1000 psi. For radial laminar flow in a crack of constant thickness h and length c encircling a cavity of radius a, the pressure drop from the cavity to the crack tip is

$$p_a = 12\mu(Q/2\pi a)c/h^3 \qquad \text{(A-19)}$$

Hence a pressure drop of 2700 psi (18.62 MPa) in a crack of length
49 mils (1.24 mm) extending from a cavity of 3/8 inch (0.95 cm) radius
implies a crack thickness of h = 0.3 mils (0.0076 mm). All the above
numbers in the example seem practical.

If the crack in the cavity is approximated by a penny-shaped crack,
a pressure distribution in the crack that decreases from the cavity
pressure to zero at the tip produces stable crack growth followed by
unstable crack growth as shown in Figure A.1; thus, some growth is
possible during the initial pressure rise of the hydrofracture record.
Such stable growth probably accounts for the maximum slope of the initial
pressure rise portions of the hydrofracture record frequently being at
pressures below the peak pressure.

Finally, differentiation of (A-17) yields the theoretical slope of
the fracture initiation versus overburden curve for both water and
glycerol hydrofracture, that is,

$$\frac{dp_a}{dp_b} = 1 \qquad\qquad (A\text{-}20)$$

which is in agreement with the experimental data for RMG 2C4 shown
earlier in Figure 3.5.

Appendix B

POROUS FLOW ANALYSIS

A porous flow analysis based on the work of Rice and Cleary[13] is presented here as an aid to understanding the decay of an explosively generated residual stress field surrounding a spherical cavity. The analytic results are formulas for the stress-induced flow of interstitial fluid in a porous solid. The formulas are used to show the relationships between pore pressure and the effective stresses acting on the solid matrix. The initial pore pressure distribution is approximated by the mean normal stress associated with a calculated residual stress field. Equations are specialized for the case of spherically symmetric motion.

The total stresses σ_{ij} acting on a material element and the pore pressure p are defined as the basic state variables and are assumed related in some appropriate fashion to the strains of the solid ϵ_{ij} and the mass m of pore fluid per unit reference volume. The linearized constitutive relations for a fluid-saturated porous elastic solid are presented for quasi-static elastic deformation in which local equilibrium of the pore fluid can be assumed.

For the strains of the solid

$$2G\epsilon_r = \sigma_r - \frac{\nu}{1 + \nu} (\sigma_r + 2\sigma_\theta) + \frac{3(\nu_u - \nu)}{B(1 + \nu)(1 + \nu_u)} p \qquad (B-1)$$

$$2G\epsilon_\theta = \sigma_\theta - \frac{\nu}{1 + \nu} (\sigma_r + 2\sigma_\theta) + \frac{3(\nu_u - \nu)}{B(1 + \nu)(1 + \nu_u)} p \qquad (B-2)$$

where G and ν are the shear modulus and Poisson ratio when the material is deformed under drained conditions, ν_u is the undrained Poisson ratio, and B is defined by the relation between initial induced pore pressure and the total hydrostatic stress acting on an element. That is,

$$\Delta p = -B \frac{\Delta(\sigma_r + 2\sigma_\theta)}{3} \tag{B-3}$$

The elastic constants ν_u and B may be determined directly from the result of a single undrained test in which the Poisson effect and induced pore pressure are measured.

For the mass of pore fluid per unit reference volume

$$m - m_o = \frac{3\rho_o(\nu_u - \nu)}{2GB(1 + \nu)(1 + \nu_u)} \left(\sigma_r + 2\sigma_\theta + \frac{3p}{B}\right) \tag{B-4}$$

where m_o and ρ_o are the fluid mass content of an element and the fluid density for the unstressed state.

The constitutive law governing pore fluid diffusion, D'Arcy's law, is

$$q = -\rho_o \kappa \frac{\partial p}{\partial r} \tag{B-5}$$

where q is the fluid mass flow rate in the radial direction per unit area and κ is the permeability.

The field equations are also developed for quasi-static response. Equilibrium of stresses requires that

$$\frac{\partial \sigma_r}{\partial r} + \frac{2}{r}(\sigma_r - \sigma_\theta) = 0 \tag{B-6}$$

The kinematic relations between strain and displacement u in the radial direction,

$$\varepsilon_r = \frac{\partial u}{\partial r} \qquad \text{and} \qquad \varepsilon_\theta = \frac{u}{r} \qquad\qquad (B-7)$$

lead to the compatibility equations as follows:

$$\frac{\partial \varepsilon_\theta}{\partial r} = \frac{1}{r}\frac{\partial u}{\partial r} - \frac{u}{r^2} = \frac{1}{r}(\varepsilon_r - \varepsilon_\theta)$$

$$\frac{\partial \varepsilon_\theta}{\partial r} + \frac{1}{r}(\varepsilon_\theta - \varepsilon_r) = 0 \qquad\qquad (B-8)$$

Use of equilibrium (B-6) and the constitutive relations (B-1 and B-2) in the compatibility condition (B-8) yields

$$\frac{\partial}{\partial r}(\sigma_r + 2\sigma_\theta + 4np) = 0 \qquad\qquad (B-9)$$

where

$$n = \frac{3(\nu_v - \nu)}{2B(1 + \nu_u)(1 - \nu)} \qquad\qquad (B-10)$$

Hence from (B-9)

$$\sigma_r + 2\sigma_\theta + 4np = C_1(t) \qquad\qquad (B-11)$$

The final governing equation is for mass conservation of the infiltrating pore fluid

$$\frac{\partial q}{\partial r} + \frac{2}{r}q = -\frac{\partial m}{\partial t} \qquad\qquad (B-12)$$

B-3

Use of (B-4) and (B-5) in (B-12) yields

$$- c \left(\frac{\partial^2 p}{\partial r^2} + \frac{2}{r} \frac{\partial p}{\partial r} \right) = - \frac{3 \sigma_o (\nu_u - \nu)}{2GB(1 + \nu)(1 + \nu_u)} \frac{\partial}{\partial t} \left(\sigma_r + 2\sigma_\theta + \frac{3p}{B} \right) \quad (B-13)$$

Combining (B-12) and (B-13) gives

$$c \left(\frac{\partial^2 p}{\partial r^2} + \frac{2}{r} \frac{\partial p}{\partial r} \right) = \frac{\partial p}{\partial t} + \frac{2(\nu_u - \nu)}{(1 - \nu_u)(1 + \nu)} \frac{dC_1(t)}{dt} \quad (B-14)$$

where c is the coefficient of consolidation and is given by

$$c = k \left[\frac{2G(1 - \nu)}{(1 - 2\nu)} \right] \left[\frac{B^2(1 + \nu_u)^2 (1 - 2\nu)}{9(1 - \nu_u)(\nu_u - \nu)} \right] \quad (B-15)$$

Use of (B-11) to eliminate σ_θ in (B-6), and integration of the result subject to the condition $\sigma_r(r = a) = \sigma_r(a)$ yields

$$\sigma_r = \frac{1}{3} \left(1 - \frac{a^3}{r^3} \right) C_1(t) + \sigma_r(a) \frac{a^3}{r^3} - \frac{4\eta}{r^3} \int_a^r \sigma^2 p(\sigma, t) d\sigma \quad (B-16)$$

Equation (B-14) governs pore pressure distribution. Equations (B-11) and (B-16) govern the change in stress associated with a change in pore pressure. For the special case of an infinite medium, $\sigma_r(\infty) = \sigma_\theta(\infty) = p(\infty) = 0$. Hence (B-11) requires that $C_1(t) = 0$.

We apply these results assuming that the 2C4 properties are not changed by the explosion. Consider the infinite region surrounding an exploded cavity. Assume that the step function shown in Figure B.1(a) approximates the initial pore pressure resulting from charge detonation. The height of the step is determined from the mean normal stress associated with a calculated residual stress field.[9] The width of the step is taken as the extent of the undyed region associated with hydrofracture of an exploded cavity sphere. Hence the initial pore pressure distribution is

B-4
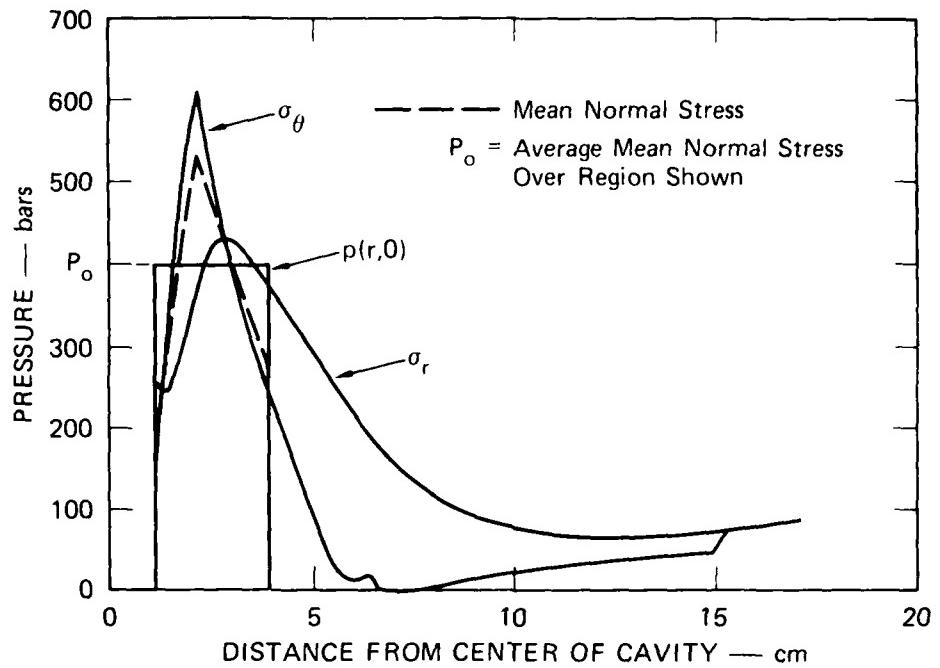
(a) INITIAL PORE PRESSURE DISTRIBUTION
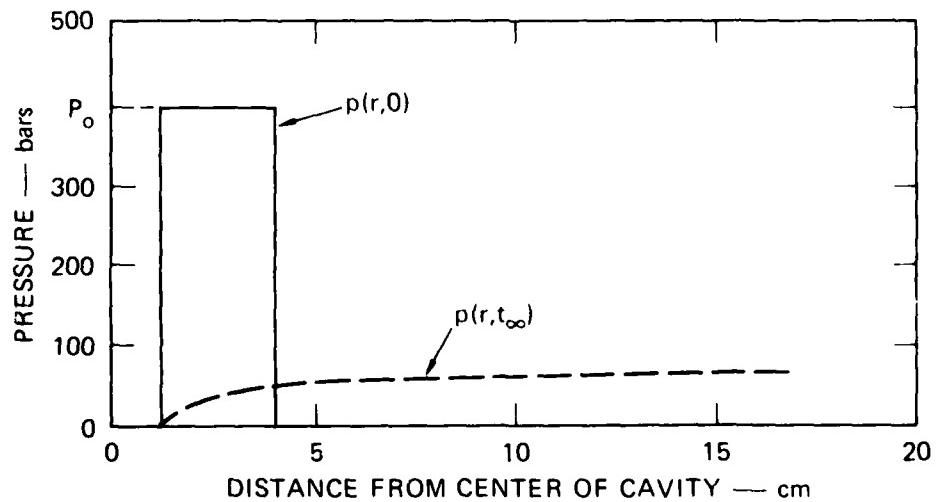
(b) LATE-TIME PORE PRESSURE DISTRIBUTION

MA-8113-54

FIGURE B.1 PORE PRESSURE DISTRIBUTION NEAR AN EXPLODED CAVITY

$$p(r,0) = \begin{cases} P_o & a < r < b \\ \\ 0 & r > b \end{cases} \qquad (B-17)$$

The radial and tangential stresses associated with (B-17) are determined from (B-11) and (B-16) with $C_1(t) = 0$:

$$\sigma_r(r,0) = - \frac{4\eta p_o}{r^3} \int_a^r \rho^2 d\rho = - \frac{4\eta p_o}{r^3} \left(\frac{r^3 - a^3}{3} \right) \qquad a < r < b \qquad (B-18)$$

$$\sigma_r(r,0) = - \frac{4\eta p_o}{r^3} \int_a^b \rho^2 d\rho = - \frac{4\eta p_o}{r^3} \left(\frac{b^3 - a^3}{3} \right) \qquad r > b \qquad (B-19)$$

$$\sigma_\theta(r,0) = - 2\eta p_o - \frac{2\eta p_o}{r^3} \left(\frac{r^3 - a^3}{3} \right) \qquad a < r < b \qquad (B-20)$$

$$\sigma_\theta(r,0) = - \frac{2\eta p_o}{r^3} \left(\frac{b^3 - a^3}{3} \right) \qquad r > b \qquad (B-21)$$

The pore pressure distribution for $t > 0$ is given by the solution (see Reference 14) of (B-14) with $C_1(t) = 0$:

$$p(r,t) = \frac{p_o}{2r\sqrt{\pi c t}} \int_a^b \rho \left[e^{-(r-\rho)^2/4ct} - e^{-(r+\rho-2a)^2/4ct} \right] d\rho \qquad (B-22)$$

For times long enough such that

$$4 ct \gg (b - a)^2 \qquad (B-23)$$

B-6

the following approximations are valid:

$$e^{-(r-\rho)^2/4ct} \approx 1 - (r - \rho)^2/4ct \tag{B-24}$$

and

$$e^{-(r+\rho-2a)^2/4ct} \approx 1 - (r + \rho - 2a)^2/4ct \tag{B-25}$$

Substituting (B-24) and (B-25) into (B-22) and integrating yields the following approximation for late-time pore pressure distribution:

$$p(r,t_\infty) \approx \frac{2p_o}{3\sqrt{\pi}} \frac{(b-a)^2}{4ct} \frac{(b-a)}{\sqrt{4ct}} \frac{2b+a}{b-a} \left(1 - \frac{a}{r}\right) \tag{B-26}$$

Numerical values of relevant material properties are shown in Table B.1. Drained and undrained shear modulus and Poisson ratio are based on acoustic measurements performed on a saturated and partially dried specimen of RMG 2C4. Permeability was measured in a water permeameter. The value for B was estimated from a table of geological properties presented in Rice and Clary.[13] The coefficient of consolidation and η were determined from (B-15) and (B-10), respectively.

Table B.1

MATERIAL PROPERTIES FOR POROUS FLOW ANALYSIS

Property	RMG 2C4
Drained shear modulus G (psi)	1.08×10^6
Drained Poisson ratio ν	0.275
Undrained shear modulus G_u (psi)	1.03×10^6
Undrained Poisson ratio ν_u	0.282
Permeability κ (cm^4/dyne-sec)	3×10^{-12}
B	0.6
Coefficient of consolidation c (cm^2/sec)	4.24
η	0.019

The region of significant initial pore pressure is specified by taking $a = 1$ cm and $b = 4$ cm in (B-17). From (B-23), the late-time approximation is valid for

$$\frac{4ct}{(b - a)^2} = 10 \qquad (B-27)$$

or

$$t_\infty = 5.3 \text{ sec} \qquad (B-28)$$

From (B-26), the corresponding late-time pore pressure distribution is given by

$$p(r,t_\infty) \approx 0.036 \, p_o (1 - \frac{1}{r}) \qquad (B-29)$$

and is shown schematically in Figure B.1(b). If the total residual stress field generated by charge detonation is approximated by $\sigma_r = \sigma_\theta = p_o$, then the maximum percentage decay due to pore fluid migration is found from (B-18) and (B-20) as follows:

$$\frac{\sigma_r(b,0)}{p_o} = -\frac{4\eta}{3} \left(1 - \frac{a^3}{b^3}\right) = 2.5\% \qquad (B-30)$$

and

$$\frac{\sigma_\theta(b,0)}{p_o} = -\frac{2\eta}{3} \left(1 - \frac{a^3}{b^3}\right) = 1.2\% \qquad (B-31)$$

Appendix C

MATERIAL PROPERTIES

Table C.1 provides the mixtures and heat curing cycles for rock-matching grout RMG 2C4, low density rock-matching grout LD 2C4, and granite simulant GS3. Table C.2 summarizes the commonly used physical and mechanical properties.

The scatter in crush strength and tensile strength associated with the testing of a large number of 2-inch-diameter (5.08-cm) cylinders is shown in Figures C.1 through C.4. These figures show that, in general, reasonable tolerance is maintained on material strength. Additional strength properties of 2C4 and GS3 are shown in Figures C.5 and C.6.

Table C.1

MIXTURES[a] FOR ROCK-MATCHING GROUT RMG 2C4,
LOW DENSITY ROCK-MATCHING GROUT LD 2C4,
AND GRANITE SIMULANT GS3

Component	RMG 2C4	LD 2C4
Type I-II Portland cement	32.691%	32.063%
Sand (20-40 Monterey)	21.896%	21.476%
Barite (barium sulfate)	20.848%	20.447%
Bentonite (gel)	2.837%	2.783%
CFR 2 (concrete friction reducing compound)	0.078%	0.077%
Water	21.650%	21.234%
Microballoons (Q-CEL 300)	–	1.920%

Component	GS3
Type I-II Portland cement	38.573%
Sand (granite)	49.295%
Melment	1.035%
CFR 2 (concrete friction reducing compound)	0.252%
Water	10.845%

[a] 28-day aging procedure: sealed in plastic and submerged
in water with the following temperature sequence: raise
to 54°C over 48-hour period, hold at 54°C for 48 hours,
lower to 25°C over 36-hour period.

Table C.2

PROPERTIES OF ROCK-MATCHING GROUT RMG 2C4,
LOW DENSITY ROCK-MATCHING GROUT LD 2C4,
AND GRANITE SIMULANT GS3

(a) PHYSICAL PROPERTIES

| Physical Property	RMG 2C4	LD 2C4	GS3
Density (g/cm^3)			
Aged	2.15	1.90	2.42
Dry	1.75	1.57	2.27
Grain	2.87	2.68	2.80
Water by wet weight (%)	18.6	17.4	6.3
Porosity (%)	39	43	18.8
Saturation (%)	100	86	81.6
Air voids (%)	0	13.4	3.5
Longitudinal velocity (km/sec)	3.29	3.13	4.82
Shear velocity (km/sec)	1.82	1.78	2.75
Modulus in compression (psi)	2.64×10^6	2.20×10^6	6.68×10^6
Shear modulus (psi)	1.03×10^6	8.74×10^5	2.65×10^6
Bulk modulus (psi)	2.00×10^6	1.53×10^6	4.64×10^6
Poisson's ratio	0.28	0.26	0.26
Permeability (μd)	3.0	–	–

(b) MECHANICAL PROPERTIES

| Material	Average Strain Rate (sec^{-1})	Compressive Strength (psi)	Tensile Strength (psi)
RMG 2C4	Static	3970	530
RMG 2C4	0.15	5330	900
LD 2C4	Static	3200	460
LD 2C4	0.15	5000	780
GS3	Static	8900	1110
GS3	0.15	15900	1620

FIGURE C.1 UNCONFINED CRUSH STRENGTH OF ROCK-MATCHING GROUT
RMG 2C4
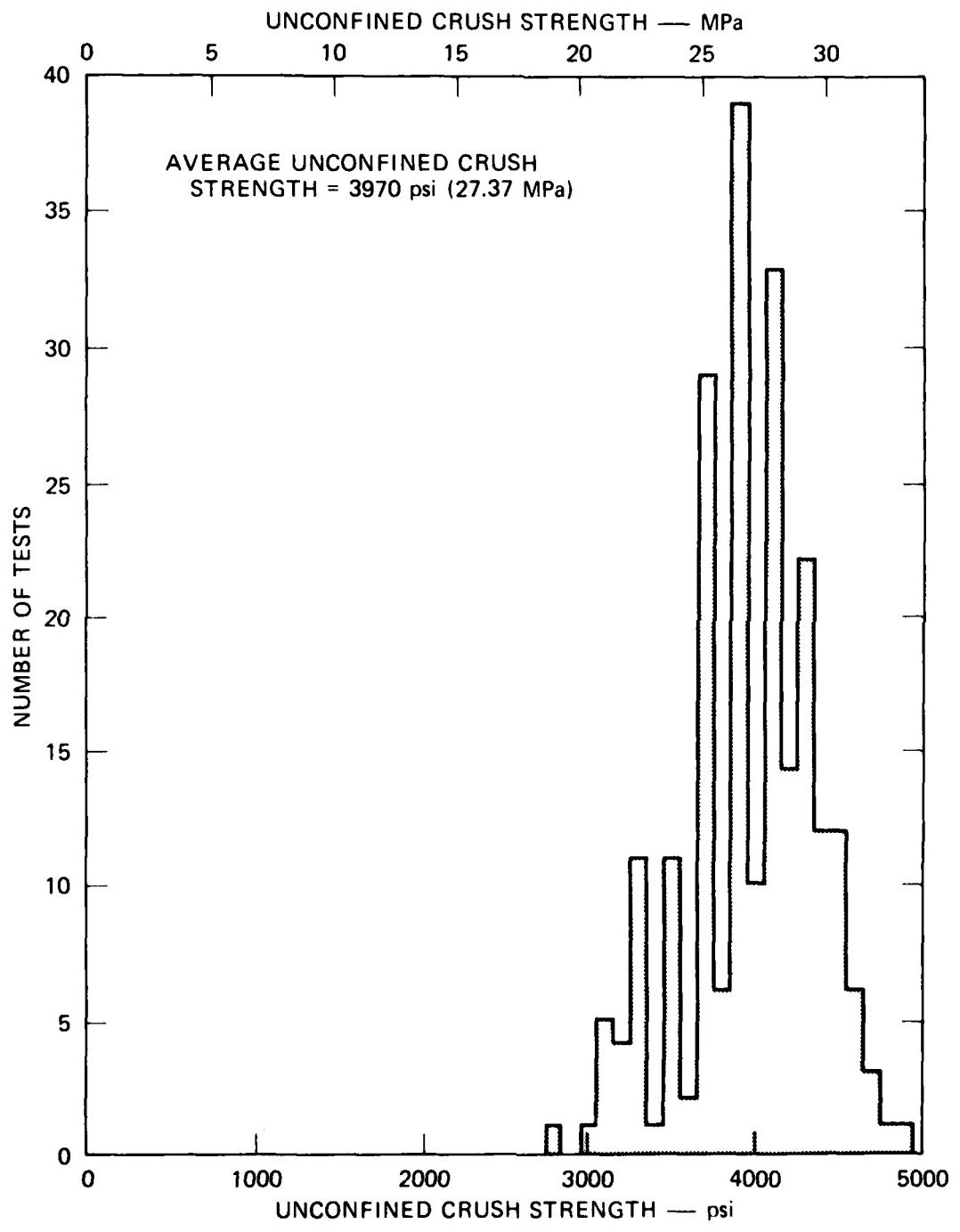
MA-5958-143A
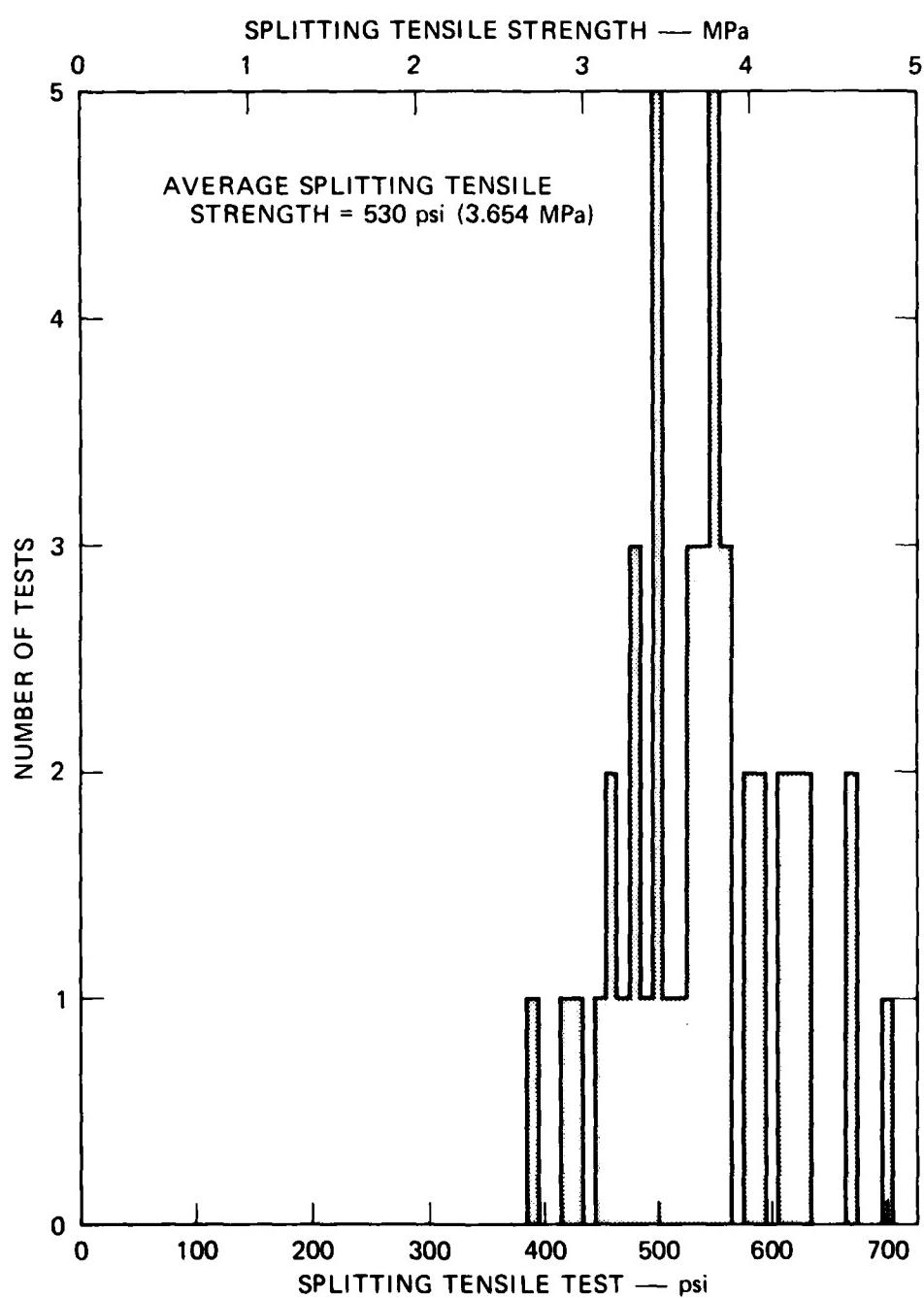
FIGURE C.2 SPLITTING TENSILE STRENGTH OF ROCK-MATCHING GROUT
RMG 2C4
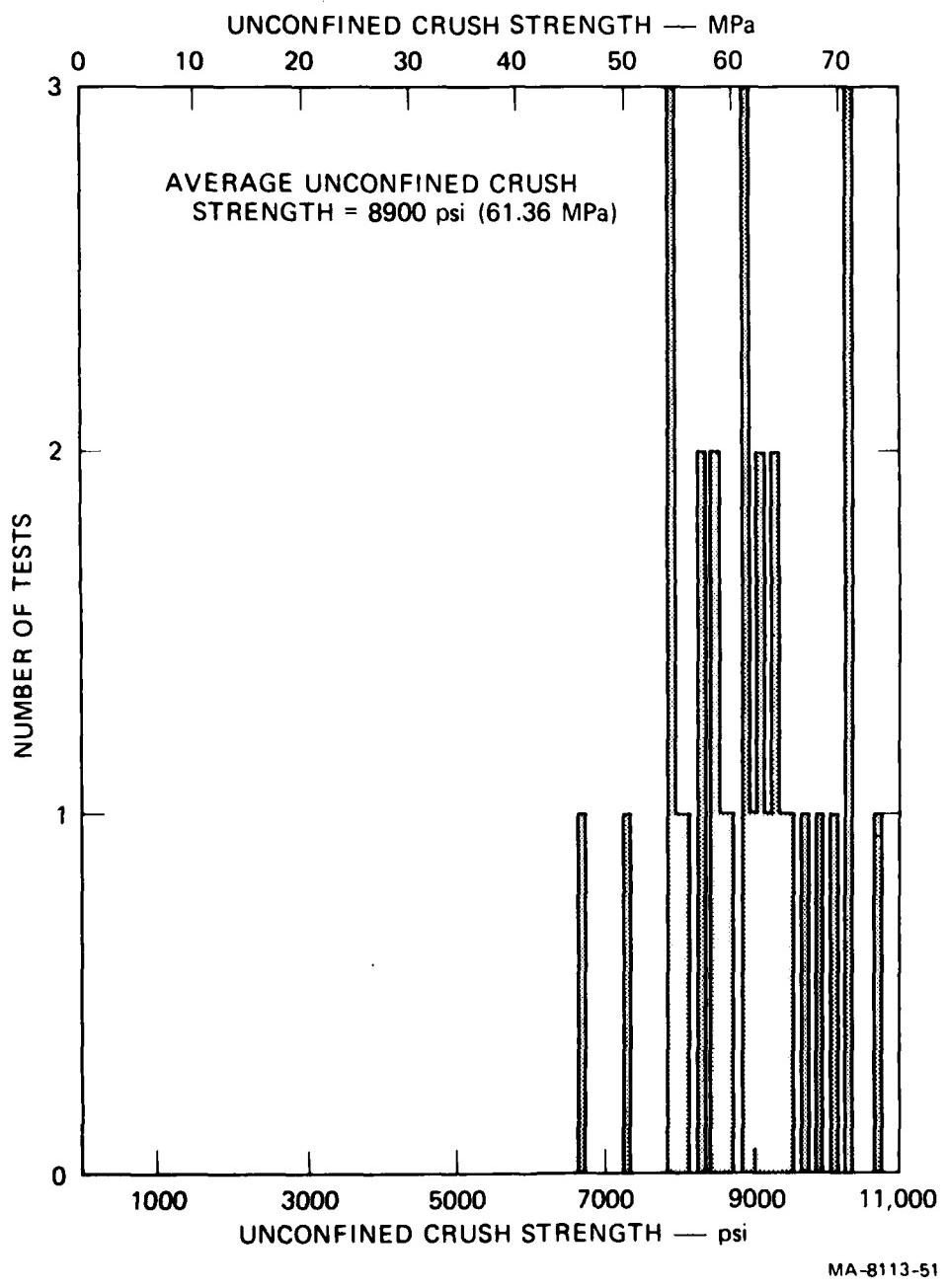
FIGURE C.3 UNCONFINED CRUSH STRENGTH OF GRANITE SIMULANT GS3

MA-8113-51

C-6
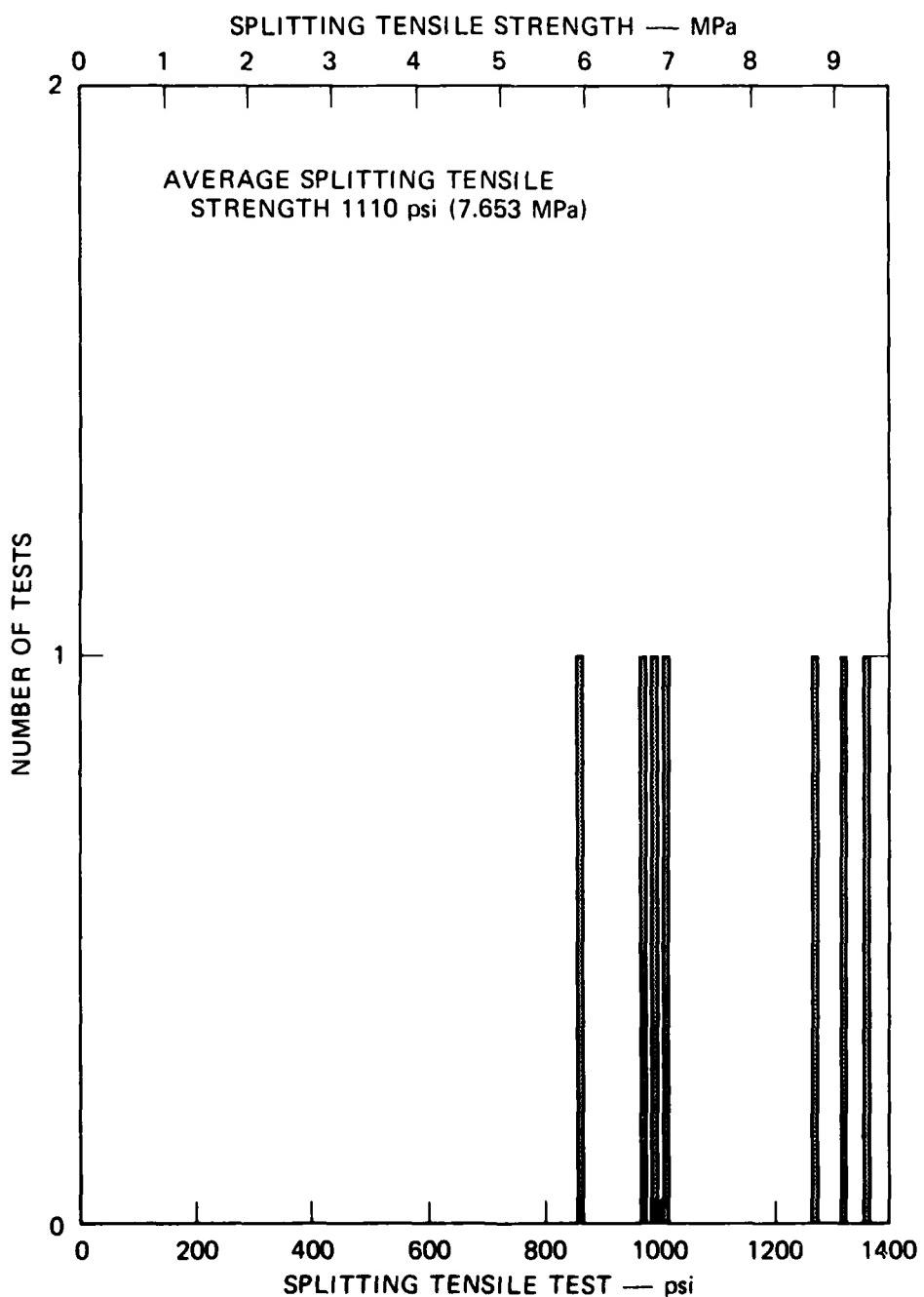
FIGURE C.4 SPLITTING TENSILE STRENGTH OF GRANITE SIMULANT GS3
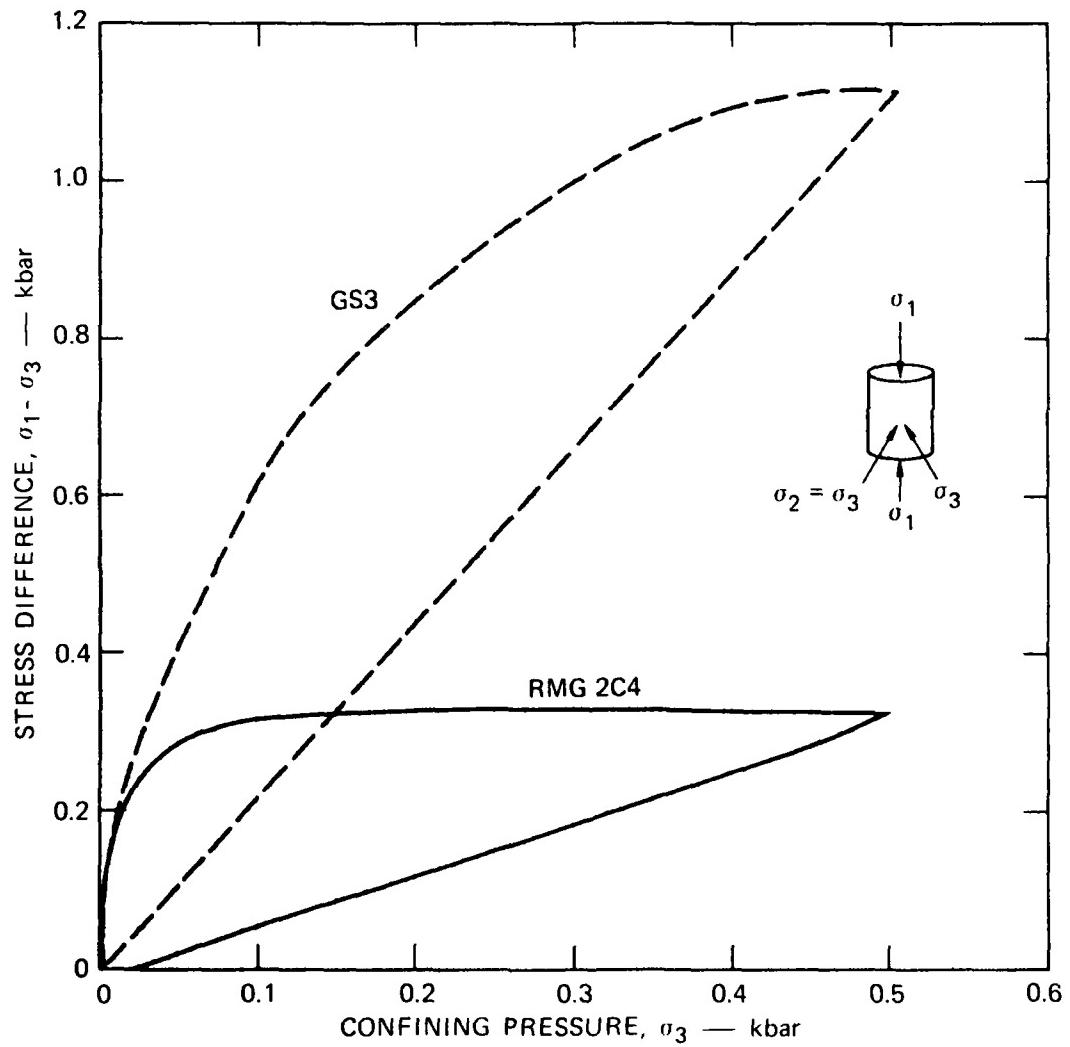
FIGURE C.5 STRENGTH PROPERTIES OF ROCK-MATCHING GROUT RMG 2C4
AND GRANITE SIMULANT GS3: STRESS DIFFERENCE VERSUS
CONFINING PRESSURE

C-8
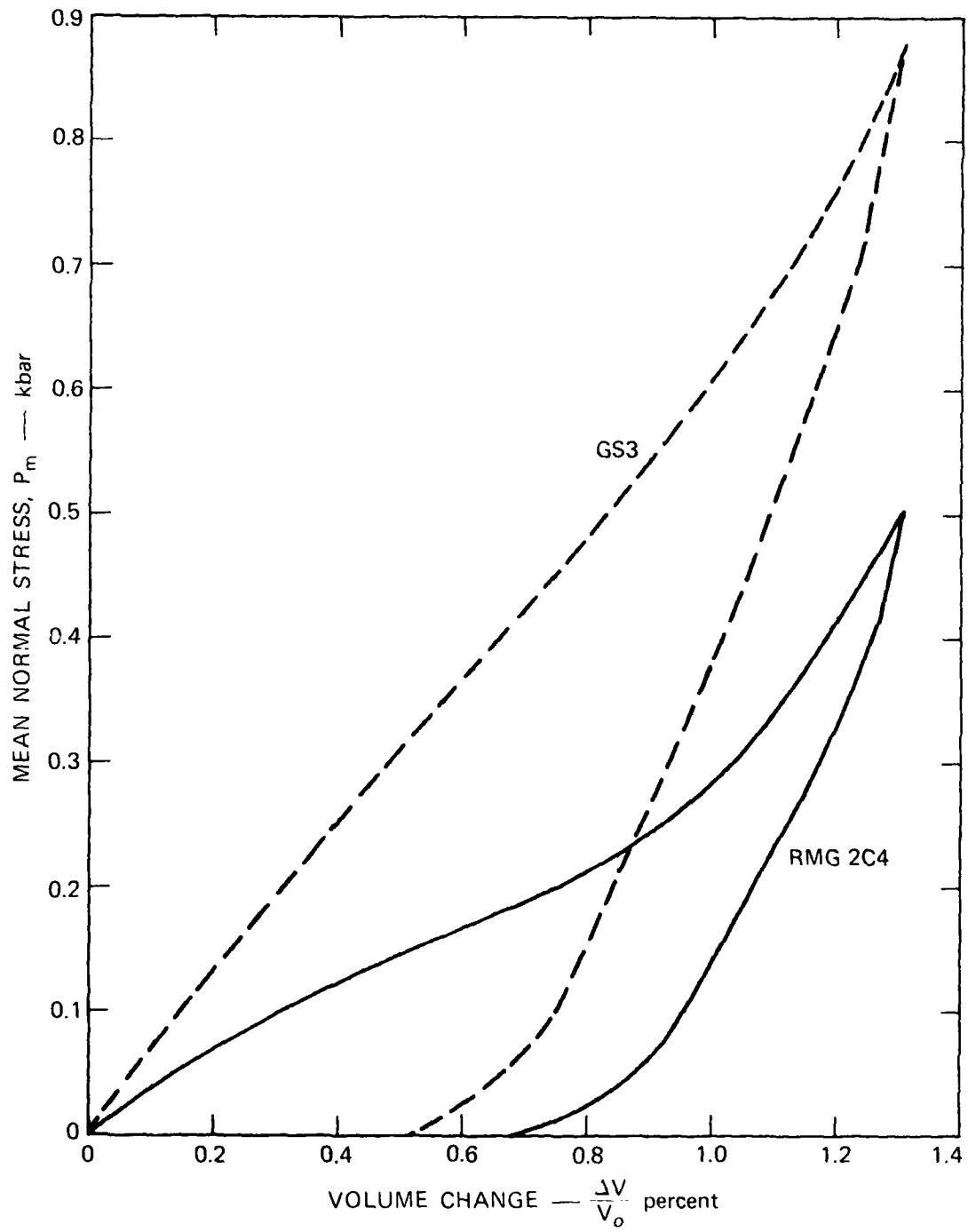
MP-5958-41

FIGURE C.6 STRENGTH PROPERTIES OF ROCK-MATCHING GROUT RMG 2C4 AND GRANITE
SIMULANT GS3: MEAN NORMAL STRESS VERSUS VOLUME CHANGE

Appendix D

SEQUENCE OF EVENTS IN UNVENTED EXPLODED CAVITY TESTS

Figure D.1 shows a schematic representation of cavity pressure and
fluid line pressure generated during a typical unvented exploded cavity
test. Charge detonation occurs at time zero and results in an initial
cavity gas pressure indicated by point A. Curve AB represents the decay
of residual gas pressure in a closed cavity as the detonation products
cool and diffuse into the surrounding medium. Point C represents the
prepressure applied to the hydrofracture fluid. Pumping begins at time
zero, and the straight line segment CD represents pressurization of the
fluid line as pumping continues. The ball valve that seals the cavity
starts to open at time zero. However, cavity gas pressure is high enough
for four seconds following charge detonation to prevent the valve from
opening. Curves BE and DE represent equilibration of cavity gas pressure
and fluid line pressure when the cavity finally opens. Hydrofracture
records for unvented exploded cavity tests start at point E, and curve EF
represents the initial portion of a typical record.

The 300 psi (2.068 MPa) at point C is the nominal prepressure applied
to the hydrofracture fluid before charge detonation. The 1176 psi
(8.108 MPa) at point D is the pressure generated in the fluid line after
four seconds of pumping at a rate of 4.26 cm^3/min. This value is obtained
from a calibration test on the closed system of 90 cm^3 of water. The
pressure in the closed system increases 3089 psi (21.30 MPa) for every cm^3
of fluid compression. The 1500 psi (10.34 MPa) at point E is the measured
value of equilibrium pressure between cavity gases and hydrofracture fluid
when the cavity first opens. The 1550 psi (10.69 MPa) at point B is a
theoretical estimate of cavity gas pressure just before the cavity opens.
The calculation is based on the assumption that, when the cavity opens,
the 3.6 cm^3 of detonation products in the cavity expand as a perfect gas
with a ratio of specific heats of 1.4.

D-1
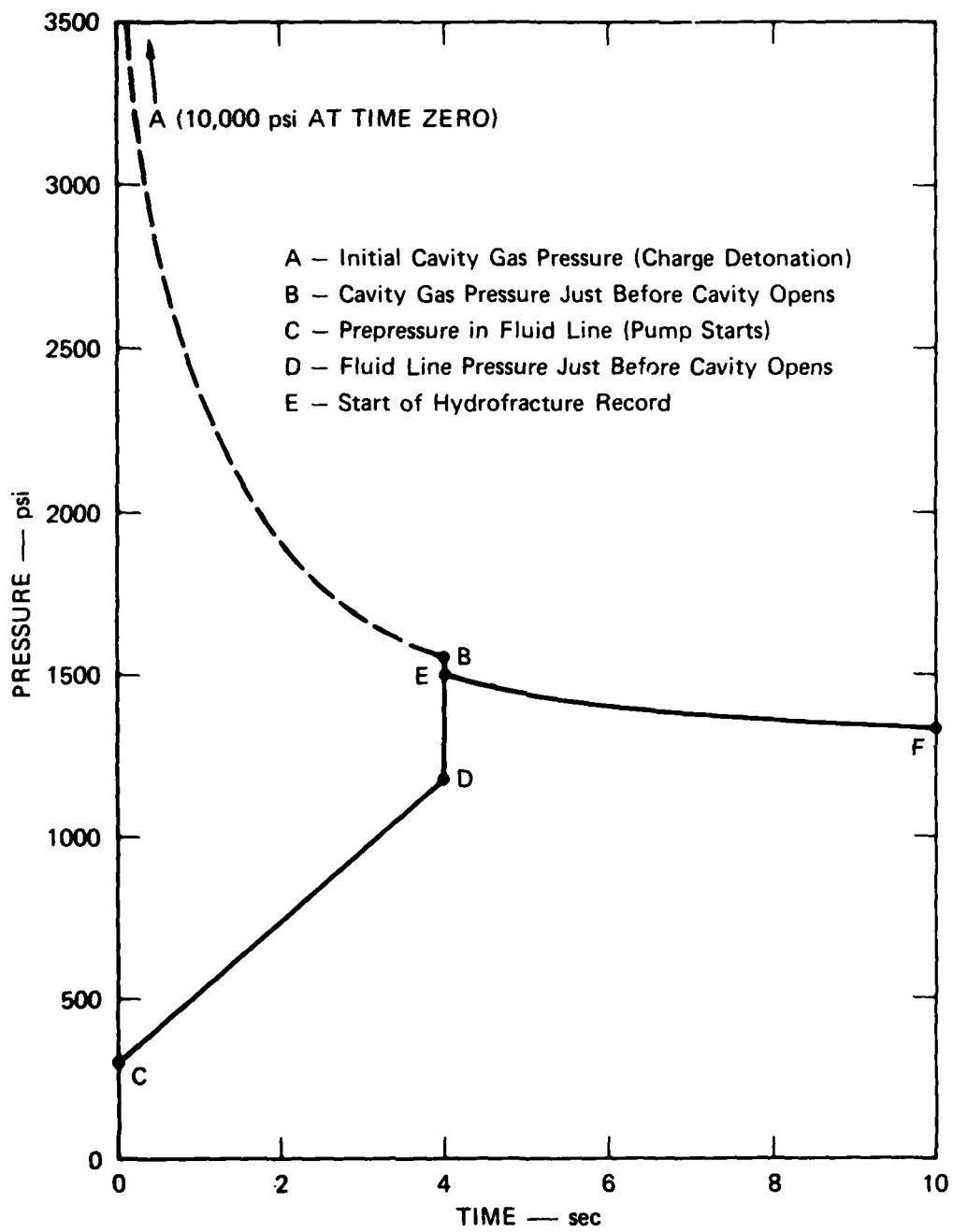
FIGURE D.1 SEQUENCE OF EVENTS DURING UNVENTED EXPLODED CAVITY TESTS

MA-8113-55

D-2

The hydrofracture records for unvented exploded cavity tests indicate that the pressure at fracture initiation depends on the minimum residual cavity gas pressure. As an aid to interpreting this dependence, Figure D.2 shows the stress history at the cavity wall together with a Mohr-Coulomb yield surface. Charge detonation results in a cavity pressure increase indicated by the path 0-1-2. Point 2 corresponds to point A in Figure D.1. Cavity gases then cool along path 2-3-4′. Point 4′ corresponds to the minimum cavity pressure. Hydrofracture results in a cavity pressure increase along path 4′-5′. Cavity fracture occurs at point 5′ where the circumferential stress σ_θ equals the static tensile strength σ_T of the material. Fracture does not occur along the path 0-1-2 because the dynamic tensile strength is large enough to withstand the dynamic loads. Figure D.2 shows that, if the cavity pressure had been unloaded to point 4″ instead of point 4′, the resulting fracture initiation pressure would have been given by point 5″ instead of point 5′. That is, a lower residual cavity gas pressure results in a lower fracture initiation pressure.

CAVITY PRESSURE = $-\sigma_r$

MOHR-COULOMB YIELD SURFACE
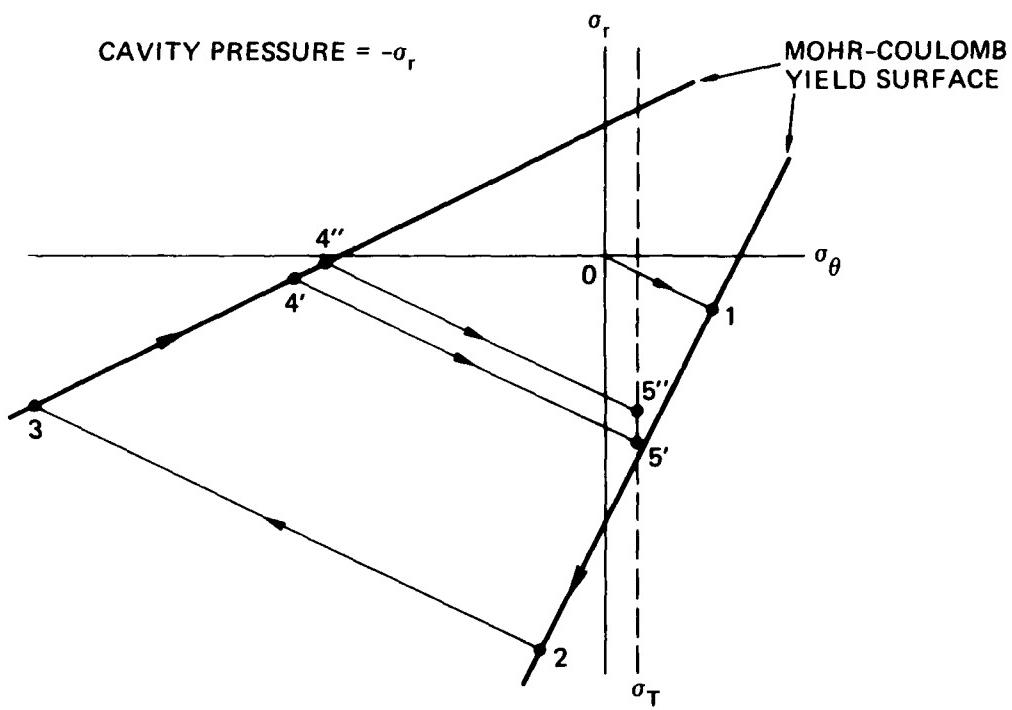
FIGURE D.2 STRESSES AT CAVITY WALL DURING UNVENTED
EXPLODED CAVITY TESTS

MA-8113-56

REFERENCES

1. R. W. Gates and C. F. Petersen, "A Laboratory Method for Studying Stemming of Line-of-Sight Tunnels in Underground Nuclear Tests," SRI Final Report DNA 3058Z, Contract DNA001-72-C-0047 (November 1972).

2. R. W. Gates, C. F. Petersen, and A. L. Florence, "Laboratory Method for Studying Stemming of Line-of-Sight Tunnels in Underground Nuclear Tests," SRI Final Report DNA 3592F, Contract DNA001-73-C-0122 (December 1973).

3. A. L. Florence, "Laboratory Investigation of Stemming of Horizontal Line-of-Sight (HLOS) Underground Nuclear Tests," SRI Final Report DNA 3684F, Contract DNA001-74-C-0101 (February 1975).

4. A. L. Florence, "Laboratory Investigation of Stemming and Containment in Underground Nuclear Tests," SRI Final Report DNA 4149F, Contract DNA001-75-C-0083 (October 1976).

5. J. C. Cizek and A. L. Florence, "Laboratory Investigation of Containment in Underground Nuclear Tests," SRI Final Report DNA 4846F, Contract DNA001-77-C-0025 (January 1978).

6. J. C. Cizek and A. L. Florence, "Laboratory Studies of Containment in Underground Nuclear Tests," SRI Final Report DNA 4847F, Contract DNA001-77-C-0025 (January 1979).

7. A. L. Florence and T. C. Kennedy, "A Simple Analysis for Containment Studies," SRI Topical Report 76-3702-2, Contract DNA001-75-C-0083 (August 1976).

8. L. Seaman, "SRI PUFF 3 Computer Code for Stress Wave Propagation," prepared for Air Force Weapons Laboratory, Air Force Systems Command, Kirtland AFB, New Mexico, Technical Report No. AFWL-TR-70-51, SRI International, Menlo Park, California (September 1970).

9. N. Rimer and K. Lie, "Spherically Symmetric Numerical Simulation of the SRI Grout Spheres Containment Experiments," Systems, Science and Software Topical Report SSS-R-79-3831, Contract DNA001-77-C-0099 (October 1978).

10. J. C. Cizek, A. L. Florence, D. D. Keough, and J. T. Rosenberg, "Experimental Study of the Effects of Faults on Spherical Wave Propagation," SRI Final Report (Draft) Contract DNA001-79-C-0261 (October 1979).

11. I. N. Sneddon, Fourier Transforms (McGraw Hill, New York, 1951).

12. H. Tada, P. Paris, and G. Irwin, The Stress Analysis of Cracks Handbook (Del Research Corporation, 226 Woodburne Drive, St. Louis, Missouri 63105).

13. J. R. Rice and M. P. Clearly, "Some Basic Stress Diffusion Solutions for Fluid-Saturated Elastic Porous Media with Compressible Constituents," Reviews of Geophysics and Space Physics, Vol. 14, No. 2, pp. 227-241 (May 1976).

14. H. S. Carslaw and J. C. Jaeger, Conduction of Heat in Solids, 2nd ed. (Oxford Press, London, 1959).

DISTRIBUTION LIST

DEPARTMENT OF DEFENSE

Defense Nuclear Agency
    ATTN: SPTD, T. Kennedy
4 cy ATTN: TITL

Field Command
Defense Nuclear Agency
    ATTN: FCT, P. Oppedahl
    ATTN: FCTT, B. Summa
    ATTN: FCTT, G. Ganong
3 cy ATTN: FCTK, C. Keller
3 cy ATTN: FCTK, B. Ristvet

Defense Technical Information Center
12 cy ATTN: DD

Field Command Test Directorate
Defense Nuclear Agency
    ATTN: FCTC, J. Lacomb

DEPARTMENT OF ENERGY

Nevada Operations Center
    ATTN: R. Newman

OTHER GOVERNMENT AGENCY

Department of the Interior
U.S. Geological Survey
    ATTN: A. Fernald
    ATTN: R. Carroll

DEPARTMENT OF ENERGY CONTRACTORS

Lawrence Livermore National Laboratory
    ATTN: J. Shearer
    ATTN: L. Makague
    ATTN: G. Higgins
    ATTN: B. Hudson
    ATTN: R. Terhune

Los Alamos National Scientific Laboratory
    ATTN: E. Jones
    ATTN: F. App
    ATTN: R. Brownlee
    ATTN: T. Kunkle
    ATTN: B. Travis
    ATTN: J. Wing

DEPARTMENT OF ENERGY CONTRACTORS (Continued)

Sandia National Laboratories
Livermore Laboratory
    ATTN: C. Mehl
    ATTN: C. Smith

DEPARTMENT OF DEFENSE CONTRACTORS

California Research & Technology, Inc
    ATTN: M. Rosenblatt

Desert Research Institute
    ATTN: D. Schulke, Sec Off for: P. Fenske
    ATTN: D. Schulke, Sec Off for: C. Case

Pacific-Sierra Research Corp
    ATTN: H. Brode

Pacifica Technology
    ATTN: D. Patch

Physics International Co
    ATTN: E. Moore
    ATTN: D. Mumma

Kaman Tempo
    ATTN: DASIAC

R & D Associates
    ATTN: P. Haas

SRI International
    ATTN: A. Florence

Systems, Science & Software, Inc
    ATTN: R. Duff
    ATTN: C. Dismukes